

**EXPERIMENTAL STUDY ON OPTIMUM
SPACE-CHARGE EFFECTS AND ENHANCED
FREE-SPACE COUPLING FOR VIRCATOR
DRIVEN BY COMPACT DRIVER**

By

Rohit Shukla

Enrolment No: PHYS01200804007

BHABHA ATOMIC RESEARCH CENTRE, VISAKHAPATNAM

*A thesis submitted to the
Board of Studies in Physical Sciences*

In partial fulfillment of the requirements

For the Degree of

DOCTOR OF PHILOSOPHY

of

HOMI BHABHA NATIONAL INSTITUTE



November 2014

Homi Bhabha National Institute

Recommendations of the Viva Voce Committee

As members of the Viva Voce Committee, we certify that we have read the dissertation prepared by Rohit Shukla entitled "EXPERIMENTAL STUDY ON OPTIMUM SPACE-CHARGE EFFECTS AND ENHANCED FREE-SPACE COUPLING FOR VIR-CATOR DRIVEN BY COMPACT DRIVER" and recommend that it may be accepted as fulfilling the thesis requirement for the award of Degree of Doctor of Philosophy.

----- *S.V.G. Menon* ----- Date :

Chairman : Dr. S.V.G. Menon

----- *Anurag Shyam* ----- Date : 27.11.2014

Convener : Dr. Anurag Shyam

----- ----- Date :

Member : Dr. Prasad A. Naik

----- *A. Z. Chaturvedi* ----- Date :

Member : Dr. Shashank Chaturvedi

----- *Lalit Kumar* ----- Date : 27.11.2014

External Examiner : Dr. Lalit Kumar

Final approval and acceptance of this thesis is contingent upon the candidate's submission of the final copies of the thesis to HBNI.

I hereby certify that I have read this thesis prepared under my direction and recommend that it may be accepted as fulfilling the thesis requirement.

Date: 27.11.2014

Place: VISAKHAPATNAM

Anurag Shyam
Guide : Dr. Anurag Shyam

STATEMENT BY AUTHOR

This dissertation has been submitted in partial fulfillment of requirements for an advanced degree at Homi Bhabha National Institute (HBNI) and is deposited in the Library to be made available to borrowers under rules of the HBNI.

Brief quotations from this dissertation are allowable without special permission, provided that accurate acknowledgement of source is made. Requests for permission for extended quotation from or reproduction of this manuscript in whole or in part may be granted by the Competent Authority of HBNI when in his or her judgement the proposed use of the material is in the interests of scholarship. In all other instances, however, permission must be obtained from the author.

Rohit Shukla
27/11/2014
Rohit Shukla

DECLARATION

I, hereby declare that the investigation presented in the thesis has been carried out by me. The work is original and the work has not been submitted earlier as a whole or in part for a degree/diploma at this or any other Institution or University.

Rohit Shukla
27/11/14

Rohit Shukla

Dedicated to
my wife Aradhana
&
my lovely kids Suramyia & Surashmi

List of publications arising from the thesis

Published in Peer Reviewed Journals:

1. **Compact, reusable inductive storage *cum* opening switch based 1.5GW single shot pulsed power generator**

R. Shukla, A. Shyam *Notes: Review of Scientific Instruments* **85** Issue 3 (2014)

2. **Low voltage, low energy and repetitive (4Hz) operation of a conventional vir-cator for microwave emission in the range of 4-8 GHz**

R.Shukla, A. Shyam *Laser and Particle Beams* **31** Issue 04 pp 627-634 (2013)

3. **Microwave Emission from a AXIAL-Virtual Cathode Oscillator Driven by Compact Pulsed Power Source**

R. Shukla, P.Bannerjee, S.K. Sharma, R. Das, P. Deb, Prabakaran T., B.K. Das, B. Adhikary, R.Verma, A.Shyam *Journal of Physics :Conference Series* (2012)

4. **Results of Compact High Voltage Pulse Transformer made using a capacitor bank assembled in the shape of primary**

R. Shukla,P.Bannerjee, S. Sharma, R. Das, P. Deb, Prabakaran T., B. Das, B.Adhikary, A.Shyam *Notes: Review of Scientific Instruments* **82**, 106103 (2011)

5. **Solid Dielectric Pulsed Forming Line Driven Electron Beam Diode for the production of microwaves**

R. Shukla, S.K. Sharma, A.Shyam *Journal of Nepal Physical Society: Conference Series* **26** No 1 pp 29-34 (2010)

Conference Presentations :

1. **Microwave Emission from an AXIAL-Virtual Cathode Oscillator Driven by Compact Pulsed Power Source**

R. Shukla, P. Bannerjee, S.K. Sharma, R. Das, P. Deb, Prabakaran T., B.K. Das, B. Adhikary, R. Verma, A. Shyam *International Symposium on Vacuum Science and Technology* VECC Kolkata, India (IVS-2012)

A recipient of **Shrimati Shakuntalabai Vyawahare memorial best poster award** in the symposium.

2. Inductive storage type pulsed power driver for the generation of Electromagnetic Radiations

R. Shukla, P. Banerjee, S. K. Sharma, R. Das, P. Deb, T. Prabakar, B. K. Das, B. Adhikary, A. Shyam *International Symposium on Microwaves* Nimhans, Bangalore, India (ISM-2010)

3. Low-Cost, Inductive storage type, Indigenous & Compact 500MW pulsed power driver for 12.5ohm load

R. Shukla, P. Banerjee, S.K. Sharma, P. Deb, T. Prabakaran, R. Das, B. Das, B. Adhikari, A. Shyam *School on Pulsed Power Technology* BARC, Mumbai, India (SPPT-2010)

4. Solid Dielectric Pulse Forming Line Driven Electron beam diode for production of microwave

R. Shukla S.K. Sharma A. Shyam *4th International conference on the frontiers of plasma physics and technology* Kathmandu Nepal (FPPT-2009)

5. Microwave radiations from Vircator driven by solid dielectric Pulse Forming Line

R. Shukla, S.K. Sharma, A. Shyam *International Symposium on Microwaves* Bangalore, India (ISM-2008)

Rohit Shukla

ACKNOWLEDGEMENTS

The guide has biggest role in a person's work pertaining to the thesis and here comes the deep and sincere acknowledgement for Dr. Anurag Shyam who has continuously been actively supportive for the work mentioned in the thesis.

I would like to acknowledge the contribution of my doctoral committee members who have spent their precious time in evaluating and suggesting me as and when was needed during the tenure of Ph D which led me to complete the research work reported in this dissertation. Dr. S.V.G. Menon (Retd. Head, Theoretical Physics Division BARC), Dr. Prasad A. Naik (Head, Laser Plasma Division, RRCAT, Indore), Dr. Shashank Chaturvedi (Head, Computational Analysis Division, BARCF Vizag) as members of my Doctoral Committee have really motivated me throughout the period of the research. Special contribution of ever-inspiring personalities of Dr. Prabal Chattopadhyay and Dr. Aseem Chattopadhyay of IPR, Gandhinagar Gujarat as my teachers during my course works can not be left unmentioned here. Acknowledgement is made towards the contribution of colleagues of the Energetics & Electromagnetics Division who took part in discussions and then leading to increased understanding about the problem. Colleagues from Computational Analysis Division has always helped in any of the requirement related to computers and various modelling related problems irrespective of the time of need sparing some of their precious time for me.

Acknowledgement is to my Late Grand Father who was really overjoyed to know that I had started my research leading to a Ph.D. My uncle, my parents and my siblings will certainly enjoy the completion of my Ph.D.

Rohit Shukla

Abstract

Ultra compact PT charges the solid dielectric PFL in $2\mu\text{s}$ and $1\mu\text{s}$ made by RG218 cable and 450kV XLPE cable in the presented results. The achieved voltage gains of PT are 1:20 in such compact geometries. PFL are made of coaxial cable to drive electron beam diode in form of vircator and are reported for the first time. The microwave emission from such compact PFL charged by new-configuration PT is reported for 1MW radiation in frequency range of 4-8GHz. The vircator is operated with the help of dry PFL at repetition rate of 4Hz and consistency of results in terms of frequency and peak power upto six sequential shots is reported in the repetitive operating mode. Shot to shot variation is also shown to be very little in terms of frequency and peak radiated power in single shot mode of operation. The cable based PFL pulsed power generator has electrical peak power delivery of 650MW and 3.3GW respectively when they are made using RG218 cable in one case and high voltage XLPE cable in the other case. A broadband conical horn antenna to maximize the radiation at the axis of vircator is designed and implemented after the vircator. 3D modelling results of the antenna are also presented. The vircator efficiency of 0.3% is also reported and extensive modelling of the results in PIC code (XOOPIC two and half dimensional code) is also presented. The vircator is reported to be operating at 50kV of A-K gap voltage which is the lowest reported in conventional vircator geometry. At these low anode cathode voltages the current densities (computed assuming uniform emission) achieved are $300\text{A}/\text{cm}^2$ which is quite close to the highest values reported in the literature i.e. $450\text{A}/\text{cm}^2$. For single shot applications ultra compact pulsed power generators using exploding copper wire as opening switch is reported for 500MW and 2GW peak electrical power delivery capabilities in two reported cases. All the switches in this generator are in air and hence device is very attractive. The experimental, modelling results of these compact generators aimed for vircator as load is presented.

SYNOPSIS

It has been seen in the past that for the microwave emission from Vircator (Virtual Cathode Oscillator) like pulsed high power microwave emitting devices, one requires high electrical input powers which are essentially delivered by the pulse-shaping and pulse-compression devices made of high dielectric strength (voltage withstand capability) and high relative permittivity (high energy density capacity) materials. The leaders in the field have been liquid dielectrics like water ($\epsilon_r = 74$ at 35°C temperature [1]) and castor oil ($\epsilon_r = 4.7$) and have been immensely used in the experiments. In such cases of liquid dielectrics, especially in the case of water, there is a need of continuous processing of the liquids to maintain its purity levels so that the dielectric property of the liquid utilized for pulse-shaping and/or pulse-compression are not changed/deteriorated to worsen the performance of the whole integrated system. The contamination like electrode erosion and humidity (in case of other than water used as the dielectric) are the main factors worsening their performance. This ends up in the requirement of associated systems and components requiring constant energy to run them, even though the system is lying idle and needs to have short readiness time at the time of need of its functioning. Moreover, the system becomes heavier because of requirement of such associated components and systems. The operation becomes really difficult to work with as the efforts required in maintaining the system in operational mode is much higher. If the mobility of pulse microwave source is also of prime concern to the user then it becomes needless to say that the usefulness of the liquid dielectric based pulsed power system driven high power microwave source is drastically reduced.

The aim of the present work is to explore the possibilities of radiation emission from a simple virtual cathode oscillator made using a dry-type and maintenance-free type pulse forming system to drive electrical input powers into it. This enhances the compactness/robustness of the system and reduces the time of readiness from idle to on-state with increased ease in mobility. Hence the experimental scope for such system in terms

of practical feasibility is needed to be explored. The work is aimed for making one such integrated system which has a compact and maintenance-free pulsed power source and a vircator device matching with the designed pulse-power-source's parameters to deliver the considerable levels of microwave emission in the frequency range starting from a few gigahertz and lying up to 10GHz. Moreover the issues to make system more compact and also about integrating the chemical energy driven primary pulse-power energy-storage are also discussed with an aim of realization of such compact and maintenance-free devices. The work reported in this thesis is aimed towards achieving pulsed microwave emission of longer durations (long anode cathode gap closure time) from a vircator driven by a compact maintenance-free dry-type pulsed power source in the frequency range of few GHz to 10GHz. The research involves solving the physics problems to design the system components and realize, characterize them in parts and then assembling such system components in order to study the physics of integrated-system made operational. The study on the effect of designed and developed antenna in view of enhancing free space coupling from the vircator is also done as part of work of research reported in the thesis. Related stage-by-stage system-modelling is also reported in the thesis which involves very fast softwares for circuit solving like spice solver PSPICE, inductance extraction programmes like FASTHENRY, EFFI particle-in-cell codes XOOPIIC and few FORTRAN/SCILAB based codes written to analyse the experimental results as a feedback mechanism while designing in the system in stages. Essentially there are two mechanisms to generate such pulses and they are as a) capacitive storage type pulsed power source by utilizing the closing switch and b) the other is inductive storage type pulsed power generator utilizing the opening switch. In both the cases the initial energy can be provided by ultra-compact high-energy-density pulsed power converters (from chemical energy to electrical energy). The first option among the two types of systems mentioned above is explored for realizing a vircator driven by a pulse forming line made of solid dielectric which is essentially high-voltage

transmission-line combination in parallel to deliver the desired source impedance and desired electrical powers. The second method of inductive storage driven compact pulsed power source was also explored and a complete modelling with circuit solver to incorporate the integration of inductive storage-*cum* opening switch driven vircator was done to define the operating parameters of such a compact pulsed power driver after validation of the model with the experimental results.

Chapter 1 is an introduction of the problem and review of literature. It also presents a picture of the aims conceived, which is to make a compact and portable pulsed power system driven virtual cathode oscillator, and need of the work presented in the thesis

Chapter 2 deals with the diagnostics used in the experiments reported for the present thesis work. The diagnostics used for the observing the primary voltage at PFL is simple resistive divider made of high voltage high energy ceramic disc resistor which is made stacking number of resistors in series to make the upper arm of the resistive voltage divider. The lower arm is made using the same type ceramic disk resistor with different composition and dimensions to give a lower arm resistance of 5Ω . The attenuation ratio resulting from this combination is 8000:1. The voltage at the diode is being measured using a high voltage probe which consists of two similar 100MHz, 100kV 1000:1 probes connected in series. The net output from this series combination of probes is having an attenuation of 20000:1 and the high voltage terminals of both the probes are made common to deliver a voltage measurement diagnostic which can withstand to twice of the voltage withstand capacity of one divider. This way we can measure the voltage up to 200kV pulse. The rise time of this probe corresponds to 12ns only as per the experimental tests reported in this thesis. For the measurement of the current passing through electron beam diode we have used one standard current transformer (CT) with 20ns rise time in one segment of ground connection of the vircator chamber which is segmented in 12 similar parts. The sensitivity of the current transformer is 10Volts/kA and thus every volt from the CT measures an equivalent current of 1.2kA passing through the

electron beam diode. For the measurement of microwaves frequency, high frequency digital storage oscilloscopes and to see the envelope of radiated microwave pulse the high bandwidth microwave detector diodes are used after suitable attenuation of microwave power density done by free space attenuation, external fixed attenuators. The sampling of radiated microwave power is done by horn antenna kept at different locations away from radiating horn antenna or waveguide of vircator.

Chapter 3 describes the system components for capacitive method based repetitive pulsed power driven laboratory based microwave radiator source and their design, fabrication and testing details which are highlighted as given under. A compact power supply, a trigger-generator and the low operating voltage (below 10kV) spark-gap for repetitive triggering was designed developed and tested. The second major component is solid dielectric based pulse forming line (compact, dry and requiring no maintenance) is made in three different experimental setups. It has advantage over Marx base or inductive storage based system in terms of the flat output pulse. The microwave emission results from these three setups and respective vircators is observed and reported in chapter 6. The first two of them being based on four parallel 50 Ω cables RG218 (180kV tested for microwave emission with vircator) to give a net 12.5 Ω source impedance of different pulse widths depending upon the cable lengths viz 8m and 12m respectively. The peak power delivery capability of these pulsed power generators is 650MW for a matched load. It is to be noteworthy here that the two pulse forming lines were charged with monopolar and bipolar voltage pulses in two cases respectively and it was found that the bipolar charging of pulse forming line deteriorates the longevity or life of overstressed pulse forming line. Then in the final and the third system only mono-polar charging of pulse forming line was done. This PFL is differently made using 450kV voltage withstand cables, each of 60 Ω impedance providing net 15 Ω source impedance. The system is deliverable to the field with very good portability and also with no maintenance during operation. The peak power delivery capability of such this system for a

matched load is 3.3GW

Chapter 4 describes the design and modelling details of three different transformers used for charging the transmission line based pulse forming line described above for driving the vircator. This was done in order to finally generate the microwave radiations from the vircator. The transformers are modelled (in the last two cases of pulse forming line) using a circuit solver for studying its electric performance whereas the design was made on the basis of 3-dimensional inductance extraction program called FASTHENRY (including physics of coupling of energy between primary and secondary) and using EFFI computer code (in the first case of pulse forming line). The code FASTHENRY is capable of handling the 3D geometry of the transformer and gives a pictorial presentation of the sample problem and solves it by considering the problem space in the forms of small straight elements of current carrying conductors. Interestingly as the transformer is air core pulse transformer hence it is essential to know the sizes of primary and secondary capacitor to demonstrate a system which is compact. The FASTHENRY code computes the primary and secondary inductances and also mutual inductance between primary and secondary and hence becomes a good design tool for a suitable air-core pulse-transformer. The primary capacitor bank is interesting and made in a novel way in last two cases. For the first time, as is reported in the literature, it has been made in such a way that the primary of pulse transformer is made using a series and parallel combination of axial lead type cylindrical capacitors. The transformers are designed in order to make a double resonant mode operation for a particular case(second setup) of pulse forming line made by RG218 cable and also to make first pulse charging in the other cases of pulse forming lines (in the first and third setup) charging. A noteworthy point is that the PFL charging within $1\mu s$ from the beginning of primary capacitor discharge was finally achieved in the experiments.

Chapter 5 deals with the details of antenna design for axial extracted vircator and for a suitable coupling with the vircator and to analyse the results of changes in the mi-

microwave emission in free space by the use of antenna in the vircator driven by compact pulsed power driver.

Chapter 6 deals with the experiments and their results in different systems using monopolar or bipolar pulses with different rise times for pulse forming line charging. The double resonant and first pulse charging in minimum rise time is aimed during the transformer design and studied in second and the third set of vircator experiments after gaining some experience from first set of experiments in which bigger pulsed power generator was used to drive the vircator. The system made by such assemblies require almost zero maintenance during their operation except the maintaining vacuum before each shot in vircator chamber and the work has been expanded towards repetitive vircator operation. The modelling of the microwave emitter was done on a two and half dimensional particle-in-cell codes XOOPIC which is available in public domain. Different cathode materials are used for the experiments.

The salient features of the conducted experiments are as given under.

1. Monopolar charging of RG218 based system was done and connected virtual cathode oscillator (VIRCATOR) load with graphite cathode demonstrates emission of microwave radiations in 1.7GHz frequency. The emitted microwaves being propagating electromagnetic fields have caused visible breakdown in gas discharge tubes like neon lamps and fluorescent tubes. X rays generated by the electron beam bombardment were also recorded and annular profile of electron beam was observed and recorded. This is first of its kind experiment as electron beams for vircator operation were produced by any cable based PFL system.
2. Double resonant operation of RG218 Cable based system with aluminium cathode and demonstration of high frequency radiations at 160kV and 180kV charging of the PFL respectively was subsequently reported. Bulk breakdown in the dielectric

of the Pulse forming line was also noticed at 200kV of pulse charging voltage in double resonant charging when the peak value of the charging voltage is achieved in $2.0\mu\text{s}$. A slight frequency shift in microwave emission was also observed in the output depending on the charging voltage. The system was modelled also using XOOPIC particle-in-cell code and the results show a very good understanding of the high frequency and low frequency signals coming out of the axial vircator.

3. As the bipolar pulses reduce the life of the solid dielectrics at high voltage stressing so we replaced the RG218 cables with other cables having a voltage withstand capability of 450kV in short pulses with the cable overall diameter of 39mm and an impedance of 60Ω . The cable based pulse forming line was charged using a pulse transformer in the first peak. For this purpose another pulse transformer was made using capacitor bank shaped in form of primary but to enhance the coupling between primary and secondary we have used the flexibility of diameter in order to use the energy of primary bank efficiently. The secondary was successfully charged and discharged in first peak which is attained in $1\mu\text{s}$ time and the radiations of vircator were recorded at these conditions. The microwave radiations from the vircator are observed using a cathode made by red velvet and the A-K gap being 3mm. It is also observed that the radiations are ranging in 4-8GHz in different shots and chirping of frequency in different shots is minimal.
4. A successful demonstration of microwave emission from a virtual cathode oscillator operating at low voltage has been achieved experimentally without any change in conventional geometry of virtual cathode which had previously been done by the application of external magnetic field for operating the virtual cathode oscillator at relatively lower voltages as per the reported literature.

5. A repetitive 4Hz operation of the vircator driven by cable based PFL is achieved and 1MW radiation with 0.3% efficiency is recorded by the vircator at low voltage operation.

Chapter 7 has the description of the inductive-storage *cum* opening-switch based compact pulsed power generators which is shown to demonstrate 500MW and 2GW of electrical powers for 200ns of duration into a 12.5Ω and 18Ω loads respectively. The 2GW power generator is less than 15kg in weight and 70cm length and 20cm diameter cylindrical dimensions. The circuit modelling to understand the physics for such system was done using action dependent resistivity (Tucker and Toth model) model. The integrated analysis of such system with a load which has formulation of voltage dependent impedance like that of vircator or planar anode cathode structure devices was also done and is being reported as assembled system of one kind. The effect of different anode cathode spacings for such generator driven vircator has been studied theoretically in terms of load power, voltage and current. This study is meant for making a single-shot integrated system for generation of high power microwaves using chemical pulsed power and foundations are planned to be laid by using this work in order to make a comparison of inductive storage -vis-a vis capacitive storage based compact pulsed power technology. The inductive storage based pulsed power source is expected to be the most compact pulsed power source as the energy density of such chemicals driving this system is very high and the pulsed power delivery from such chemicals is very high. This way they form a complete single shot system but as the nature of chemicals used in such devices is such that they release enormous energies in very short durations they cannot be used in laboratory based controlled and environment. The work includes the spice modelling and the experimental results of laboratory based inductive storage system. Further modelling in terms of analysis of the inductive storage system was also done in order to predict the assembly behaviour of the system for different load impedance

which includes the pspice modelling of voltage dependent impedance of the vircator diode which is $137(d/R)^2/V_{diode}$.

Chapter 8 finally has conclusion of the experiments reported in the thesis. This chapter also includes some of the suggestions for the future experiments.

LIST OF ABBREVIATIONS

FWHM	Full width half maximum
PFL	Pulse Forming Line
Vircator	Virtual Cathode Oscillator
HPM	High Power Microwave
PT	Pulse Transformer
PIC	Particle-in-Cell
XOOPIC	Object oriented particle-in-cell code with X windows
FFT	Fast Fourier Transform
STFT	Short Time Fourier Transform
μH	microhenry
nH	nanohenry
μs	microsecond
ns	nanosecond
ps	picoseconds
μF	microfarad
S.S.	Stainless Steel
VSWR	Voltage Standing Wave Ratio
PE	Poly-Ethylene
XLPE	Cross Linked Poly-Ethylene
TLT	Transmission Line Transformer
rms	root mean squared
BW	Band Width
HV	High Voltage
dB	Decibel

SYNOPSIS	1
List of Abbreviations	10
List of Figures	14
List of Tables	20
1 INTRODUCTION	21
1.1 Compact Pulsed Power Generators : Literature survey	23
1.2 Overstressing primary energy storage capacitors: Literature survey . . .	24
1.3 Coaxial cable used for compact pulsed power: Literature survey	25
1.4 Opening switches for inductive storage: Literature survey	26
1.5 Vircator: Basics	29
1.6 Work Summary	31
2 DIAGNOSTICS	35
2.1 Voltage Measurement	36
2.1.1 PFL charging voltage measurement	36
2.1.2 Diode voltage measurement	39
2.2 Current Measurement	42
2.3 Microwave Diagnostics	43
2.4 Electron Beam Impression	45
2.5 X-ray Diagnostics	46
2.6 Conclusion	46

3	SOLID-DIELECTRIC PULSE FORMING LINE	47
3.1	RG218 Cable PFL for first and second set of vircator experiments	49
3.2	450KV cable PFL for third set of vircator experiments	54
3.3	Modelling of PFL with vircator for power calculation	58
3.4	Conclusion	63
 4	 COMPACT PULSE-TRANSFORMER	 65
4.1	PT for the first set of vircator experiments	70
4.2	PT for the second set of vircator experiments	73
4.3	PT for the third set of vircator experiments	82
4.4	Conclusion	87
 5	 CONICAL HORN ANTENNA	 89
5.1	Antenna Basics	90
5.2	Antenna Analysis	93
5.3	Conclusion	102
 6	 VIRCATOR RESULTS	 104
6.1	Vircator Experiments:Set1	107
6.2	Vircator Experiments:Set2	113
6.2.1	Experimental Setup	115
6.2.2	Experimental Results	119
6.3	Vircator Experiments:Set3	121
6.3.1	Introduction	121
6.3.2	Experimental Details	127
6.3.3	Energizing the vircator	130
6.3.4	Experimental Results	136
6.4	Conclusion	138

7	INDUCTIVE-STORAGE-CUM-OPENING-SWITCH DRIVEN VIRCATOR	142
7.1	500MW SYSTEM AND ITS MODELLING WITH THE VIRCATOR .	143
7.1.1	Experimental arrangement	144
7.1.2	Experimental Results	148
7.2	1.5GW Compact Generator	153
7.2.1	Introduction	153
7.2.2	Experimental Results	157
7.2.3	Discussion with Analysis of Results	159
7.2.4	Summary	161
7.3	Conclusion	166
8	CONCLUSION & FUTURE WORKS	167
	Bibliography	171

List of Figures

1.1	Cable PFL driven vircator assembly with antenna	33
2.1	Resistive Voltage Divider	36
2.2	Resistive Voltage Divider Performance	37
2.3	High BW Resistive Voltage Divider	38
2.4	High BW Resistive Voltage Divider Performance	40
2.5	Cascaded High Voltage Probe	41
2.6	Cascaded high voltage probe performance analysis	41
2.7	Calibration curve of Self Integrating Rogowski coil for primary current measurement (sensitivity is 1V/kA)	43
3.1	Pulse forming line made of RG218 cable	50
3.2	Punctured RG218 cable (blackened spot is the place where cable is punctured)	51
3.3	Charging voltage waveform of cables constituting a damaged PFL	53
3.4	RG218 cable with connector for fitting	55
3.5	PFL made of 450kV (Impulse) XLPE cable	56
3.6	High voltage XLPE cable with connector for fitting	57
3.7	Estimated peak load power for the two PFLs	59
3.8	Simulated vircator(different A-K gaps, 60mm cathode diameter) impedance for 12.5 Ω 180kV PFL	60
3.9	Simulated vircator (different A-K gaps,60mm cathode diameter) power for 12.5 Ω 180kV PFL	60
3.10	Simulated vircator(different A-K gaps,50mm cathode diameter) impedance for 15 Ω 450kV PFL	62

3.11 Simulated vircator(different A-K gaps,50mm cathode diameter) power for 15 Ω 450kV PFL	62
4.1 Primary capacitor and pulse transformer for experiments of first set . . .	71
4.2 PFL voltage and the primary current waveform	72
4.3 Simulated PFL Voltage for 12kV charging of primary capacitor	74
4.4 Compact pulse transformer using capacitor bank as its primary	77
4.5 Voltage time history of PFL charged by the compact transformer	80
4.6 Voltage time history of PFL (output spark gap is in air)	81
4.7 Voltage time history of PFL (output spark gap is in oil)	82
4.8 High Voltage Pulse transformer	83
4.9 Fasthenry input drawing for the transformer (discretized geometry) . . .	85
4.10 PFL charged to 250kV by high voltage pulse transformer Red is ac- quired signal and blue is numerically filtered waveform	86
5.1 Excitation signal given to the input port in the modelling	89
5.2 Far field radiation pattern at 6GHz for first mode	90
5.3 Antenna gain value at 6GHz in polar coordinates for first mode $\Phi = 0$.	92
5.4 Antenna gain value at 6GHz in polar coordinates for first mode $\Phi = 90$.	93
5.5 Far field radiation pattern at 6GHz for second mode	94
5.6 Antenna gain value at 6GHz in polar coordinates for second mode $\Phi = 0$	95
5.7 Antenna gain value at 6GHz in polar coordinates for second mode $\Phi = 90$	96
5.8 Antenna gain versus theta at $\Phi = 0$ for first mode at different frequencies	97
5.9 Antenna gain versus theta at $\Phi = 90$ for first mode at different frequencies	97
5.10 Antenna gain versus theta at $\Phi = 0$ for second mode at different fre- quencies	98

5.11 Antenna gain versus theta at $\Phi = 90$ for second mode at different frequencies	99
5.12 Antenna gain versus theta at $\Phi = 0$ for third mode at different frequencies	99
5.13 Antenna gain versus theta at $\Phi = 90$ for third mode at different frequencies	100
5.14 antenna reflection coefficient at different frequencies for different modes	101
5.15 S11 parameter on dB scale at different frequencies for different modes .	101
5.16 VSWR of the horn antenna for different modes	102
6.1 Schematic of Vircator Chamber assembly with cable based PFL	104
6.2 Vircator Assembly	105
6.3 Pulsed power system and vacuum field emission diode	106
6.4 Impression of electron beam on S.S. mesh	107
6.5 Impression of electron beam on thermal paper	108
6.6 Exposed dental X-ray film (exposure in five shots)	109
6.7 Microwave envelop as shown by detector diode	110
6.8 Received microwave signal	110
6.9 FFT of received microwaves	111
6.10 Glowing of neon lamps (red)	112
6.11 Glowing fluorescent tube in front of microwave radiations	112
6.12 Voltage applied across the anode cathode gap	113
6.13 Axial virtual cathode oscillator System	114
6.14 Stainless Steel Cathode	114
6.15 PFL Charging Voltage and PFL Discharge Current	116
6.16 Receiving Antenna (kept at 1.2Meters from cathode) signal and envelop seen by the microwave detector diode (vircator operating with PFL at 160kV)	116
6.17 FFT of receiving antenna signal (vircator operating at 160kV PFL Voltage)	118

6.18 PFL Charging Voltage and PFL Discharge Current	119
6.19 Receiving Antenna kept at 1.2Meters from Cathode signal and envelop seen by the microwave detector diode vircator operating at 180kV PFL Voltage	120
6.20 FFT of Receiving antenna signal vircator operating at 180kV PFL Voltage	121
6.21 Picture of virtual cathode oscillator assembly fitted with the cable based PFL	122
6.22 Geometrical drawing of the virtual cathode oscillator system	123
6.23 Simulation Voltage, total Current and the current after foil measured in the XOOPIC simulation	124
6.24 Power radiated in the simulation	125
6.25 Instantaneous FFT of the radiated power and halfed frequency to find the frequency spectrum of radiation in simulation.	126
6.26 U_z versus z for the electrons trapped between cathode and virtual cath- ode at 18.66ns.	127
6.27 Number of simulation particles with time	128
6.28 PFL charging Voltage and the diode voltage waveforms	129
6.29 Diode voltage and diode current waveforms	130
6.30 Diode voltage versus diode current showing single pulsed power dissi- pation	131
6.31 Microwave pulse with 40dB external attenuator measured at 2.5 meters from radiating antenna in 8 shots. (Power stability in different shots) . .	131
6.32 Instantaneous FFT of the acquisitions of previous electric field measure- ment. (Frequency stability in different shots)	132

6.33	Microwave pulse with 40dB external attenuator measured at 1.5m, 2.5m and 3.5m from radiating antenna at the axis. (showing r^2 power attenuation) X-axis scale 200ns/div	133
6.34	Electric field measured at 2.5meters from radiator when the receiving antenna is scanned from -45degree to 45degree on axis varying in angle of 7.5degree	133
6.35	Power measured at 2.5meters from radiator when the receiving antenna is scanned from -45 degree to 45 degree on axis varying in angle of 7.5 degree	134
6.36	Instantaneous FFT of the signal of previous figure showing frequency stability between different shots. (Frequency(Hz) vs. Time(seconds)) . .	136
6.37	4Hz discharge of the primary capacitor bank for the generation of the microwave in vircator; y-axis in volts	137
6.38	Radiation of vircator at 4Hz (6shots electric-field recorded) shifted in time scale to show the peaks and modulation	139
7.1	Schematic of inductive storage type pulsed power supply	143
7.2	Experimental Setup with Marx generator	144
7.3	Short Circuit current of driver	145
7.4	Total current (pink) 5kA/div, Exploding wire Current (yellow) 5kA/div, Load Voltage (blue) 10kV/div: Horizontal Scale 200ns/div	146
7.5	PSPICE model of inductive storage system	147
7.6	Total current (red) 10kA/div, Exploding wire current (Green) 10kA/div, Load Voltage (blue) 10kV/div: Horizontal Scale 100ns/div	148
7.7	PSPICE model of inductive storage system with vacuum diode	149
7.8	Load Voltage (red) 50kV/div, Load Current (Green) 5kA/div, Load Power (blue) 500MW/div: Horizontal Scale 100ns/div	150

7.9	Normalized resistance of exploding copper wire	151
7.10	Action on wire and energy dissipated in wire	152
7.11	Experimental setup for the pulsed power source	154
7.12	Short circuit current of the circuit	155
7.13	Load voltage and total current as well as fuse current of the circuit . . .	155
7.14	The power and energy dissipated in the 10.5Ω load	157
7.15	Modelling results of the pulsed power generator with 10.5Ω load with- out including delayed burst	158
7.16	Original and modified resistivity of copper based on action integral . . .	159
7.17	Modelling results of the pulsed power generator with 10.5Ω load includ- ing delayed burst	160
7.18	The computed diode voltage for different A-K gap	161
7.19	The computed diode current for different A-K gap	163
7.20	The computed diode power for different A-K gap	164

List of Tables

3.1	Coaxial Cable Details	63
4.1	Pulse transformer details	88
5.1	First six modes used for computation	94
6.1	Summary of vircator experiments	140
7.1	Marx Generator driven Inductive Storage based pulsed power generator	165

1

INTRODUCTION

It has been already shown by different research groups working for the generation of High Power Microwaves utilizing quite bigger pulsed power generators that the input electrical powers required for the successful operation of these generators is in the order of GW. This also requires the high voltages in hundreds of kilovolts as the impedances of such devices is mostly in tens of Ω s. The simplicity in construction and operation alongwith tunability in radiation frequency by changing geometry makes the vircator among the most favourite devices for microwave production. Electrical to microwave power conversion efficiency of axial-vircators (which is simpler in construction among different vircator variants) is limited. The efficiency of vircator is not seen increasing more than a few per cent in terms of electrical to microwave peak power conversion. Mostly the generators used to drive the vircators are heavy and big in size and also demand some other sub-systems during system operation and they find a difficult way to come out of laboratories. The aim of the work reported in this thesis is towards making the pulsed microwave generating system such that the experiments which are to be done out of laboratory space may easily be conducted with them. In order to attain this objective we have tried making pulsed power generators in compact and essentially dry

configurations which are capable of driving the axial-vircator load with a quite good efficiency even at moderately high electrical pulsed powers as input. Given the limitations in the size/compactness of the pulsed power generators for laboratory applications it becomes very interesting to see towards the problem of operating a high power microwave device which, in the present case, is an axial vircator by using a moderate power but quite compact pulsed power generator as a driver. This generator may not be giving extremely high voltages as are possible by some big pulsed-power generators but still running vircator in repetitive mode.

If we go through the literature survey of the high power microwave sources then we find that there have been several attempts/efforts made in the past to develop them using compact pulsed power generators. Effectively the complete problem is bifurcated in two directions. The first one being design and development of a compact pulsed power generator by any method/scheme of pulsed power compression/conditioning which, of course, is based on the physics of energy storage (high energy density physics) and associated dielectric breakdown in dielectrics and the second one being exploration of the optimized radiation from the vircator with the electrical powers being fed by these designed and developed compact pulsed power sources. The first part, even though appearing to be too simple to be considered, has been very crucial in the development or evolution phase. This has invited very nice and interesting works to be pursued and resulted in the publications also related to the compact pulsed power source development for HPM applications. Even though the development phase is a kind of vertical or one dimensional study on the topic, but still it could not have been possible without considering some relevant applied physics concepts. The application of pulsed microwave of high powers is not limited to the interference effects in the electronic devices but also for microwave plasma interactions [4].

1.1 Compact Pulsed Power Generators : Literature survey

Recently a high voltage cable based 2Ω pulsed power generator for 25GW in 10Ω $CuSO_4$ load is reported by [53] with an aim of rectangular pulse generation into a high power microwave source. It is noted as advantage in this approach that the other schemes like Marx generators and flux compression generators are having a drawback of not capable of providing a rectangular flat top pulse. The weight of this pulsed power generator is 3ton and its dimensions are 4mx2mx1.2m. A Marx generator type pulsed power generator [141] which is made very compact and weighing 37.5kg is used for driving reflex triode oscillator at a pulse repetition rate of 10Hz. This generator is tested to deliver nearly 200kV voltage pulse into an 18.5Ω impedance load. In another interesting article [47] a pulsed power generator suitable for HPM application is made using capacitor bank driving an exploding foil opening switch and then after the compact pulse transformer uplifting the voltage produced by exploding foil switch opening action. It is also proposed to finally replace the capacitor bank with their previously deigned flux compression generators named FLUXAR configuration. Necessary to mention here is that flux compression generators have served the requirement of the most dense/compact pulsed power generators and have been employed in the field in order to substitute the very huge pulsed power generators which were made in various laboratories for the generation of high power microwaves. Also to add is that the devastating nature of the chemicals used in the power amplification in these generators may not be a choice by many of those who are interested in studying interaction of high power microwaves with the matter like plasma. Moreover the study related to the effect of repeated interactions in matter may also not be possible by these devices. The power levels produced by such devices may always be argued to be very attractive in the case of the bigger and heavier

devices but use of chemicals to make them compact may not be an easy choice for the user. The compact pulsed power generators without chemicals (used for energy sources) may be operated in repetitive mode to have a burst of microwave pulses.

1.2 Overstressing primary energy storage capacitors: Literature survey

As far as the primary energy storage capacity of any pulsed power system is concerned, capacitors mostly play a very important role in their realization. Domingos et al [42] have reported the testing results of different types of capacitors for application at far higher voltages as compared with the maximum voltages they were rated for. The average breakdown voltage is found to be exceeding upto a factor of 8 in some cases which is quite interesting. In another article by Shkuratov et al [43] a voltage overstressing of a factor of more than four was reported for some mica capacitors. The capacitors used to make compact primary energy storage in the case of inductive energy storage reported in this thesis were also overstressed upto a factor of 2.5. In an independent study they are operated with twice overstressing than their rated stress for a repetition rate of 50Hz [44]. The capacitor used have a shape of cylindrical capacitors with axial threaded leads at its two ends. The diameter of these capacitors is 45mm and cylindrical length is 95mm. The capacitors, when opened, are found to be aluminium foil covered plastic film capacitors . The capacitors which are rated for 2kV DC are charged upto 5kV whereas the capacitors which are rated upto 5kV are charged to 10kV. 2kV capacitors charged to 4.2kV have reported a life of more than 1000shots under 50Hz operation and low inductance ringing discharge.

1.3 Coaxial cable used for compact pulsed power: Literature survey

Solid dielectrics are widely used in making of coaxial cables. Most commonly used dielectric in the cables is polyethylene(PE). Compared with oil paper or mass impregnated cable, PE insulated cables are almost maintenance free, have a lower weight and offer smaller thermal resistance for a given voltage and conductor cross section [14]. With the improvements in the PE in the form of HDPE (high density poly ethylene), LDPE (low density poly ethylene) and cross linked polyethylene (XLPE) the cables have gone through various useful changes specially in their high voltage withstand capacities. High voltage transmission using XLPE coaxial cables have made its way upto 500kV and hence the availability of these cables and technological advancement going in the field of cable technology suggest the possibility of using ready made cables for making a pulse forming line in order to eventually build a compact pulsed power source which requires no-maintenance during the operational life of the pulsed power source. The XLPE cables have been used for the development of advanced generators, transformers and pulsed power sources [5, 9, 53, 61]. The breakdown of XLPE has been studied under DC voltage [8] and the impulse breakdown superposed on AC voltage [6] is also reported. Production of partial discharges in low voltage cables has been studied and reported by Steiner [7]. Extensive study on the coaxial XLPE cable is done by Riechert et al [12–14] regarding breakdown occurring under DC pre-stress and also under unipolar and bipolar impulses. These results suggest reduction in impulse breakdown strength of the cable than that at the same DC voltage. It is explained that as homopolar space charge gets developed around the inner conductor under DC high voltage, it reduces the field strength inside the insulator of the cable thereby increasing the dielectric strength of cable. Whereas, under influence of unipolar impulses the

space charge does not get time to be developed and hence no screening of electric field is possible. This leads to the lowering of impulse breakdown strength than to DC breakdown strength in the coaxial cable. As far as the bipolar pulse breakdown is concerned, the homo polar charge developed in first polarity leads to the hetero polar charge cloud development around the current carrying conductor in the second polarity field stress. This finally leads to the enhanced electric field inside the insulator of the cable and therefore further reduces the breakdown strength of the cable. The correlation of space charge buildup and breakdown strength of the cable is studied and reported [15] very interestingly. Other references [10, 11] also have reported a good study on the topic related to the coaxial cable dielectric breakdown strength. As a conclusion XLPE can be used safely under 100kV/mm impulse stresses and also for repetitive operation. The dielectric constant of PE is also reported to be 2.26 in the literature [51]. Reduction in the dielectric strength of the cable under high temperature and also under temperature gradient inside the sample is also reported [14].

1.4 Opening switches for inductive storage: Literature survey

The application of exploding wires and foils are very widespread [16, 17], [48] and include but not limited to the production of nano-particles, high-voltage generation, high-pressure impact studies, pinch-driven fusion events, under-water electrical wire explosion (UWEE). The behaviour of exploding wire/foil opening switch for power conditioning application, for high voltage generation experiments in electrical loads, strongly depends upon its environment for the two reasons; one being the dependence of change of resistivity on the environment and the other is dependence of voltage breakdown strength on its surroundings. The inter-dependence of one effect on the other can

also not be ruled out. In the present context of high voltage generation the important parameters of exploding wires are their breakdown strengths and the rate of rise of the resistivity depending upon the rate of current rise which they are undergoing across. Literature is full of the evidence where the breakdown strength of as high as 60kV/cm in short lengths and 4kV/cm in longer lengths of exploding wires have been achieved in the current loadings where the rate of rise of current ranges from few hundred MA/s to some TA/s. Cho et al [18] have shown the application of exploding copper wire phenomenon towards nano-particle formation. Mao et al [19] reported their work towards single wire explosion for nano-particle generation. This also reveals the generation of nearly 10kV/cm field inside the exploding wire of copper when subjected to superheating under the current rise time of 5GA/s loading. Vlastos [20–23] has reported much about the dwell-time, restrike channel resistance and also tried explaining the mechanism for current restrike. The study conducted by Sinton et al [125–130] is nice demonstration of 1kV/cm dielectric strength in exploding wires used for generating extra long arcs with wire lengths upto 100meters. N.Shimomura et al [133–135] have elegantly reported production of approximately 20kV/cm field across the exploding copper wire loaded with an electrical pulse of 2GA/s. In his experiments a high impedance 20kohm impedance probe was connected as load. Vitkovitsky et al [24] have reported a dielectric strength as high as >20kV/cm in small fuse lengths (upto 3cm) which is again shown to be exceeded upto 40kV/cm in smaller (1cm) fuse lengths by B.M.Novac et al [25]. Taylor [26] has reported 180MA/s current rise time study done on copper wires with relatively slower current rise times. R.Baksht et al [27] has also shown for the similar rise time loadings that the plasma formation occurs before the conductor vaporizes in aluminum foils surrounded by air. Korobenko et al [28] for aluminum and Rakhel et al [29] for tungsten reported the behaviour of wire at current heating rate reaching as high as 50-100GA/sec. The electric field as high as 60kV/cm in tungsten wire is reported

in these experiments even though any external load is not connected in parallel to the opening switch except the voltage probe. In the work related to underwater electrical wire explosion experiments [37–41] the resistance evolution of the exploding wires of copper are very well described for the microsecond (20GA/s), the sub-microsecond (400GA/s) and the nanosecond discharges (1TA/s). However, the experimental setup for these experiments is not connected with a parallel load, except a high impedance probe, connected with opening switch. These experiments are essentially related with the high pressure generation studies by the exploding wires. Reinovsky et al [31] have reported that even for 5TA/second current rise times, 7kV/cm dielectric strength in aluminum foil fuses is achievable for the inductive loads. Recently it has been reported by Stephens et al [34,35] about their preference for the aluminum as exploding metal conductor material and also presented a good study below 1GAmp/sec current loadings on fuses. Elsayed et al [32] have reported 14 silver wires in pressurized gas environment based opening switch which is driven by explosive driven pulsed power source and delivers nearly 400kV voltage pulse on a vircator load of 30ohms impedance. The length of the fuse in the experiment is 56cm which is kept inside special geometry of 28cm length elegantly. Length-wise the dielectric strength is 7kV/cm which is improved in the housing to reach as high as 14kV/cm. The current rise time used for the loading of fuse for these experiments is nearly 20GA/seconds. In a similar current rise time loading experiment reported by Demidev et al [33] a load impedance of 25Ω was driven by 177kV Voltage generated by 13cm long (15kV/cm dielectric strength) copper wires used as fuse elements primed by explosively driven generator device. A very interesting analysis by Reinovsky et al [30] in the context of opening switches reports limit on the ratio of conduction time to the interruption time by a factor of 10 for capacitor discharges and with a factor of 50 for the explosively driven generators. Suggestion of this study is existence of a limit or finite upper value for the ratio of conduction time to

the interruption time in the operation of electro-explosive based fuse opening switches. The action is defined as the time-integral of current density squared passing through the exploding wire cross section. In fact it is well established that the action is a very critical parameter for deciding the burst phase of exploding wire after which the resistance rise overshoots and the wire resistance is mainly decided by its component in the vapor phase. Action to burst is well defined for various metals but a variation of a factor of 2 for current density variation by a factor of 10 is reported [138] and here comes the role of experimental boundary conditions which decide this variation which can be physically explained by the fact that the environment surrounding the exploding wire decides this variation. The work reported Stephens et al [34, 35] and Sinars et al [36] for insulated coating wires used as electro-explosive fuses is important in this context.

1.5 Vircator: Basics

As far as the microwave generation from the vircator is concerned it is based on very simple scheme of forcing a flow of charge carriers i.e. a current far exceeding the space charge limiting current inside a drift tube also known as a waveguide. The interaction of the charge particle beam with the drift tube causes the formation of electron cloud also known as the virtual cathode. Now the following charges of the beam get trapped between real and virtual cathode start oscillating and start radiating at the microwave frequencies decided by distance between real and virtual cathode which is also decided by the anode cathode gap. The virtual cathode also starts radiating at the plasma frequency of its constituents decided by the charge density of virtual cathode. Interestingly as we move towards making the compact pulsed power generator we struggle to attain very high voltages (because of limited breakdown strength of insulators) and hence the voltages produced are moderately high. At these generated voltages the current inside

the vircator should be above the space charge limiting currents. The velvet cathode is found to be a good choice as later it is pointed out that it emits nearly similar current densities as that at high voltage application. Velvet has as low as 20-50kV/cm breakdown strength at the application of 100nS pulses as is mentioned in the literature [51].

Under non relativistic cases the space charge limited electron beam current density (J) between parallel electrodes may be given by equation 1.1 [45]. The assumption is the gap (d) between cathode and anode is smaller than the cathode radius (R). Here V is the voltage applied across the anode and cathode, ϵ_0 is permittivity of the free space and e, m_0 are charge and mass on an electron. v' is the velocity with which anode cathode gap is reduced by the expanding plasmas at the anode and cathode and t is the time elapsed since this reduction in gap has begun.

$$J = \frac{4\sqrt{2}}{9}\epsilon_0\sqrt{\frac{e}{m_0}}\frac{V^{3/2}}{(d-v't)^2} \approx \frac{4\sqrt{2}}{9}\epsilon_0\sqrt{\frac{e}{m_0}}\frac{V^{3/2}}{d^2} \quad (1.1)$$

this leads to defining a diode impedance (Z_{Load}) as given under provided V is in Mega-volts.

$$Z_{Load} = 137\left(\frac{d-v't}{R}\right)^2/\sqrt{V} \approx 137\left(\frac{d}{R}\right)^2/\sqrt{V} \quad (1.2)$$

As far as the propagation of electron beam of radius r_b through a drift tube of radius r_0 is concerned the space charge limiting current (I_{SCL} in Kiloamperes) is given by following equations.

$$I_{SCL}(annular) = \frac{8.5}{\ln(r_0/r_b)}(\gamma_0^{2/3} - 1)^{3/2} \quad (1.3)$$

$$I_{SCL}(solid) = \frac{8.5}{1 + \ln(r_0/r_b)}(\gamma_0^{2/3} - 1)^{3/2} \quad (1.4)$$

Here γ_0 is called relativistic factor for electrons moving with velocity v and is defined as

$$\gamma_0 = \sqrt{\frac{1}{1 - (v/c)^2}} \quad (1.5)$$

c is the speed of light.

When the current of diode exceeds this space charge limiting current a virtual cathode is formed and the oscillations of virtual cathode occur at approximately the relativistic plasma frequency (f_p) which is given by equation 1.6 where n is density of electrons in the charge cloud.

$$f_p = \frac{1}{2\pi} \left(\frac{ne^2}{\epsilon_0 m \gamma_0} \right)^{1/2} \quad (1.6)$$

for the non relativistic case the virtual cathode oscillation frequency (f_{vc}) is given by

$$f_{vc} \propto \frac{V^{1/2}}{d} \quad (1.7)$$

The radiation frequency (f_r) of reflexing electrons (T being period of reflexing) between cathode and virtual cathode is given by

$$f_r = \frac{1}{4T} \quad (1.8)$$

For non relativistic case the above relation simplifies to

$$f_r(\text{GHz}) = 2.5 \frac{\beta}{d} \quad (1.9)$$

Where $\beta = v_b/c$ while v_b is electron velocity and c is speed of light and anode cathode gap d is in centimetres.

1.6 Work Summary

In our experiments it has been successfully established that microwave power conversion efficiency as much as 0.3% can be achieved for the vircator operation even at very low voltages i.e. 50kV. The second interesting thing found was that even at these low

voltages the currents densities as high as reported at higher voltages or limiting cases can be produced using velvet cathode. We have achieved a current density as high as $300A/cm^2$ in our experiments. Moreover as far as repetitive vircators are concerned it is shown that a reflex triode type vircator has been operated at 10Hz operation and has delivered four sequential microwave pulses without any change in the radiated microwave power. In our experiments we operated at 4Hz of operation and found that an almost stable radiation is seen up to 6 consecutive pulses of conventional vircator in terms of frequency content and power of the radiation. To understand the physics at low voltage operation of vircator extensive modelling with the help of various particle in cell codes have been conducted. It is also shown that the modelling results are being reproduced by the experimental results. Since the acceleration potential of the electrons is not very high they are not attaining very high velocities and even in the very low anode cathode space the transit time is consistent to provide the radiation in microwave range. Supposing that the applied voltages are very high and then in order to get the reflex frequency in the GHz range one has to keep anode cathode gap larger otherwise in lower gap spacing the frequency will be quite higher. Working towards studying the challenges towards development of compact pulsed power generators for the high power microwave generation purposes, we have used the transmission line based pulse forming line for driving a vircator like load and seen the dielectric breakdown inside the transmission line under different shaped pulses even though some scitation [53] is there to make a pulsed power generator employing a transmission line based pulsed power generator. This is established evidence that the solid dielectric can be successfully used for the generation of microwaves by vircator and requires no processing of the dielectric which is water and oil in bigger systems.

Figure 1.1 shows the assembly drawing of the vircator driven by coaxial cable based PFL. In order to compactize the primary energy storage scheme charging the pulse form-

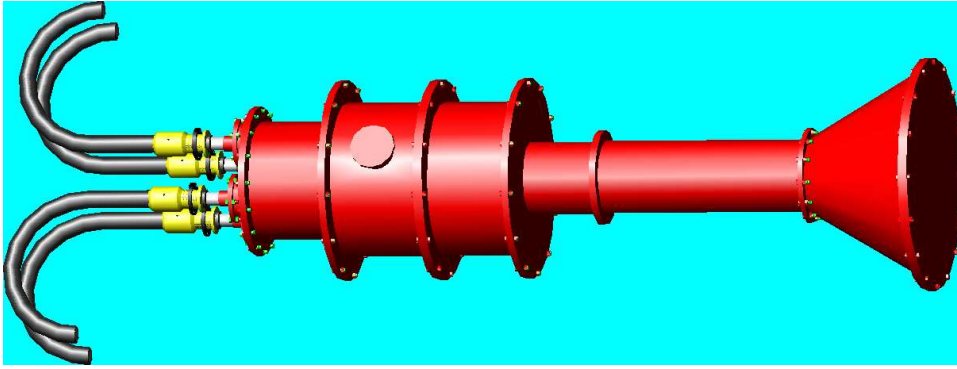


Figure 1.1: Cable PFL driven vircator assembly with antenna

ing line, we have reported a scheme in which the primary capacitor bank is interestingly shaped in form of primary turn of the pulse transformer designed to operate in either a double resonant or non-resonant mode. It is well explained in various literature that the most compact energy storage scheme between any capacitive and chemical method is inductive energy storage method and hence we attempted to even more compactize the pulsed power system for driving the vircator. Interestingly the system is one of the most compact system and is capable of delivering 1.5GW of electrical power in 10.5Ω loads. While comparing with a different type of compact pulsed power generator, it is found that the present system is even more compact with a Marx generator designed [141] to directly drive a reflex triode vircator which can certainly be advantageous for repetitive operation at 10Hz as compared to the system reported in this thesis. In all these experiments we have attempted the axial virtual cathode oscillator configuration which is relatively simple to design and also quite easy to couple with pulse forming line based coaxial output pulsed power generators.

The optimization of the space charge as is mentioned in the title of the thesis reflects the efforts done in order to get sufficient amount of the electron beam current so that, the space charge limited current is exceeded by a considerable amount leading to the formation of the virtual cathode eventually leading to the generation of pulsed microwaves

in repetitive mode. Working with the constraint of driving the vircator by the compact pulsed power driver to generate the microwave radiations, use of velvet cathode and smaller anode cathode distances (3mm) were experimentally done in order to optimize the space charge effects which finally lead to the formation of virtual cathode. Enhanced free space coupling was also aimed and with the designed and developed horn antenna a peak at the line of sight and 30° beam width of the radiation is recorded with the vircator which is driven by a compact pulsed power driver. After having achieved microwave radiations of 1MW power at 4Hz repetition (at 50kV of anode cathode voltage), after putting the efforts mentioned in the thesis, the work opens the way for the next stage of development for enhancing the electrical pulsed power and increasing the microwave emission from the device which is essentially run by a compact pulsed power generator. There is open scope of increasing the pulsed power in the system as is evident by the details reported in following chapters.

2

DIAGNOSTICS

The diagnostics are important part of the experiment as their performance decides the correctness of the results obtained from it and the correctness of the analysis of results done after the acquisition. Different kinds of diagnostics are used for different objectives of the experiments reported in this thesis like current measurement, voltage measurement etc. and are being reported as given under. Needless to say that the every diagnostics used for a particular purpose should have a rise time with which we want to resolve our acquisition or the information. Moreover the used diagnostics should be able to withstand to the maximum values of the variable which is expected to measure and should not distort the performance when it is inserted in the system for its objective of measurement.

2.1 Voltage Measurement

2.1.1 PFL charging voltage measurement

For the measurement of high voltages generated at different stages of experiment the resistive divider method have been used. For this purpose the high bandwidth voltage probes have been designed and implemented in the experiments. In Cable PFL based experiment, the primary capacitor bank charging voltage is always measured with a standard DC probe of $40kV$ peak voltage ratings with a voltage attenuation of 1000:1 connected to a DC voltmeter with a digital display. In the first set of experiments the



Figure 2.1: Resistive Voltage Divider

PFL charging voltage measurement was done using a standard $20MHz$ voltage probe which could measure a peak voltage up to $160kV$ peak. Later it was thought to be replaced with another probe which is made in-house and is reported below as the rise time of the pulse to be measured was not in the nanosecond region. The transformer performance study and the PFL charging voltage of the subsequent sets of experiments (second and third set of experiments detailed in chapter 6) is observed using a resistive voltage divider, developed in-house, which is having stack of disk resistors connected in series to make its upper arm and the lower arm is made using another disk resistor of low value as compared to the upper arm resistance. These disk resistors are seen to have no change of resistance up to $5MHz$ applied voltage signals across them during

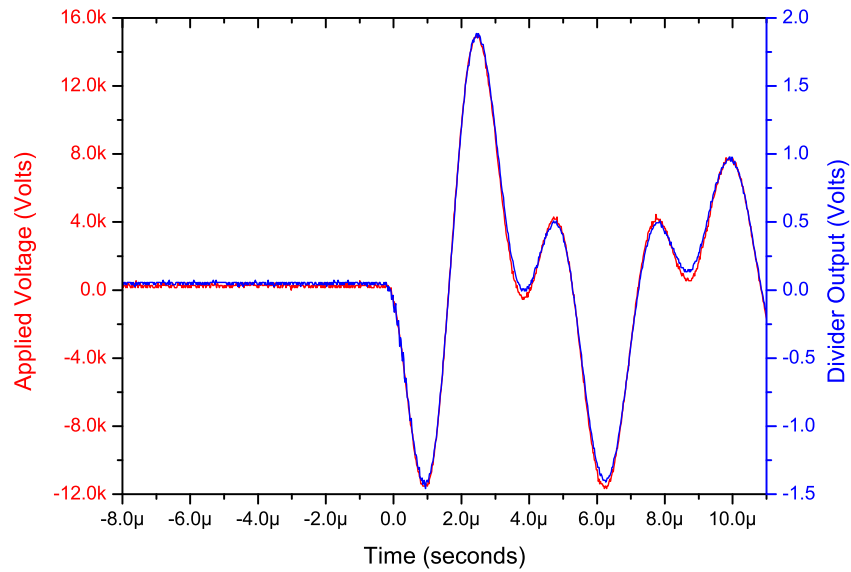


Figure 2.2: Resistive Voltage Divider Performance

their individual testing. It has 5Ω disk resistor in its lower arm whereas the upper arm is made of $40k\Omega$ impedance disk resistor. The attenuation ratio observed by the divider is $8k : 1$. The upper arm which is stressed to the most of applied voltage (lower arm is $8k$ fraction of upper arm) is enclosed in an transformer oil tube made of perspex. This helps in increasing the voltage values to which this divider can be successfully applied for voltage measurement. The length of oil filled upper arm is nearly one meter and hence is expected to successfully measure $450kV$ peak charging voltage applied on the pulse forming line. This divider is shown in figure 2.1. The performance of the voltage divider is shown in figure 2.2. For the calibration purpose Northstar make high voltage probe PVM-5 has been used in the experiment. Since the charging of the PFL is in μs & sub- μs pulses the rise-time requirement for the voltage diagnostics is not very stringent.



Figure 2.3: High BW Resistive Voltage Divider

2.1.2 Diode voltage measurement

For the measurement of the voltage applied between the anode and cathode of the virtual cathode oscillator, we used another high-bandwidth probe developed in house. This is in fact a cascade of two voltage probes. The output of the first high voltage divider is fed to the input of the second voltage divider (commercially available) operating at relatively lower voltage. This high bandwidth high voltage divider was made using a $CuSO_4$ liquid resistor column. The column was made in such a way that the resistivity of the liquid in upper and lower arms are same. This has been done in order to rule out possibilities of change in attenuation ratios caused by change in liquid resistor concentration with time as ratio remains fixed if the both arms have same resistivity all the time. It was made in the same way as is reported in the reference [46]. The resistive divider is shown in figure 2.3 and figure 2.4 shows the response of the first stage resistive divider to a fast voltage pulse applied across it. The rise time shown by the divider is approximately 7ns and hence can be used for the anode cathode gap voltage measurement. The length of total liquid column is 40cm and the lower arm is sampled from 1cm distant electrodes placed inside the liquid resistor column. Attenuation of a factor of 40 is being offered by the resistive voltage divider. To further attenuate the voltage to a level where we can safely send the signal to the oscilloscope, another resistive and high bandwidth voltage divider of 1000 : 1 attenuation, 20kV DC voltage, 40kV peak voltage, 75MHz bandwidth(Tektronics make 6015A) is used with the lower arm of the main high voltage divider already made of liquid resistor column. The importance of first high voltage probe is because of its higher voltage measurement capabilities provided by the 40cm long liquid resistor column. This probe is used in the experimental results of the first set reported in the chapter 6.

Another high bandwidth probe for high voltage measurement was made using commercially available two similar probes each of which has a bandwidth of 75MHz and can

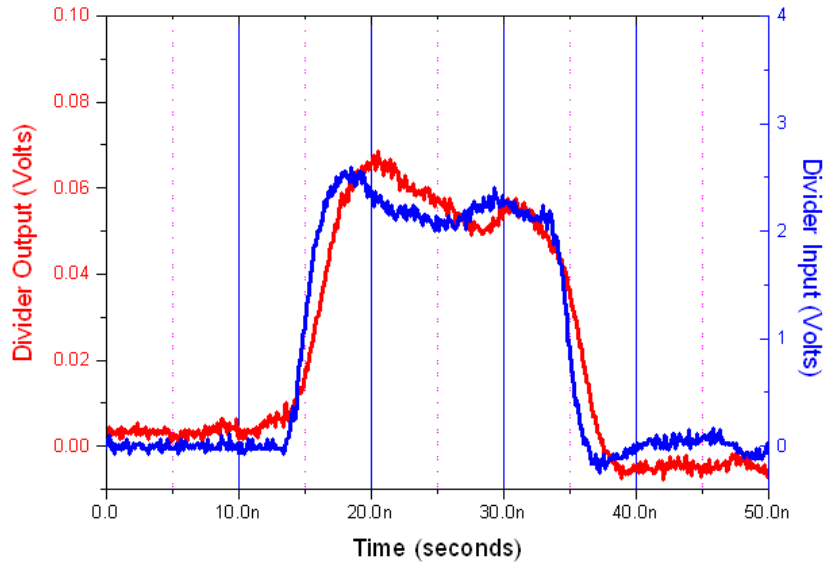


Figure 2.4: High BW Resistive Voltage Divider Performance

measure a peak voltage of $100kV$. For the case of $450kV$ charging of the PFL voltage, expected diode voltage is nearly $225kV$ for exactly matched load conditions. To measure this expected voltage a rugged probe was devised. This was made by connecting the input terminals of these two probes such that high voltage terminal of the two probes were connected. What one gets is a probe with two input terminals, to be connected to the HV side, but having two output ports. In order to protect the oscilloscope from application of very high voltages, one has to essentially ensure, that the output end of the probe which is connected with the ground should be used. This way the attenuation provided by the cascaded probe is twice viz $2000 : 1$ to that of single probe which in the present case is $1000 : 1$. This probe has advantage that it has no liquid resistor and hence there is no issues related to the orientation while fixing the probe with the viricator system. The resistive high voltage probe made by cascading the same two probes is shown in figure 2.5.

As the rise time ($BW.t_{rise} = 0.35$) of each probe is nearly $4ns$. To determine the rise time



Figure 2.5: Cascaded High Voltage Probe

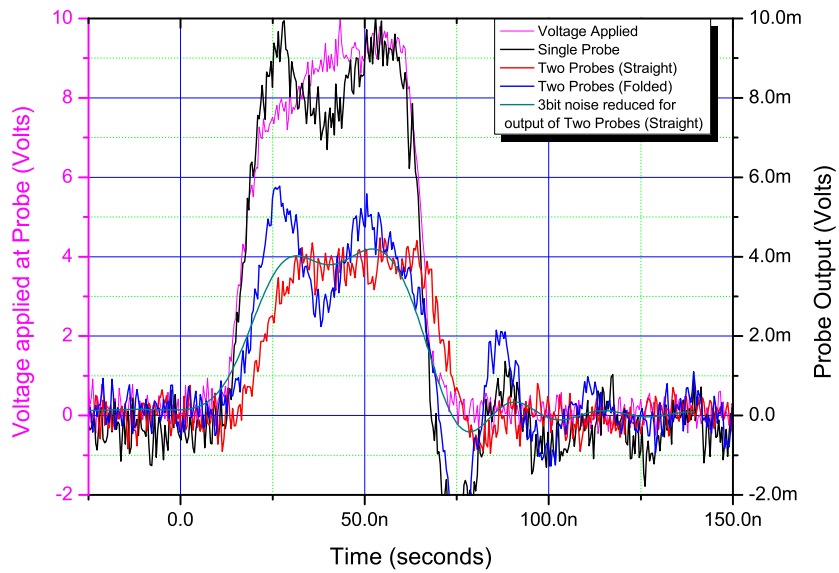


Figure 2.6: Cascaded high voltage probe performance analysis

of the probe combination/cascade, experiments were separately conducted based on examiner's suggestion which was to consult the supplier's technical head, Dr. Richard Adler regarding this arrangement. Subsequently, it is further noted that [50] two probes may be connected in series for measurement of still higher voltages as is done by me. Moreover 40ns rise time pulse is simply expected to be reproduced based on the past experience. The exact bandwidth may be found by using a fast pulse generator like Agilent 3320A and then observing the shape of the measured voltage by the probe made after series combination. We have done such experiment with the signal generator and found out that the bandwidth of probe is sufficient to show a voltage pulse of 44ns with the rise time of 12ns. The results of such testing are shown in figure 2.6. The better method of series connection is also suggested [50] in which the high voltage end of one probe is connected with the ground point of the other probe. It is also suggested [50] to short the unused lower arms of the probes used in making series combination but not connected to the oscilloscope. This is suggested in order to reduce the high voltage generation at these portions of the probe caused by stray capacitances. This is interestingly understood that series connections of many such probes may be done to increase voltage range of probe provided the bandwidth is separately checked with the pulse generator.

2.2 Current Measurement

In the first set of experiments the primary discharge current of the pulse transformer was measured. It was done by designing self integrating Rogowski coil which works on the principle of L-R integration. A calibration curve of the self integrating Rogowski coil is shown in figure 2.7. M/S Pearson make current transformer is used for the calibration purpose of the self integrating current transformer developed in the lab. The subsequent current measurement in the experiments is done by the standard current transformer

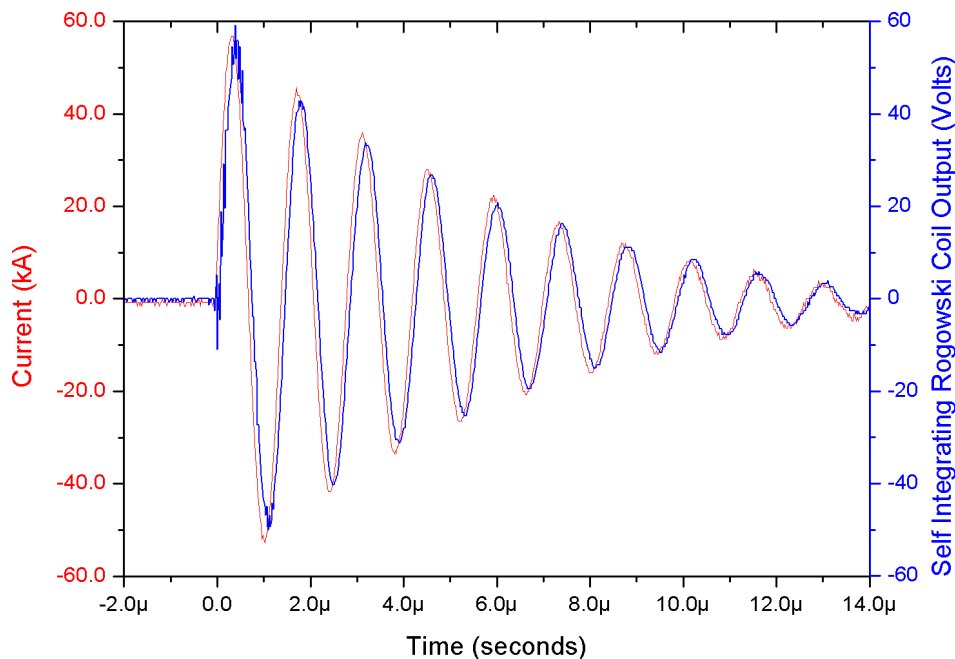


Figure 2.7: Calibration curve of Self Integrating Rogowski coil for primary current measurement (sensitivity is 1V/kA)

available commercially for the beam current measurement in the experiments reported in the thesis. The current transformer used for this purpose are having $2kA$ peak current measurement capability and have a rise time of $5ns$. Hence the return current is divided in 12 similar channels and the current transformer is inserted around one such channel. The current transformer inserted in one channel and two current transformers inserted in two channels give same total current and hence single current transformer in any channel gives the correct measurement of total current.

2.3 Microwave Diagnostics

The frequency of the radiated microwave from the vircator is measured using high bandwidth oscilloscope connected to a receiving antenna with required external attenuation to bring down the level of signal below 5Volts which is safe limit for the oscilloscope. High bandwidth oscilloscope has 50Ω impedance. For the first set of experiments the

bandwidth of oscilloscope used for the frequency measurement was limited to 5GHz whereas for subsequent sets of experiments the bandwidth of the oscilloscope used in the measurement is 10GHz. The connection between receiving antenna is done using very high band width cable of 12GHz bandwidth. In all the measurements the oscilloscope is kept inside the shielded enclosure which has 100dB radiation attenuation up to 10GHz frequency. All the in and out signal cables were inserted through a waveguide port of 20mm inner diameter and 15cm length. The oscilloscope in these experiments was battery powered. To avoid the reflections of microwaves from surroundings the microwave absorbers were used in a proper way allowing attenuation of microwaves (more than 30dB) after being reflected from unavoidable neighbourhood like walls and floor. Ultra-fast microwave detector diodes of very having a rise time of nearly 2ns are used for observing the microwave pulse envelop shape in the first and second set of experiments. They are effective in showing the information regarding the duration of radiated microwave pulse and also about the variation of power in the single pulse with respect to time. As a very simple way to find out whether the radiations are taking place or not in the first set of experiments neon lamps were put in front of radiating waveguide of viricator. The back light illumination of neon lamps from viricator was stopped by using black paper in between them. Tho glow of the neon lamps was observed and recorded using open shutter photography done at the time of viricator operation. Similarly a fluorescent tube was also kept in front of the radiating waveguide and it was seen glowing in the first set of experiments during viricator operation. For the measurement of microwave power we have used quad-ridge receiving antenna which has nearly flat frequency response in a very broad frequency range up to 12GHz. The received power is measured by V^2/R method where R is the input resistance of oscilloscope and V is the voltage measured by the oscilloscope. The external attenuation inserted in the connection between antenna and oscilloscope is taken into account for this calculation. Now in order to calculate the

radiated power from the received power, the free space attenuation equation 2.2 (Friis transmission equation [49]) from transmitting antenna to receiving antenna is considered. If the power received at the receiver antenna is P_r then the transmitted power (P_t) from the transmitter is given by

$$P_t = P_r \frac{4\pi^2 R^2}{\lambda_0^2 G_t G_r} \quad (2.1)$$

Here the G_r and G_t are the gains of receiver and transmitter antenna respectively, R is the distance between transmitter and receiver and λ_0 is the wavelength of radiation under consideration. In dB units same equation can be rewritten as

$$P_t(dBm) = 32 + 20\log_{10}(fR) + P_r(dBm) - G_t(dBm) - G_r(dBm) \quad (2.2)$$

here f is frequency and should be in GHz and R , the distance between transmitter and receiver, should be in meters. It is to be noted that before applying this equation it was confirmed in the experiment that the r^2 attenuation of power is being followed in the measurement zone. For understanding the energy distribution in the radiated power or the mode of radiation radiated signal was scanned in a plane changing its angular position by a angular displacement of 7.5° while going from -45° to 45° from the axis of radiating antenna.

2.4 Electron Beam Impression

In the beginning or in the first set of experiments to find out the electron beam profile, a thermal paper was used which got blackened by the heating done by the electron beam bombardment. It was kept before the anode mesh and hence obstructs the way of the emitted electrons. Later it was seen that an impression of electron beam bombardment is also found in the SS mesh used in the experiment as cathode. It is integrated image of

different sequential shots of the experiment.

2.5 X-ray Diagnostics

In the first set of experiments, in order to see the X-ray generation effects of electron beam bombardment on the anode mesh made of stainless steel, a dental X-ray film was kept in front of output window of waveguide. A stainless steel washer was used as the obstruction in the path before film for X-rays. The image of obstruction on the film is demonstration of electron beam production and propagation. X-ray dosimeters are also used for measurement of integrated doze of number of shots.

2.6 Conclusion

This chapter summarizes the details of the diagnostics used in the experiments reported in this thesis. At the end of this chapter it is understood that many high voltage probes may be cascaded in series, to enhance the voltage range of measurement, and their bandwidth can be determined experimentally at low but faster pulses.

3

SOLID-DIELECTRIC PULSE FORMING LINE

There has been several attempts previously to use commercially available solid dielectric coaxial cables for pulse compression purposes and simple pulse forming line, Blumelein [54], Transmission line transformers (TLT) have been reported to be made out of these cables. Some of them have been used for relatively low voltage applications (References [55–59]) and some of them are meant for high voltage pulse output. It is certainly the most easily available coaxial tubes which can easily be used for such purposes, if the maximum voltage required for the applications can be withstood by these cables without occurrence of breakdown till the desired event is over. Standard RG214 coaxial cable has been used by Rivaletto et al [62]. URM67 cable based pulse forming lines have also been reported by Rossi et al [67, 68], Tuema et al [64] and Turnbull et al [65] in their respective works. RG218 cable being a thicker cable has also been used for making PFL and is reported [63, 66, 69–72, 103]. Another special cable made of cross linked polyethelene (XLPE) is also recently used [53, 61] for making cable based pulsed power generator. It is very interesting to note among all these references that

the first attempt to make a source impedance which is lower than the single coaxial cable impedance i.e. 50Ω aimed to drive a load of $10\text{-}20\ \Omega$ (approximating vircator impedance) is made by R. Shukla et al [103] using RG218 high voltage cable and a pulsed voltage of $100\text{-}120\text{kV}$ was achieved in these conditions. The voltage spike above 120kV (reaching to 180kV for very short duration of few tens of nanoseconds), as is shown in the same article [103], is ignored in the present context because its occurrence in the subsequent analysis of results is not supported by the modelling of the cable based pulse forming line. Electron beam generation by this 12.5Ω cable based pulsed power generator is also reported in the same paper. Subsequently the generation of microwaves from a vircator system driven by this 12.5Ω impedance coaxial cable based PFL is also reported [73, 101] at maximum PFL charging voltages of 180kV . The experimental results are mentioned in detail in chapter 6. Another attempt to reduce the generator impedance below $50\ \Omega$ was done by Lindblom et al [61] but the generator impedance is reported to be 25Ω only whereas the cable impedance is also the same (load impedance is equal to the constituent cable impedance). Advantage in this scheme over use of single coaxial cable was the enhancement of operating voltage ratings of PFL upto 170kV . Recent article [53] demonstrated the performance of an ultra powerful 25GW generator of very low impedance i.e. 2Ω for a $10\Omega\ \text{CuS O}_4$ load aimed for similar application. It is also mentioned in the same reference that the ultra powerful generator has 2.5tons of weight without water and 3tons of weight with water. Recently we have reported a 15Ω generator [52] made by 4 number of 60Ω cables of 500kV pulsed-voltage ratings (procured from M/S Scandiflash AB) and demonstrated the microwave radiations measured to be 1MW of power for 4Hz repetitive operations in the radiation frequency lying between $4\text{-}8\text{GHz}$. The results of this setup in detail are also mentioned in chapter 6.

3.1 RG218 Cable PFL for first and second set of vircator experiments

The length of the compressed electrical pulse fed to the vircator is decided by the length of the cable and is equated to twice of the electrical transit time of the cable. The equations 3.1, 3.2, 3.3, 3.4, 3.6 make the relevant set of equations of a coaxial PFL or transmission line and are used for the characterisation purposes of the PFL. This coaxial pulse forming line has r_1 as inner radius and r_2 the outer radius, ϵ_r is the relative permittivity of the medium of the pulsed forming line and μ, μ_r are permeability and relative permeability of the medium. The capacitance per unit length C of the pulsed forming line is

$$C = 2\pi\epsilon_0\epsilon_r/\ln(r_2/r_1) \quad (3.1)$$

The inductance per unit length L is

$$L = (\mu/2\pi)\ln(r_2/r_1) \quad (3.2)$$

The impedance Z_0 of coaxial pulse forming line is given by the square root of inductance to capacitance ratio and is as give under.

$$Z_0 = 60(\mu_r/\epsilon_r)^{1/2}\ln(r_2/r_1) \quad (3.3)$$

The pulse width τ of the output pulse from the pulse forming line of length l is

$$\tau = 2l\sqrt{LC} \quad (3.4)$$

The electric field (E) at any point at radius r between the inner and outer coaxial cylinders is given by the equation 3.5. Here V is voltage applied at the inner electrode.

$$E = \frac{V}{r \ln\left(\frac{r_2}{r_1}\right)} \quad (3.5)$$

The magnitude of this electric field is maximum (E_{max}) at the surface of inner cylinder and is given by

$$E_{max} = \frac{V}{r_1 \ln\left(\frac{r_2}{r_1}\right)} \quad (3.6)$$

Additionally if a load of Z_{Load} impedance is connected after spark gap with the PFL of Z_s impedance which is charged to a voltage V_s at the outset, the power transferred (P_{Load}) to the load is given by

$$P_{Load} = \frac{V_{Load}^2}{Z_{Load}} = \frac{V_s^2 Z_{Load}}{(Z_s + Z_{Load})^2} \quad (3.7)$$

The RG218 cable based pulse forming line is shown in figure 3.1. The first set of



Figure 3.1: Pulse forming line made of RG218 cable

experiment is conducted using 8meters length of the cables and hence the pulse width generated is expected to be $88ns$ whereas in the second set of experiment the length of the cables are increased to $12meter$. This leads to a pulse width of approximately

132ns. The Pulse forming line in the first set of experiments is being charged by a mono-polar voltage pulse, generated from quite a bulkier pulsed power system which has a big capacitor with mounted spark gap on it (weighing 100kgs) and a separate pulse transformer. Even though the system is double resonant and the primary spark gap could not be triggered below 14kV of the charging of the capacitor bank, It was chosen to discharge the pulse forming line in the first pulse only. And it is seen that at 22kV primary voltage charging the PFL was charged to 120kV of voltage in nearly 1.2 μ s. The charging power supply for the primary capacitor bank used in the first set of experiments is explained in the reference [60].

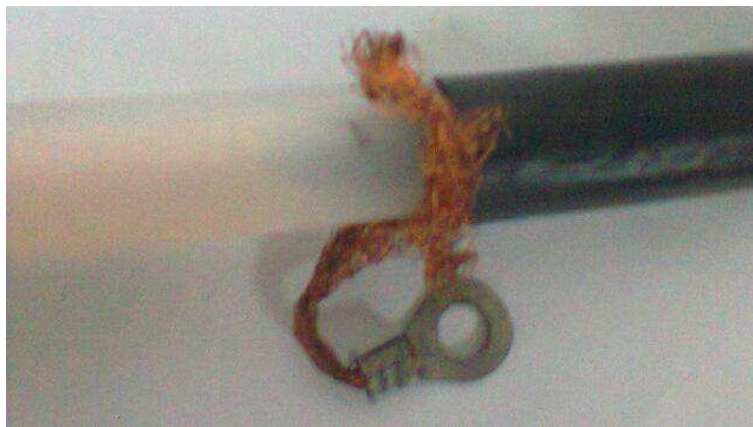


Figure 3.2: Punctured RG218 cable (blackened spot is the place where cable is punctured)

It was considered in the successive improvements towards compact pulsed power system design that the fast charging of the pulse forming line may lead to higher voltage over-stressing of the transmission line successfully because the charge is retained for lesser time and hence the successive arrangements were made for faster charging of the pulse forming line. A compact pulsed power seed system by using special technique was made in which the pulse transformer and the primary capacitor bank are integrated in very small configuration. This transformer *cum* primary capacitor-bank assembly (weighing <10kgs) is double resonant with the pulsed forming line capacitance which

is connected in the secondary of it in the second set of experiments. The power supply for this setup is very simple as compared with the power supply of the first set of experiments. In order to maintain continuity for the explanation of the improvement it is being mentioned that a peak double resonant pulse charging of the same PFL was made possible for a peak voltage of 200kV but with a very limited life which could not exceed couple of shots. In this case the peak voltage appears after $2\mu\text{s}$ from the beginning of primary capacitor discharge. Moreover since the operation of Tesla transformer was made double resonant to increase the energy efficiency of the complete assembled system, the charging pulse appearing across the PFL was bipolar in nature and is expected to stress the PFL even more as compared with the monopolar pulse charging.

Breakdown in RG218 cable PFL

It was seen that even single shot of 200kV was deteriorating the insulation characteristic of pulse forming line and the life of the pulse forming line was drastically reduced to couple of shots only. It was concluded that even though the PFL was charged with the faster pulse, the bipolar pulse was reducing its life as the breakdown occurred inside the cable rather at the ends which has sharp edges as is shown in figure 3.2 by dark spot at the end of cable. This suggested of the bulk breakdown in the material of the transmission line dielectric. Once the bulk breakdown occurred, all the cables were disconnected from each other and were separately charges using the same charging assembly at very low charging voltage so that the secondary voltage does not exceed 40kV voltage. The cable which was damaged showed a different discharge waveform as is shown in figure 3.3 clearly showing that it is deteriorated by breakdown whereas others respond in a quite similar fashion with the applied voltage. The deteriorated cable was selected to be replaced for the next assembly and next shot. The connector of the RG218 cable is shown in figure 3.4 which directly connects with the spark gap chamber feeding the vircator. This connector helps in reducing the field enhancement

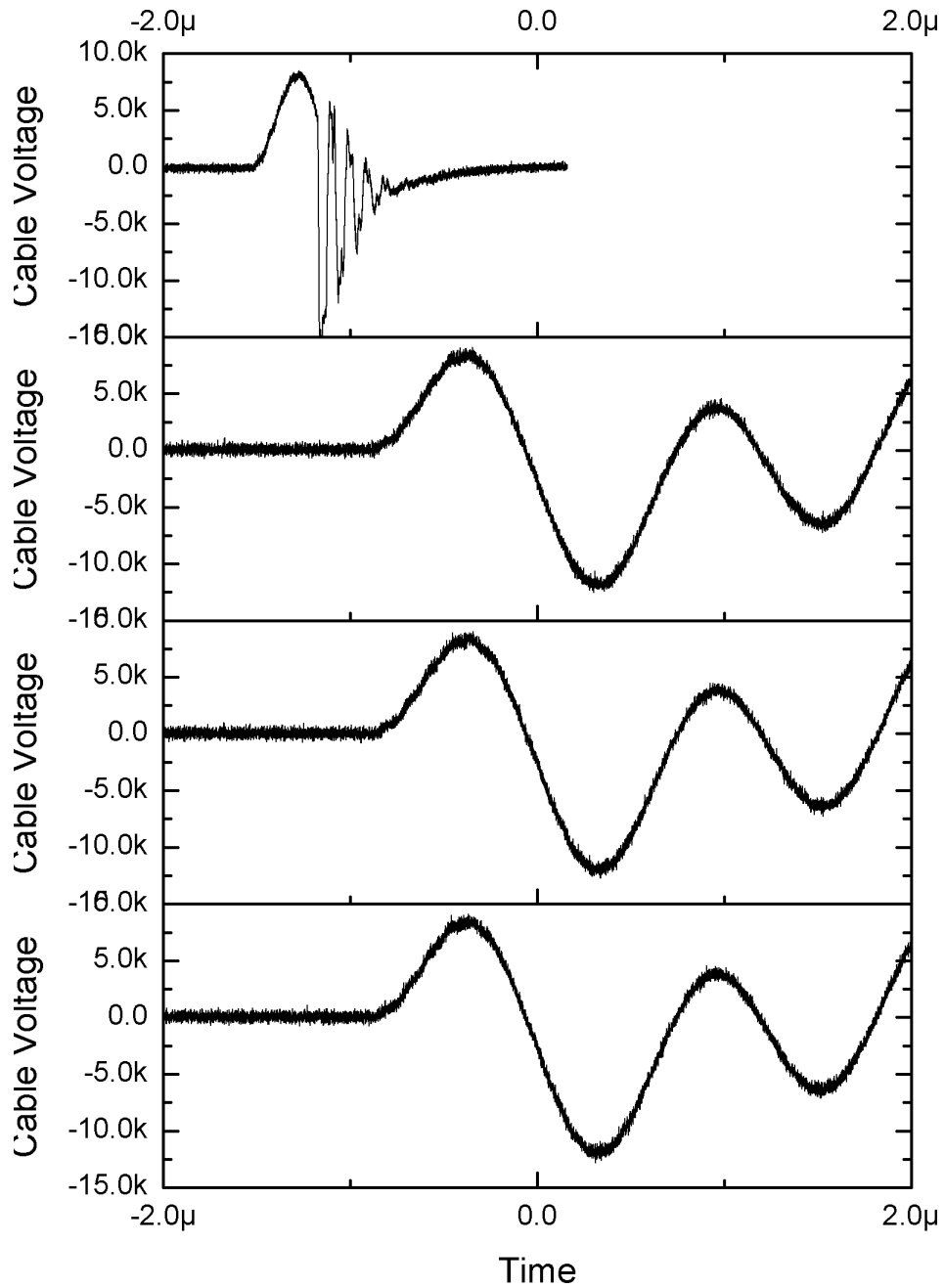


Figure 3.3: Charging voltage waveform of cables constituting a damaged PFL

effects of sharp edges of the braid wires of the coaxial cable at the ends of cable. The sharp wires are smoothly terminated at this connector and hence the field enhancement caused by sharpness/pointedness of the ends of braid wires is mitigated. With all these efforts of protecting the ends (both; charging as well as discharging) of the cable, it was found that the bulk breakdown of the cable initiated inside the coaxial cable itself (not only at ends) in the attempts to charge the PFL beyond 180-200kV of voltages. It was considered to be maximum withstand voltage for RG218 cable. At 200kV charging the maximum electric power that can be transferred to a matched load by this RG218 PFL is 800MW. The option to replace the RG218 cable based PFL in subsequent experiments with another cable which could have withstood even higher voltages was exercised and is reported in the next section of this chapter.

3.2 450KV cable PFL for third set of vircator experiments

Since the charging of the RG218 cable beyond 200kV was nearly impossible with the efforts reported in previous section, thicker-cable based pulse forming line (peak charging voltage of 450kV) was used for the final set of experiments reported in the chapter 6. Figure 3.5 represents the end of vircator which is being fed by 450kV rating high voltage cable based PFL. Subsequently, in these third set of experiments, the monopolar but very fast charging of the Pulse Forming Line was aimed and finally the designed PFL is charged within $1\mu s$ from the beginning of the primary capacitor bank discharge of the compact pulsed transformer. In this set of experiments, the energy efficiency of the integrated system was reduced to 56% (from 80% of the second set of experiments) but the coupling of the pulsed transformer was enhanced to 0.8. Since the primary energy was stored in very compact configuration, wasting 44% of energy was not a serious



Figure 3.4: RG218 cable with connector for fitting

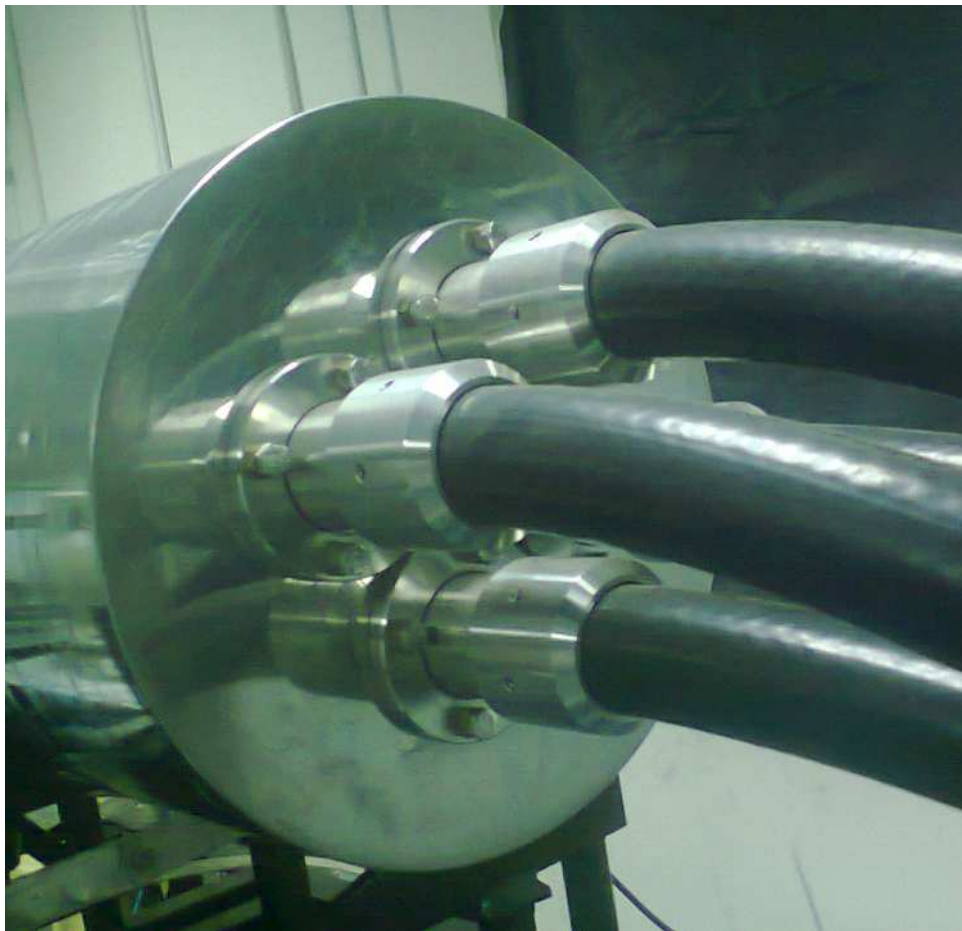


Figure 3.5: PFL made of 450kV (Impulse) XLPE cable

consideration in attaining goal of compactness of the driver. Interestingly at the peak charging voltage, the PFL designed can deliver nearly 3.375GW of electrical power to the matched load of 15Ω . The PFL is presently being charged and discharged to peak voltage of 225kV which amounts to a peak power delivery capability of 825MW again to a matched load. The PFL for the third set of experiments reported in chapter 6 has



Figure 3.6: High voltage XLPE cable with connector for fitting

a cable length of five meters each and approximately a total of 1meter length is peeled off from both the ends. This PFL has four number of such XLPE cables. This leaves four meters of PFL length and a pulse width of 40-50ns is expected to be produced by this pulse forming line. The connector of the high voltage XLPE cable is shown in fig-

ure 3.6 which directly connects with the spark gap chamber feeding the vircator. The charging end was in air and the discharging end of the PFL is enclosed in pressurised air housing at 2.5 atmospheric pressure. This cable is different from the RG218 cable as for field smoothening purpose, a thin layer of semicon material is covered over the insulator. The braid/outer conductor of this cable is placed over semicon coating. Since the bulk breakdown of the cable is expected to be occurring at much higher voltages like 450kV, the charging end of the cable is expected to be more prone to the surface breakdown of the insulator surface if placed in air. Hence a long length is to be peeled-off for charging the cable to 450kV voltage successfully in air. The other promising method would be use two twice length cables in place of four cables and connecting their four ends together at the one end of spark gap feeding vircator. In this case, the charging point on PFL can separately be fed at the same end of spark gap managing the desired insulation strength easily and eventually solving surface breakdown problem.

3.3 Modelling of PFL with vircator for power calculation

Applying the maximum power transfer theorem from PFL to a fixed impedance to define the peak power delivery capability the equation 3.7 has been solved and the results are shown in figure 3.6. The peak powers estimated are for different load impedances connected to the two types of PFLs are shown in this figure. This figure shows the power delivery capabilities for different values of load impedances which are fixed in time for the present consideration. It turns from these calculations that the peak power delivery capability for matched load conditions are 650MW and 3.3GW respectively for the RG218 cable (12.5Ω) and XLPE cable based PFLs (15Ω). These values are for peak charging of PFLs to 180kV and 450kV respectively. Here it is noteworthy, that

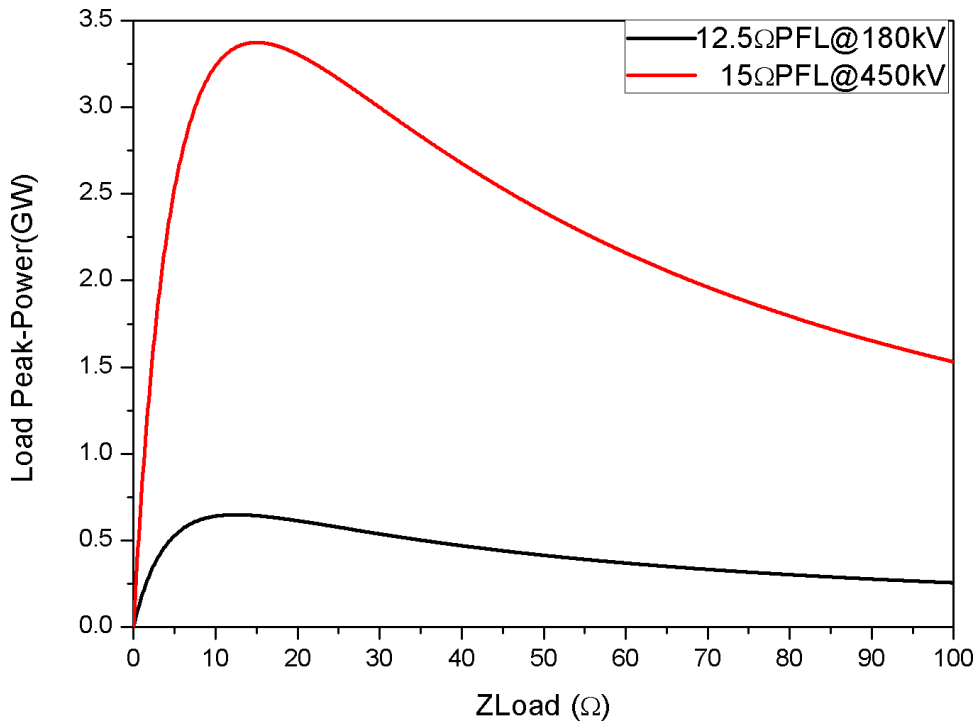


Figure 3.7: Estimated peak load power for the two PFLs

the reported vircator experiments in the chapter 6 are for a variable impedance device whereas the present figure depicts fixed load impedance performance. The second set of experiments reported in the chapter 6 are conducted at 180kV of the RG218 PFL voltage and this figure suggests that a peak power not more than 650MW could have been delivered by the PFL in these experiments irrespective of the profile of the evolution of dynamic impedance of the vircator. At the same time it is quite evident from these modelling results of the 450KV cable PFL that the peak power of exceeding 3GW can be ensured in a load having an impedance in the range of 10-30Ω using this pulse forming line.

The time varying impedances are considered in following analysis. The modelling of the vircator load, having a voltage dependent impedance as is suggested by R. B. Miller [45] for the case of non relativistic planar diode and mentioned in equations 1.1 and 1.2, with the cable based PFL is done for the both the cases of RG218 cable and high voltage

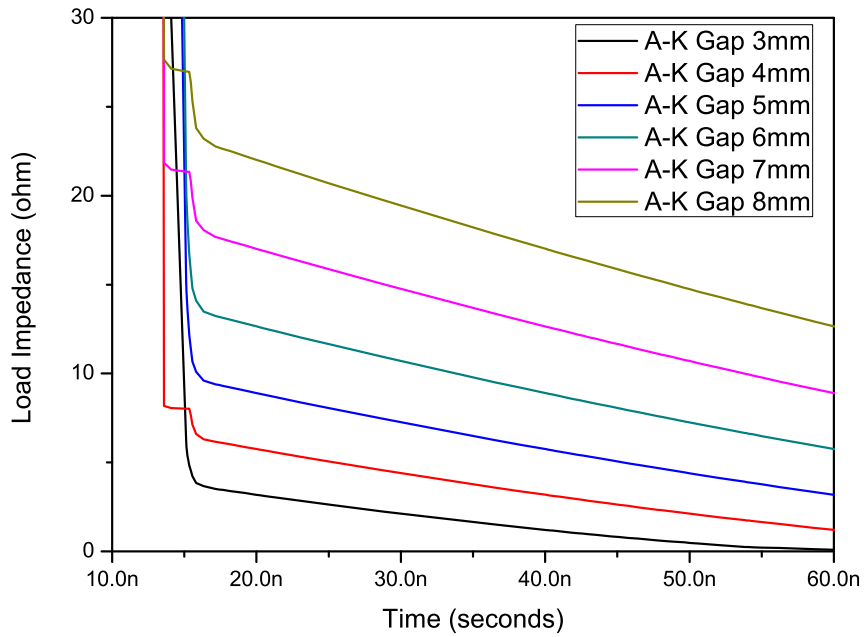


Figure 3.8: Simulated vircator(different A-K gaps, 60mm cathode diameter) impedance for 12.5 Ω 180kV PFL

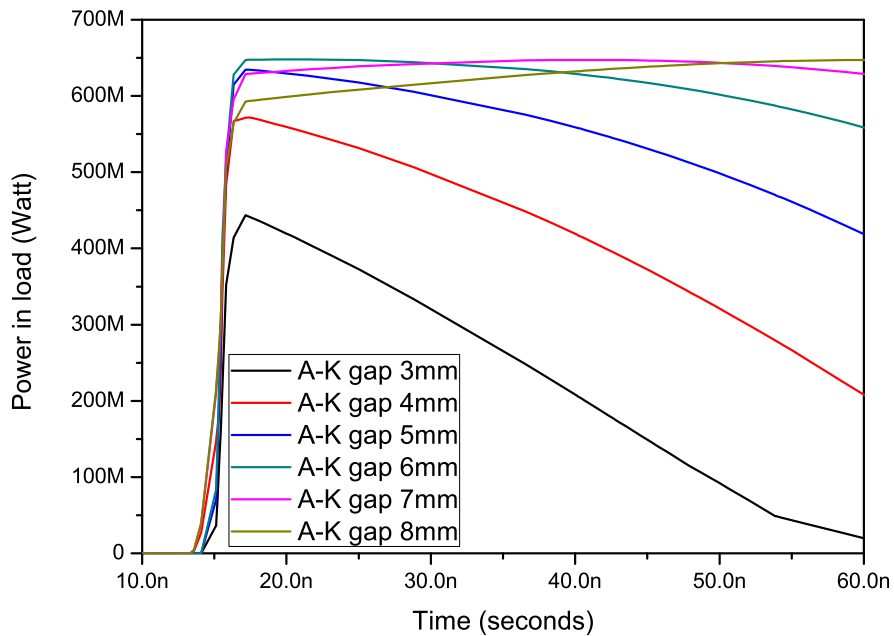


Figure 3.9: Simulated vircator (different A-K gaps,60mm cathode diameter) power for 12.5 Ω 180kV PFL

XLPE cable. The pulsed width assumed in the modelling is 50ns and discharge of PFL starts from 10ns time in both the cases. The effects of plasma expansion from anode and cathode is also included by using a closure velocity of $5\text{cm}/\mu\text{s}$ which is assumed to be $2.5\text{cm}/\mu\text{s}$ from either side. The charging voltage kept in these modelling are 180kV and 450kV respectively. This has been done in order to estimate the coupled performance of the PFL with vircator which are mentioned in the chapter 6 as second and third set of experiments. The resulting time varying impedances for the diode with 60mm cathode diameter and varying anode cathode gap spacings (from 3mm to 8mm in steps of 1mm) are presented in figures 3.8. As far as impedance collapse is concerned it can be seen that 4mm anode cathode gap starts with 8Ω impedance and settles very fast to nearly 1Ω impedance in 60ns with 5km/s closure velocity. The corresponding load powers delivered are being shown in figure 3.10. This also represents the peak power delivery capability of the PFL developed because PFL could not be used for a charging voltage beyond 180kV with the vircator. the power starts at 550MW and then gets reduced to 225MW as per the modelling results during the time in which the impedance collapses to nearly 1Ω . It needs to be noted here that as the diode impedance reduces, as per the modelling results the voltage applied across anode cathode gap also reduces accordingly whereas the current does not increase proportionately. Even the diode closure velocity is dependent upon the physical properties like vacuum inside the chamber, cathode and anode material, current densities etc. Still rather simplified modelling results mentioned here give good insight about the experimental setup used in the second set of experiments reported in the chapter 6.

In order to electrically model the experimental setup reported in the third section of chapter 6 the similar modelling results as mentioned above are being reported. In this modelling the PFL impedance is 15Ω and the charging voltage is 450kV which is peak charging capability of the PFL being used in the experiments. This gives the under-

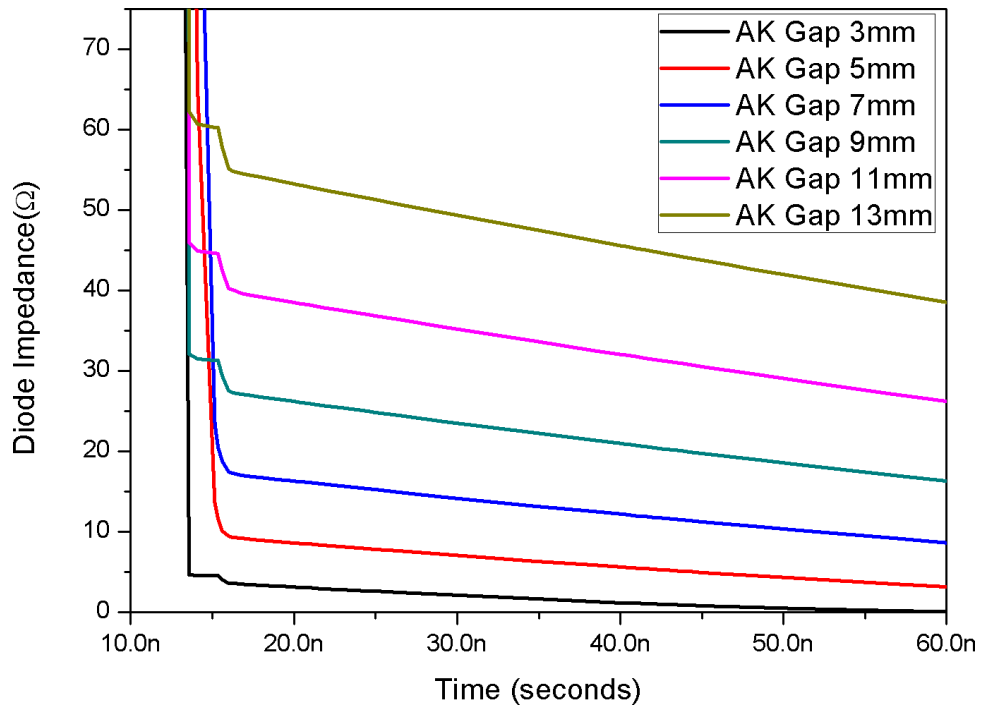


Figure 3.10: Simulated vircator(different A-K gaps,50mm cathode diameter) impedance for 15 Ω 450kV PFL

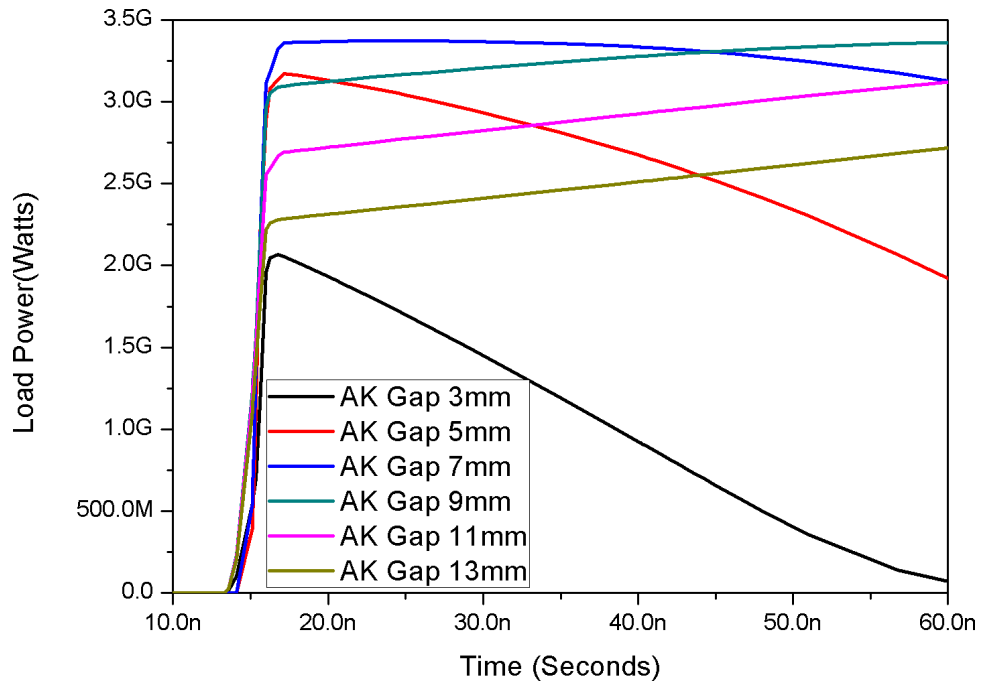


Figure 3.11: Simulated vircator(different A-K gaps,50mm cathode diameter) power for 15 Ω 450kV PFL

standing of the peak performance which is aimed with this setup and forms the basis of future works. The resulting time varying impedances for the diode with 50mm cathode radius and varying anode cathode gap spacings (from 3mm to 13mm in steps of 2mm) are presented in figures 3.9. The load powers delivered by these pulsed power generators made of coaxial cables are shown in figures 3.11. It is quite interesting to note here that this pulse power generator is capable of delivery nearly stable powers above 2GW to diodes which start with impedance value of 30Ω i.e. the diodes which have initial anode cathode spacings of 9mm and a cathode diameter of 50mm.

3.4 Conclusion

A completely dry type PFL is aimed to be used in the experiment to achieve a compact pulsed power generator driving vircator. In the first two sets of experiments reported in the chapter 6, RG218 cable based pulsed forming lines have been made and used. In the third and final set of experiments, the PFL is made using a 450kV rating high

Table 3.1: Coaxial Cable Details

	RG218	Ref. [52]	Lindblom et.al. [53]	Lindblom et.al. [61]
$r_2(mm)$	12	30	25.5	16
$r_1(mm)$	6	5	11.5	9
$Z_0(\Omega)$	50	60	30	25
$E_{max}normalized$	2.6	1	1.18	2.1
<i>Dielectric</i>	PE	XLPE	XLPE	XLPE

voltage cable. The details of the cables used in these experiments are listed in table no 3.1 and their geometries have been compared with other cables used in making other pulsed power systems [53, 61]. As far as experiments reported in this document are concerned we have used transmission lines based pulsed forming lines (coaxial cable in parallel) to achieve the desired impedance of the pulse forming line. In all the three sets

of experiments reported in the chapter 6, we have used four number of cables in parallel and hence achieved a generator impedance of 12.5Ω and 15Ω respectively. Standard cables of RG218 having impedance of 50Ω for the first two set of experiments and other cable (tested for 450kV with sufficient shot life) 60Ω impedance for the last and also the third set of experiments have been used. The electrical model results give good insight about the experimental results reported in the chapter 6.

4

COMPACT PULSE-TRANSFORMER

Some of the radiation sources, which require pulsed accelerators as their driver, operate with low energies (working with nearly 200Joules), whereas the power requirement for their operation is very high (in Gigawatts). These pulsed accelerators have unique characteristic of having very high power delivery capability. The main components of such accelerators are energy storage components and voltage amplifiers operating in the order of 100s of kVs to few mega volts. These voltage amplifiers may be either any Marx generator or any Tesla/Pulse/Linear transformer. The major factor deciding the size of such voltage amplifiers is either energy required by the radiation source or the voltage levels of operation of the radiation source. Eventually the high voltage applied in the radiation source is provided by a capacitor which may be oil or water capacitor or erected capacitor of Marx generator in any of above mentioned two cases of voltage amplifiers. Application point of view of such radiation sources forces everyone involved to think about compact energy storage schemes and compact voltage amplifiers.

The pulse transformer is the device used to uplift the voltage in the secondary of it when the input voltage is provided to the primary side of it. Since the transformer is passive device and the objective is to pulse charge the pulse forming line and thereby over

stressing PFL to its DC ratings. This is done in order to protect the PFL dielectric from continuously applied high voltage. That is why a pulse transformer is required which can handle the high pulsed power being supplied from the primary storage. In order to avoid any saturation possibilities by these very high power inside the transformer air core transformer is chosen for the purpose which certainly has the disadvantages of slightly poor coupling as compared to the magnetic core transformers. The weight of the air core transformer is also low so has scope of making a compact and light weight pulse transformer. The experiment started from the bigger pulsed power system and at the end of work reported in this thesis, it reached to a very efficient pulse conditioning device suitable for driving a vircator. In order to increase the power handling and transfer capability it is preferred that the discharge circuit from the primary side is very fast. To achieve this the primary is made primarily as single turn in the form of sheet which reduces the primary inductance. The secondary of the pulse transformer can be made either spiral or helical in shape. In the present work it has been chosen to make secondary in the shape of helical winding which has been effectively made very compact. Equation 4.1 and equation 4.2 are the typical governing equations for the discharge pattern of a primary capacitor C_p charged to V_0 voltage initially and L_p and L_s being the primary and secondary side inductance of the pulse transformer. The mutual inductance between primary and secondary of the transformer are defined by M where the equation 4.3 relates the mutual inductance with the coupling coefficient (k) of the transformer. C_s is the capacitance of the capacitor connected to the secondary of the pulse transformer which is the PFL in the present case of study.

$$L_p(di_p/dt) + (1/C_p) \int (i_p dt) - M(di_s/dt) = V_0 \quad (4.1)$$

$$L_s(di_s/dt) + (1/C_s) \int (i_s dt) - M(di_p/dt) = 0 \quad (4.2)$$

$$M = k \sqrt{L_p L_s} \quad (4.3)$$

The condition for the 100% energy transfer from the primary capacitor bank to the secondary capacitor bank is explained by the point of time when the secondary capacitor is charged at its maximum and the voltage at the primary side capacitor as well the currents in the primary and secondary side of the transformer are zero. The possible solutions for realization of this condition can mathematically be found by solving above equations which are formulated under the assumption of negligible resistive losses in either primary or secondary side of the transformer discharge circuit [85]. It is found that 100% energy transfer from primary capacitor to the secondary capacitor will take place only when

1. The resonant frequency ω_p of the primary circuit (with open secondary) is equal to the resonant frequency ω_s of the secondary circuit (with open primary) where the resonant frequencies of primary and the secondary are defined as

$$\omega_p = 1 / \sqrt{L_p C_p} \quad (4.4)$$

$$\omega_s = 1 / \sqrt{L_s C_s} \quad (4.5)$$

2. Coupling coefficient values are in discrete numbers like 0.6, 0.385, 0.27, 0.222, 0.18, 0.153 etc. and the secondary voltage peaks at 2nd, 3rd, 4th, 5th, 6th and 7th half cycle respectively

The equations can be solved on the computer for any value of the coupling coefficient and resonant frequencies. The effects of non zero primary and secondary circuit resistances may also be studied. As we go for lower values of k, the charging time of the secondary capacitor increases. It is desirable to have short charging time of the PFL as the electric breakdown of the PFL is inversely proportional to the third root of the

charging time [108]. in this context if the equations are solved for k values ≥ 0.8 (also called single resonance mode) the secondary voltage peaks at first half cycle itself. This reduces the charging time but also reduces the energy efficiency. In another interesting publication [83] an off-resonant Tesla-transformer was designed with $k = 0.525$ and the frequency ratio $\omega_p/\omega_s=0.69$ with an understanding that the primary current is not reversed before secondary current peaks. Two types of the secondary windings are generally used in the pulse transformers [109].

1. Helical Winding

2. Radial or Spiral Winding

In the case of helical winding, secondary winding is on an insulator former and is done with a conductor of a cable with its insulation and outer shield removed. Primary winding covers the secondary winding completely. Primary or secondary winding can be made tapered to attain higher values of coupling coefficient. The system has advantages like (1) simple to be made and (2) being suitable for 1-5MV systems as air or liquid insulation can be used. Helical winding has disadvantages like (1) poor coupling coefficient (2) requires high turns ratio for given voltage and hence the inductance and the charging time increases (3) low inter-turn capacitance hence the windings are not capacitively graded leading to requirement of extra protection of HV side from the breakdown. In the case of spiral or radial winding, the winding is done in radial direction with thin sheet of conductor and solid-sheet insulator (like any of poly-propylene, mylar, poly-ester etc.) taken together. The advantages are (1) the system is compact (2) high coefficient of coupling (3) The secondary winding is capacitively graded whereas the disadvantages are corona initiated breakdown in the solid insulator which is in the form of sheets. Considering above mentioned advantages and disadvantages, helical winding has been selected. It is also noteworthy that the compact pulse transformers

made for the second and the third set of experiments do not require any insulator environment (other than air) for their placement and hence the complexities related with the handling of transformer oil are not involved.

EFFI Code [2] calculates Electromagnetic Forces, Fields and Inductances due to an arbitrary distribution of current carrying circular loops, circular arcs and straight lines. As is described in Ref [2] The code uses algorithm which is based upon combination of direct as well as numerical integration using Biot-Savart law. As the singularities are associated for the computation near conductor in the filamentary approximation method (negligible conductor cross sectional area), the errors are large. But in the case of EFFI code calculations this error difficulty is solved by deriving the expressions from Biot-Savart law 4.6 for a volume current distribution.

$$\vec{B}(\vec{r}_2) = \mu_0/4\pi \int_l \int_S J \frac{d\vec{l}(\vec{r}_2 - \vec{r}_1)}{|\vec{r}_2 - \vec{r}_1|^3} dS \quad (4.6)$$

Here J is current density in conductor, $d\vec{l}$ is a vector differential line element parallel to the current flow dS is cross sectional element orthogonal to $d\vec{l}$. \vec{r}_2 is the position vector of the field point and \vec{r}_1 is the position vector of the source point. All the integral of equation 4.6 are solved analytically for the case of straight conductor segment. For the same volume distribution of current the vector potential 4.7 is defined as

$$\vec{A}(\vec{r}_2) = \mu_0/4\pi \int_l \int_S \frac{J d\vec{l}}{|\vec{r}_2 - \vec{r}_1|} dS \quad (4.7)$$

where the symbols have the same meaning. The electric field due to varying magnetic field is obtained from equation 4.7 using Maxwell relation (equation 4.8)

$$\vec{E} = -\partial\vec{A}/\partial t \quad (4.8)$$

It is quite easier to calculate the inductance of the coil using equation 4.7. The flux linkage and hence the inductance is found by integrating vector potential over the conductor region. For the case of arbitrary conductor shape the general coil is approximated by assembly of circular arc and straight conductor segments of uniform current density and constant rectangular cross section which is reasonable for most coils. By this approximation, It becomes possible to represent the integrals in terms of finite products and sums of elementary functions.

4.1 PT for the first set of vircator experiments

Pulse transformer design and testing with the PFL

The first pulse transformer, made for conducting the first set of vircator experiments is being reported. It is having a single primary turn and is a Tesla transformer in its basic configuration. The primary turn is made of a 2mm thick copper sheet rolled over a cylindrical tube which is made of Perspex insulator. The mean diameter of the primary turn is 25cms and the length of the primary turn is 30cm. The primary capacitor (the capacitor connected on the primary side of the transformer) of $7.1\mu\text{F}$ and 44kV peak charging voltage ratings with a mounted spark gap, discharges its energy in the primary turn of the Tesla transformer through low inductance double braid cables connecting the two. Figure 4.1 shows the arrangement of the capacitor and pulse transformer which are kept vertically. The secondary winding of the pulse transformer is immersed in the transformer oil. The connecting wires from the secondary winding come out from the top of the transformer enclosure for further connections with the RG218 cable based PFL as is shown in the figure 4.1. The connections between primary capacitor and the transformer primary turn are such that, at the time of discharge of the capacitor bank a θ -direction current flows in the primary turn of the transformer. The secondary of the



Figure 4.1: Primary capacitor and pulse transformer for experiments of first set

transformer is made using RG213 coaxial cable, of which outer jacket and shield is removed and only the inner conductor with its polyethylene insulation is used for winding the coil. The secondary winding is having 63 turns rolled on the diameter of 17.5cms. The pitch of the secondary winding is 10mm and hence the length of secondary coil is nearly 64cm. The primary is coaxial to the secondary and the centres of both of them coincide. Nearly 17cm length of the secondary winding is extended out of the primary turn from both the sides. The effective diameter of the secondary coil is 18.5cms. The secondary winding was placed in the transformer oil to protect it from the possibility of high voltage breakdown occurring into it. The transformer was designed to operate in the double resonant mode and hence a condition of double resonance was tried to be met which states $C_p.L_p = C_s.L_s$ and also the coupling coefficient should be 0.6 as discussed earlier. The primary inductance is 200nH and the secondary inductance is 256 μ H which match closely with the modelling results done on EFFI computer code for self and mutual inductance calculations. For these geometries the computed mutual

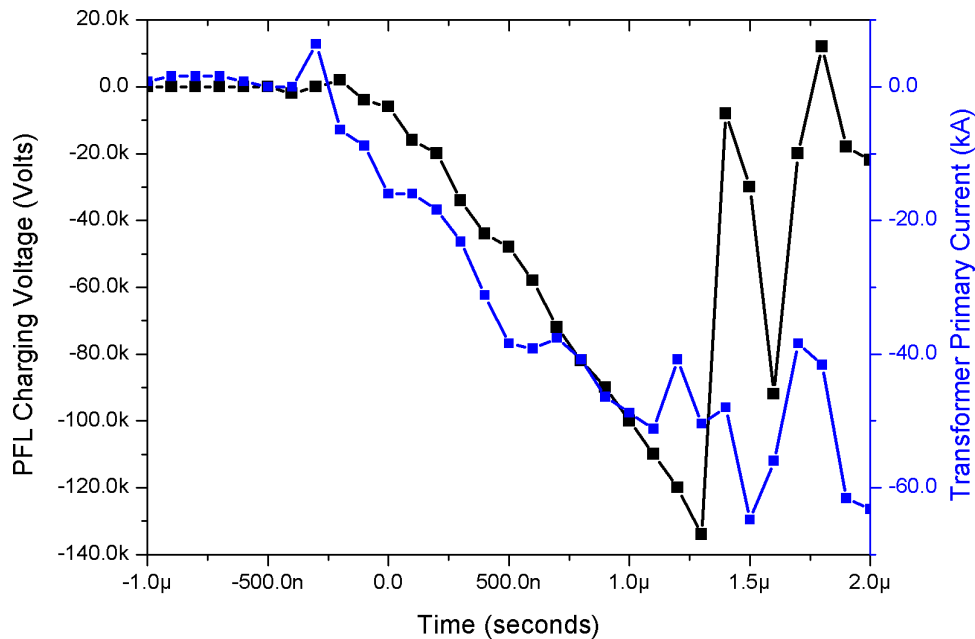


Figure 4.2: PFL voltage and the primary current waveform

inductance between primary and secondary of the transformer is $3.9\mu\text{H}$. This infers that the coupling coefficient of the transformer is nearly 0.545 which is quite close to the aimed 0.6 value of the coupling coefficient. The transformer was designed to be operated in double resonant mode with $7.1\mu\text{F}$ primary capacitance and 6.5nF PFL capacitance. The typical waveforms of the transformer with the PFL made of RG218 cable of 6.5nF is shown in figure 4.2. The double-resonant condition simulated waveform with 6.5nF capacitor are shown for reference in figure 4.3. In this modelling the primary capacitor is charged to 12kV only. In these first set of experiments the cable based PFL was charged to 140kV in $1.5\mu\text{S}$ from the beginning of the primary capacitor discharge. Similar pulsed power system is operated and reported previously for the electron beam generation study [103]. Considering the non-zero inductance of connecting cables and joints between primary capacitor and primary winding, the modelling and experimental results are in close agreement to each other. The pulse forming line was undergoing its tests for high voltage withstand capability and hence faster rise time charging was desired. So it was decided to operate the system without any resonant operation and hence the secondary PFL capacitance was slightly reduced to 3.2nF in subsequent experiments. The vircator results are reported in chapter 6. The power supply for the primary capacitor charging is described in detail elsewhere [60].

4.2 PT for the second set of vircator experiments

As is discussed in the beginning of this chapter, the pulsed voltage transformer is one of the schemes to uplift the voltages such that a pulse forming line can be charged to high voltages. Pulse forming line is a capacitor assembly which can with stand to certain high voltages for driving the matched loads requiring high electrical pulsed powers. One of the objective of experiments reported in this thesis was to drive a vircator by a compact

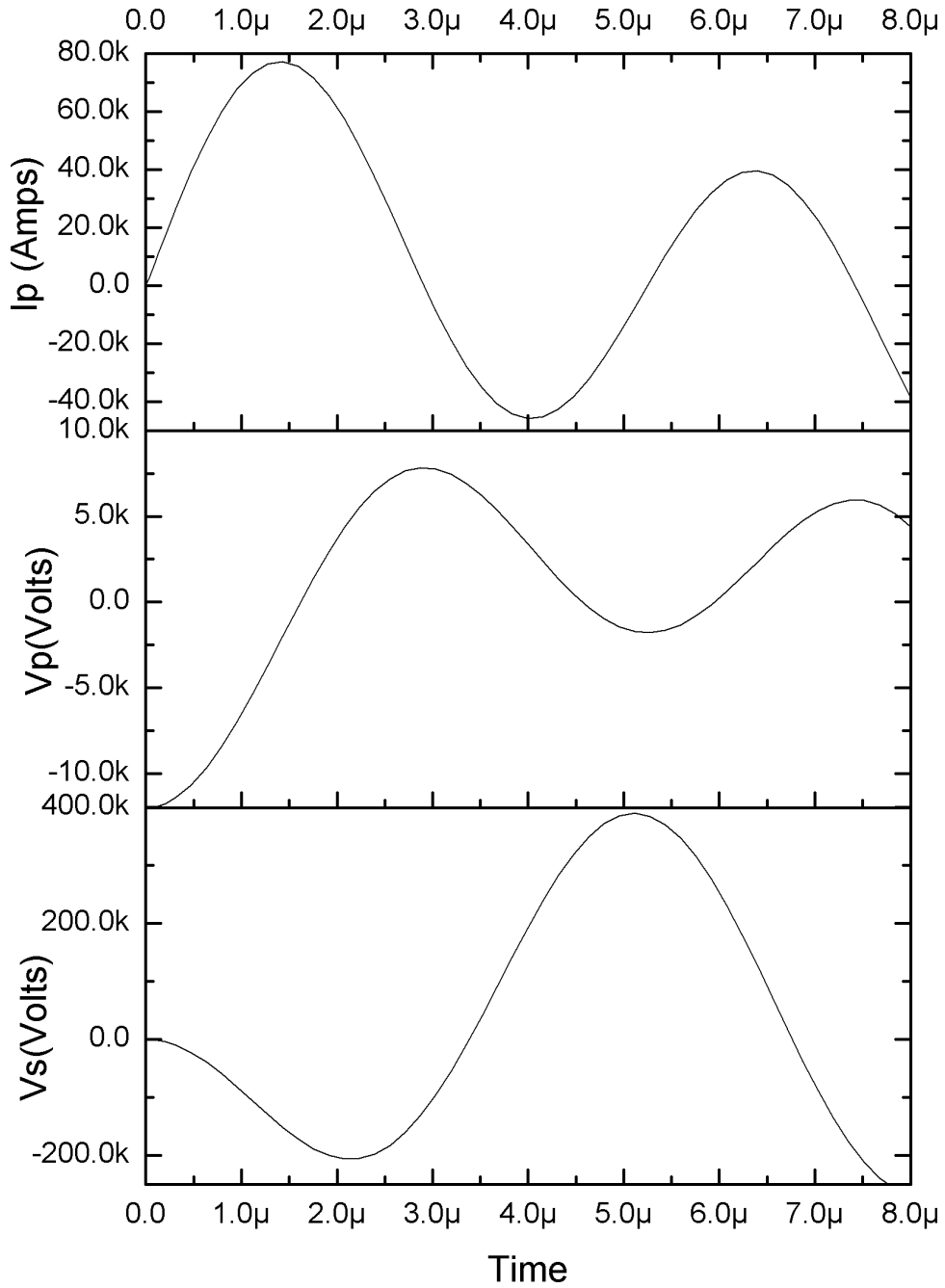


Figure 4.3: Simulated PFL Voltage for 12kV charging of primary capacitor

pulsed power supply.

It is very difficult to design or make compact fast pulsed transformer using magnetic cores, as one has to struggle with core saturation for attaining compactness in high voltage transformer. Cores pose saturation limits depending upon its size. As the size is reduced the cores get saturated with relatively lesser magnetic flux (also energies) and hence are difficult to use. The other reason for not using the magnetic cores is that their presence makes the system slow by increasing the primary and secondary inductance higher by a factor of permeability and hence the system components around the transformer including the insulators or dielectrics used in the transformer are overstressed by high voltage applied for longer durations and hence transformer becomes more prone to the voltage breakdown. Last, but not the least, reason of not using the cores is of course the cost of the cores.

All the above mentioned advantages far over weigh the only serious disadvantage associated with air core that is the poor coupling between the primary and the secondary of the transformer. To overcome this disadvantage people [75–90] have already reported use of Tesla transformer for high voltage generation purpose. The other direction in which people are working to make compact pulse transformer is by using self-magnetic insulation technique [91]. As mentioned above, if the energy required is low and systems are operating very fast i.e. in one or two microseconds then the dielectric strength of all the components is quite different to that of it which would have been in the case when such systems are operated in few tens of microseconds. In moving the direction of compact and fast pulse transformer we are presenting a pulse transformer which has its primary capacitor bank shaped in form of primary single turn winding. This reduces the flux losses in external circuit caused by the connections of capacitor bank to the primary of the transformer and increases the compactness drastically as is shown in following text.

Compact Pulse Transformer

In this section the experimental and modelling results of a compact pulse transformer are being presented. It is primed by a capacitor bank which has been fabricated in such a way that the capacitor bank and its switch takes the shape of the primary of the transformer. This has been done in order to avoid the flux losses in external inductive circuit formed in making the connections between capacitor bank and primary of the transformer however the gap between the primary turn and secondary turn limits the maximum possible flux coupling in between the primary and the secondary. This primary of transformer-*cum*-capacitor bank assembly is made rectangular in the shape rather being circular as is the case of most of the transformers to accommodate four axial capacitors in series. The primary is single turn primary to reduce the inductance so that capacitor bank delivers its energy to the high power level. The primary of the transformer is made of cylindrical capacitors with axial leads at its two ends. A parallel combination of five capacitors is used to make one of the four arms of rectangular shaped primary. The total capacitance of primary capacitor bank is $2.46\mu\text{F}$ and can be charged up to a maximum voltage of 18kV successfully.

The transformer is made with air core in order to avoid saturation effects of magnetic cores. The secondary of the transformer is made in the shape of helix, having multiple turns, wound on the rectangular cross section former to enhance flux coupling. The secondary is placed inside the primary which has rectangular cross-section bigger than secondary coil. The insulation between the primary and secondary is provided by the multiple layers rolling of mylar sheet. A high voltage capacitor assembly is connected with the secondary of transformer so that the performance of the transformer with its primary capacitor bank may be tested. During the initial testing of the transformer with 5nF load capacitor, connected at the output of transformer, the voltages achieved at secondary capacitor were 160kV in second peak which appears in less than $2\mu\text{s}$. As the

primary capacitor bank can be charged to a maximum of $18kV$ in which has expected voltage delivery of nearly $360kV$ in similar capacitive load is expected. A final voltage of $200kV$ with increased probability of a breakdown in the PFL is successfully achieved in this configuration of capacitor bank *cum* pulse transformer.

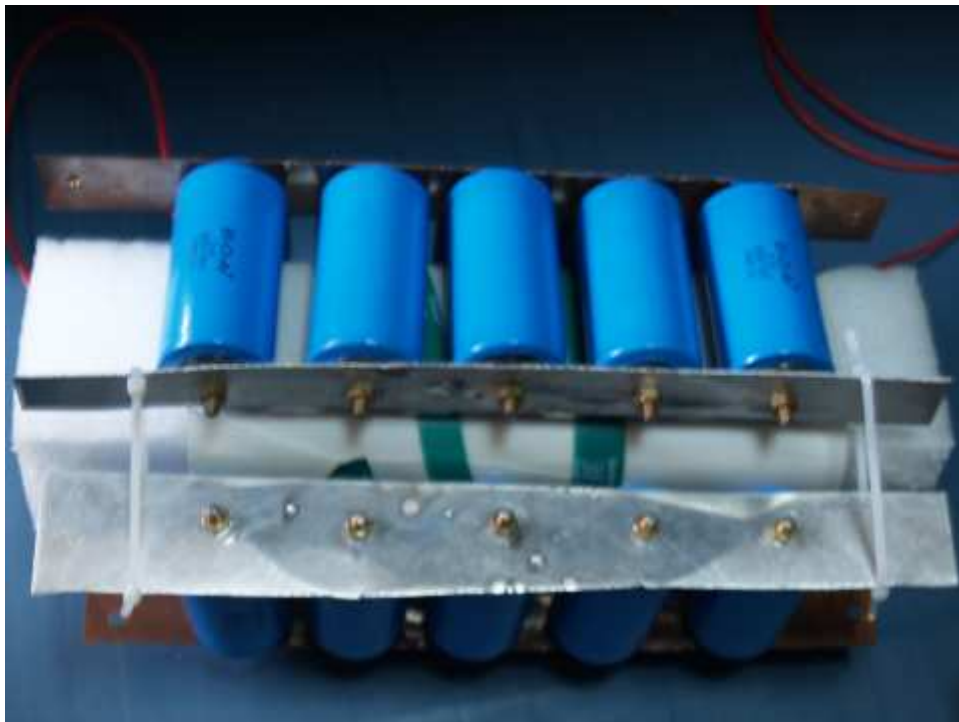


Figure 4.4: Compact pulse transformer using capacitor bank as its primary

Details of experimental setup

In figure 4.4 we have shown the compact pulsed transformer that includes its primary capacitor bank as its single-turn primary. Capacitor bank is made by 20 capacitors which are each of $2.1\mu F$ and can be charged to $4.5kV$ maximum even though they are rated for $2kV$ voltage [102]. These capacitors have a tested current delivery capacity of $15kA$ each at $4.5kV$ charging voltage. The capacitors are arranged in such a way that the complete assembly takes the shape of one turn of primary of the pulse transformer which is rectangular in shape and contains four sides. Each side contains five capacitors in par-

allel. This way the capacitor bank can be charged up to 18kV maximum. The width of the transformer is nearly 35 cms, whereas the distance between the ends of the capacitor leads of each arm is 22cm. The capacitance of primary shaped capacitor bank is $2.46\mu\text{F}$. Effectively the primary has a rectangular cross section of 15cm x 15cm. The secondary is wound on a rectangular cross section former of dimensions 9cm x 9cm and has a total of 30 turns distributed in the width of 22cms. Measured values of primary inductance L_p and secondary inductance L_s are 80nH and $41\mu\text{F}$ respectively. The mutual inductance (M) between primary and secondary windings is measured to be 905nH which suggests that a coupling coefficient (k) achieved in this geometry is 0.5. Interestingly the ratio ($\frac{L_p \cdot C_p}{L_s \cdot C_s}$) of product of primary capacitance and primary inductance to the product of secondary capacitance and secondary inductance is 0.94 which is very close to an aimed value 1.0. It reveals that under experimental limitations, the tesla machine is made to a good extent using this novel pulse transformer. Few layers of Mylar sheet are wound on secondary of transformer before putting it inside the primary to provide insulation between primary and the secondary. The transformer is low-weight because any heavy magnetic core is not used. Instead it is an air-core transformer.

The secondary capacitor used for the testing of this pulsed transformer is made using four pieces of RG218 cables each of nearly 12 meters. The total capacitance of the secondary capacitor is 5.1nF as is described in chapter 3. The power supply used to charge the primary capacitor bank is made using a high voltage transformer giving 12kV output voltage with input voltage rating of 230V. The output of high voltage transformer is connected to a high voltage diode rectifier chain made of 1kV, 1A diodes connected in series. A total of thirty diodes are connected in series in order to make this rectifier chain. The high voltage transformer output is directly connected to the primary capacitor bank using this rectifier chain without using any current controlling external resistor. This helps in fast charging of the primary capacitor bank eventually opening

avenues for repetitive operation of the complete system. To control the output voltage (also charging voltage of the primary capacitor bank) of the high voltage transformer we have connected a variac to control the input voltage in the high voltage transformer. By controlling the input voltage by variac we can control the charging voltage of the capacitor bank. The transformer is lightweight and the weight of the transformer along with its primary which also contains the capacitor bank is less than 10kg. The switching of the primary capacitor bank is done using a spark gap switch connected in between two ends of the primary capacitor bank shaped in form of rectangular single turn loop. For the measurement of secondary capacitor voltage or pulsed forming line voltage a high bandwidth (25MHz) high voltage probe having attenuation ratio of 10000 : 1 is used.

Results with the compact pulse transformer

In the figure 4.5 we have presented the experimental results obtained from the pulse transformer reported in this paper. The secondary voltage of 160kV at pulse forming line of 5.1nF is achieved by the charging of primary capacitor bank at 8kV only and then discharging it through the switch at the primary side of the transformer. The capacitor bank can be safely charged upto a maximum voltage 18kV which will theoretically lead to 360kV of secondary voltage. Moreover the charging of PFL is done very fast which is within $2\mu\text{s}$ from the beginning of discharge in the primary capacitor bank. As far as energy efficiency of the system is concerned it is higher than 80% in the present configuration considering the second peak of secondary voltage waveform. This means that 80% of the primary energy is transferred to the secondary side when the secondary side is at its second peak voltage. One more important thing in the achieved results is that the second peak in secondary (nearly 160kV) is nearly twice of the first peak (80kV) which is in opposite polarity and hence the control on the operation of the PFL switch i.e. PFL output switch is highly improved.

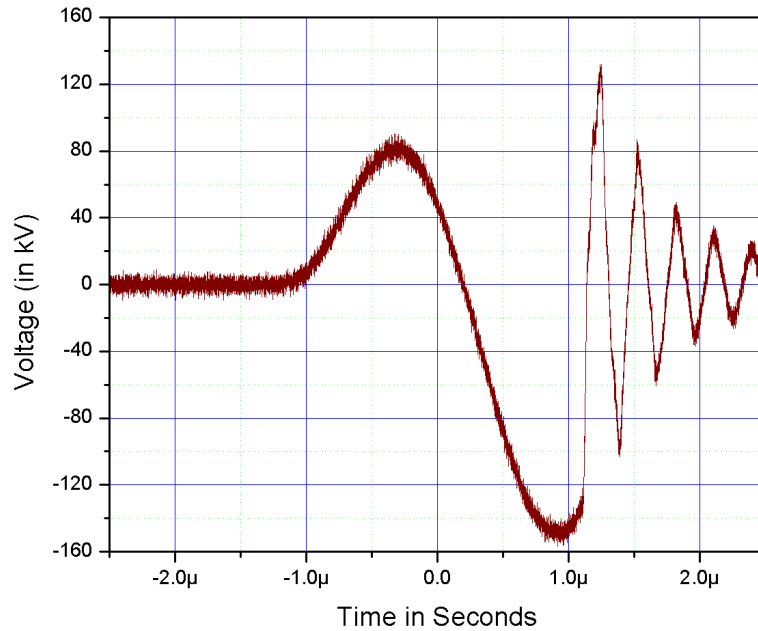


Figure 4.5: Voltage time history of PFL charged by the compact transformer

Initially when the spark gap connecting the PFL with vircator was filled in air, the peak voltages possible were not exceeding 160kV on PFL and consistent breakdowns took place at the output side beyond 160kV. The PFL charging voltages under these circumstances are shown in figure 4.6 collectively. These waveforms represent the breakdown of the output switch at 160kV. Irrespective of the primary charging voltages values, which were varied from 8kV to 12kV in steps of 2kV, the output voltage could not exceed 160kV. To enhance the voltages on PFL and also to test the peak voltage delivery capability of the pulse transformer without any changes for insulation management on the compact pulse transformer, the spark gap connected at the output side of the pulsed forming line was filled with transformer oil and the gap was accordingly reduced to hold a maximum of 200kV which is also shown in figure 4.7 This is one of its demonstration of its charging capabilities to 200kV without any insulation management like filling the secondary winding in oil. It is also possible to put the transformer in oil or pressurised

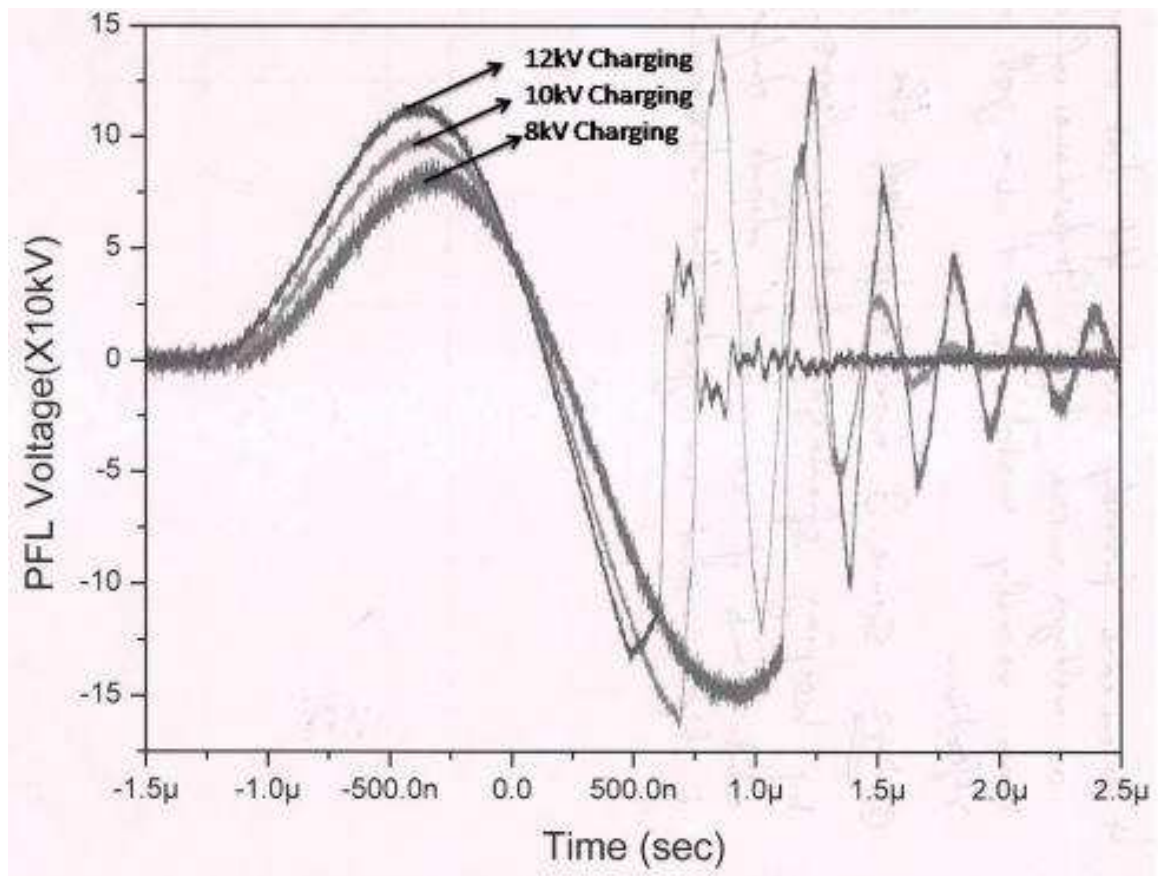


Figure 4.6: Voltage time history of PFL (output spark gap is in air)

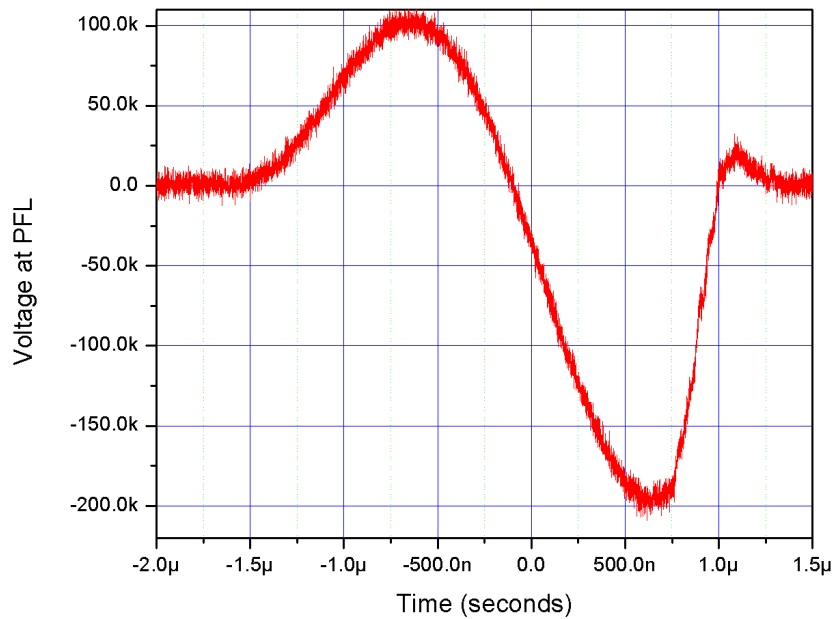


Figure 4.7: Voltage time history of PFL (output spark gap is in oil)

chamber easily, if required, for attaining very high voltages. So far up to 200kV there are no signs of high voltage breakdown in the secondary of this compact pulse transformer.

4.3 PT for the third set of vircator experiments

After learning the method to make compact pulse transformer reported in the previous section, a PFL of 450kV cable was made and to protect the cable from high voltage breakdown it was preferred to charge the PFL using monopolar charging pulse with a new compact pulse transformer with high coupling coefficient. As it is clear from the previous study that the capacitors used for making the primary of the transformer have finite thickness or very specifically the diameter which is 40mm. In order to enhance the coupling between primary and secondary we had to increase the diameter of the primary and secondary so that the unavoidable gap between primary and secondary caused by

the finite thickness of the capacitor does not consume uncoupled flux volume.

After achieving this condition, a high voltage pulse transformer is made with a higher



Figure 4.8: High Voltage Pulse transformer

coupling (80%) in between its primary and its secondary. The transformer is made using the same technique [122] in which the capacitor bank is shaped in form of its single turn primary but to have a higher coupling ratio. Figure 4.8 is showing the figure of high coupling coefficient transformer. The primary capacitor bank has an assembly of

7 axial-capacitors of $2\mu\text{F}$, 5kV each connected in parallel and four such combinations connected in series in order to provide a net capacitance of $3.5\mu\text{H}$ and a peak voltage rating of 20kV. The primary inductance is computed to be 215nH considering sheet equivalent of the primary turn with 320mm diameter. The secondary of transformer is made using Teflon insulated wire wound 40-turns at a pitch of 10mm on a cylindrical former of 280mm diameter made of perspex. The computed secondary inductance is $240\mu\text{H}$ and mutual coupling is as high as 0.8 with a mutual inductance of $5.75\mu\text{H}$. The energy efficiency if computed for the first peak (of secondary) comes out to be nearly 56%. Figure 4.9 is showing the Fasthenry equivalent for high coupling coefficient transformer. The Fasthenry program is available with complete documentation [3] for linux users. The package computes the self as well as mutual inductance of any number of current carrying conductors. The conductors are discretized sized to number of straight elements defined with two nodes. The computation by this code is fast and accurate as is shown by various sample problems. The resistance computation is also done by the code with frequency dependent analysis for each conductor at desired frequency. It is to be noteworthy here that the designed transformer is chosen to have an energy-efficiency less than 100% in order to get monopolar charging of the pulse forming line. The primary capacitor bank of the pulse transformer discharges its energy in the form of single turn loop through a spark gap which is at present operating in self breakdown mode by overvolting of the spark gap beyond its dielectric strength. The spark gap can also be triggered using optical isolation to have repetitive operation at such low energy and low voltage with advanced provisions. As far as the charging of the primary capacitor bank is concerned, it is done by very simple method which involves a high voltage step up transformer delivering 14kV in secondary when the primary is fed at 230Volts. The output is half wave rectified using a diode chain of 25Amperes and 1000V ratings. Some inductive isolation is also provided between primary capacitor bank and the high

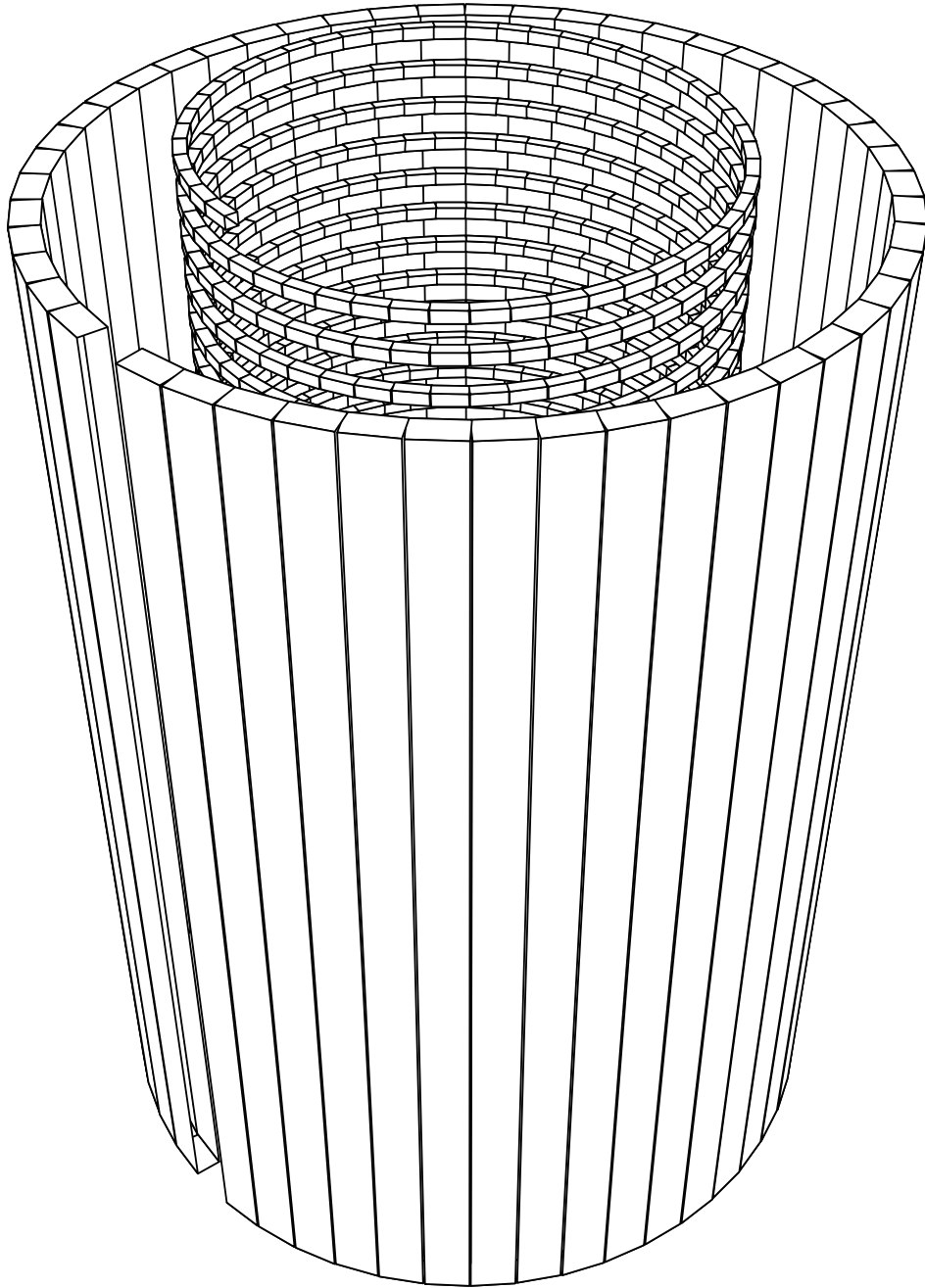


Figure 4.9: Fasthenry input drawing for the transformer (discretized geometry)

voltage step up transformer output terminals in order to isolate the rectifier diode chain during the discharge of the primary capacitor bank. The charging voltage of the primary is controlled by using a variac which limits the input voltage of high voltage step up transformer from 0volts to 230volts eventually leading to the limiting of high-voltage step-up transformer output going to the primary of the capacitor bank. Interestingly the

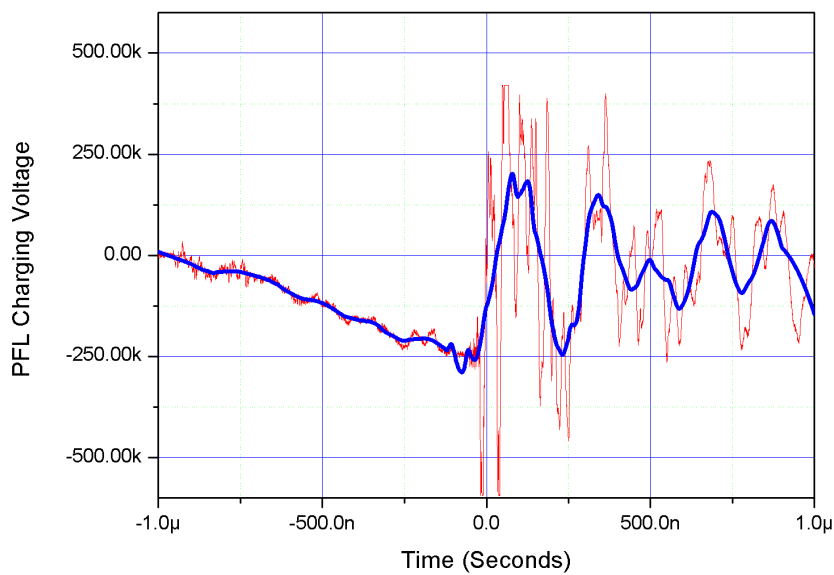


Figure 4.10: PFL charged to 250kV by high voltage pulse transformer Red is acquired signal and blue is numerically filtered waveform

figure 4.10 shows a charging of the high voltage cable based PFL up to 250kV using compact pulsed power supply and compact pulse transformer with high coupling coefficient. The blue waveform in this figure represents the 25MHz filtered waveform of the red waveform which is sampled at very high sampling rate viz 1Gsa/sec. The dimensions of the pulse transformer are mentioned in the table 4.1. The measured weight of the pulse transformer along with the capacitor bank of 700joules maximum energy rating is 19kgms.

4.4 Conclusion

The pulse transformers for the second set and the third set of experiments are compact and novel in their design as they have their primary capacitor bank shaped like primary turn giving enhanced compactness. For the second set of experiments, a compact pulse transformer is designed, developed and tested for the voltage gains of 1:20 in the reported configuration of primary and secondary capacitance. It is characterised for 160kV secondary voltage in operation in air and further work towards insulation enhancement on the PFL's output switch has led to a peak charging of 200kV of PFL or secondary capacitor. The transformer is very compact (6kg in weight) and novel in design by using the capacitor bank assembly in shape of the single turn primary winding.

Table 4.1: Pulse transformer details

Sr. No	Description	PT for first set	PT for second set	PT for third set
1	Primary Capacitance C_p	$7.1\mu\text{F}$	$2.46\mu\text{F}$	$3.5\mu\text{F}$
2	Primary Inductance L_p	200nH	80nH	215nH
3	Secondary Capacitance C_s	6.5nF	5.1nF	2.0nF
4	Secondary Inductance L_s	$256\mu\text{H}$	$41\mu\text{H}$	$240\mu\text{H}$
5	Mutual Inductance M	$2.9\mu\text{H}$	$0.9\mu\text{H}$	$5.75\mu\text{H}$
6	Coupling Co-efficient k	0.545	0.5	0.8
7	Width primary	30cm	22cm	30cm
8	Width secondary	64cm	22cm	40cm
9	Transformer length	100cm	35cm	60cm
10	Mean primary Cross-section	Circular 25cm dia.	Rectangular 15cm x 15cm	Circular 32cm dia.
11	Mean secondary Cross-section	Circular 18.5cm dia.	Rectangular 9cm x 9cm	Circular 28cm dia.
12	Secondary turns	63	30	40
13	Output Voltage	140kV @ $1.5\mu\text{s}$	200kV @ $2\mu\text{s}$	250kV @ $1\mu\text{s}$
14	Capacitor bank voltage	22kV	10kV	8kV
15	Energy efficiency		>80%	56%

5

CONICAL HORN ANTENNA

Antenna is very well explained in the detail in reference [92]. The radiation characteristics of the conical horn antenna are mentioned in detail in reference [97]. another important reference in the field of conical horn antenna describes the electromagnetic fields of conical horn antenna [96]. A nice compilation of results of compact conical horn antenna for reflex-triode for enhancing the radiation in the axis of antenna is presented by Becker [95].

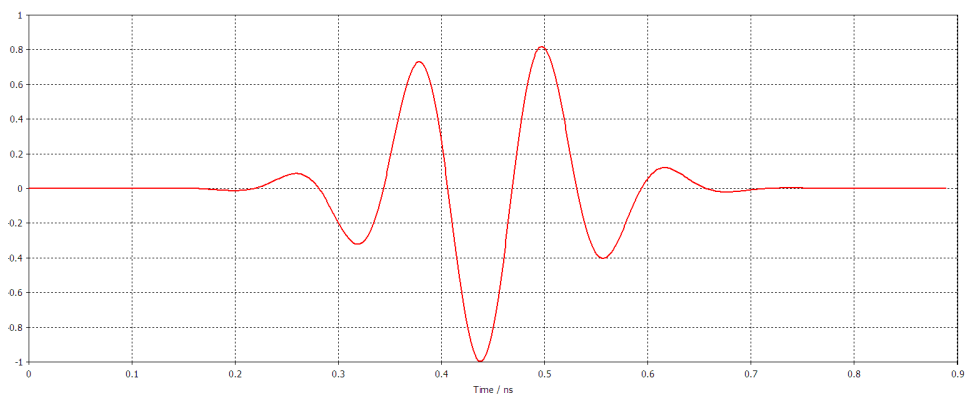


Figure 5.1: Excitation signal given to the input port in the modelling

5.1 Antenna Basics

The modal patterns for circular waveguide are enumerated and plotted in [93, 94]. The salient results as concluded in above references related to the conical horn antenna are as mentioned under. The directivity (D) for a conical horn antenna for wavelength λ with an aperture efficiency ϵ_{ap} , aperture circumference C and aperture radius a is given as

$$D(dB) = 10\log_{10}[\epsilon_{ap}(4\pi/\lambda^2)(\pi a^2)] = 10\log_{10}[C/\lambda]^2 - L(s) \quad (5.1)$$

The first term is directivity of uniform circular aperture and the second term is referred as loss figure ($L(s)$) and is a measure of loss in directivity due to aperture efficiency. The loss figure can be computed by

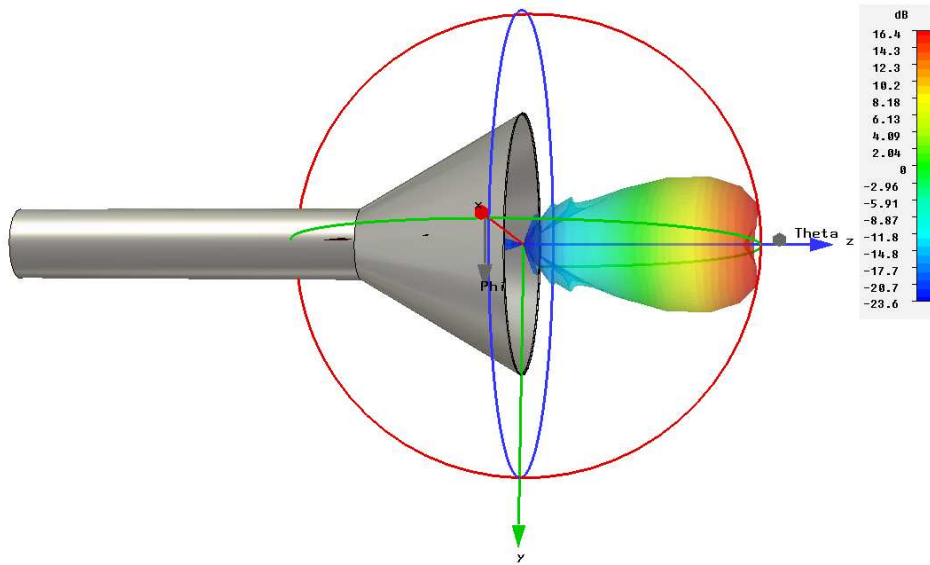


Figure 5.2: Far field radiation pattern at 6GHz for first mode

$$L(s) = 1 - 10\log_{10}[\epsilon_{ap}] \cong 0.8 - 1.71s + 26.25s^2 - 17.79s^3 \quad (5.2)$$

Where s is maximum phase deviation in (number of wavelengths) and it is given by

$$s = [d_m^2/8\lambda l] \quad (5.3)$$

The directivity of conical horn is optimum when the diameter is equal to

$$d_m \cong \sqrt{3l\lambda} \quad (5.4)$$

which corresponds to a maximum aperture phase deviation of $s = 3/8\lambda$ and a loss figure of 2.9dB or an aperture efficiency of about 51%. Here l is the extended length of the cone from its vertex to aperture perimeter.

In the first two sets of vircator experiments reported in chapter 6 horn antenna was not used for radiating out the generated microwaves from the vircator. In the third set of experiments the antenna was used after the vircator to assist the radiation in the field or for enhance free space coupling of the radiation. In order to measure the power and pattern of radiated microwaves an antenna was essential. Hence a conical horn antenna was designed and developed. As is mentioned by Becker [95] the aim of antenna to be designed for high power microwave radiator is to have TE_{11} radiation mode, it is found in the experiments reported in the chapter 6 that the radiation pattern from the vircator and antenna is having a peak at the axis of antenna which is an aim of applying antenna. Antenna was designed in such a way that it was supporting the radiation and propagation of the microwave signals by which it is fed at the input end. A conical horn antenna was designed and made for this purpose because the feed for it was having a cylindrical waveguide. It was designed to having same input waveguide diameter as that of the drift tube of the vircator and hence it takes all the propagating microwave signals of the drift tube into it for further radiation from the other end of large aperture.

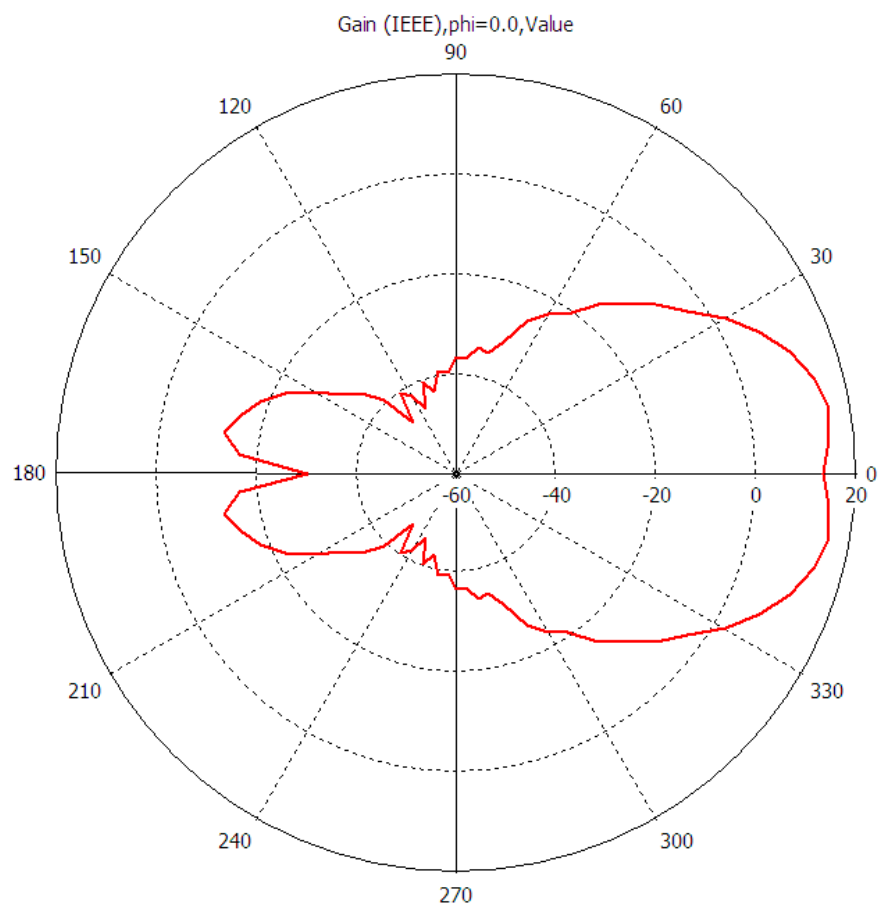


Figure 5.3: Antenna gain value at 6GHz in polar coordinates for first mode $\Phi = 0$

5.2 Antenna Analysis

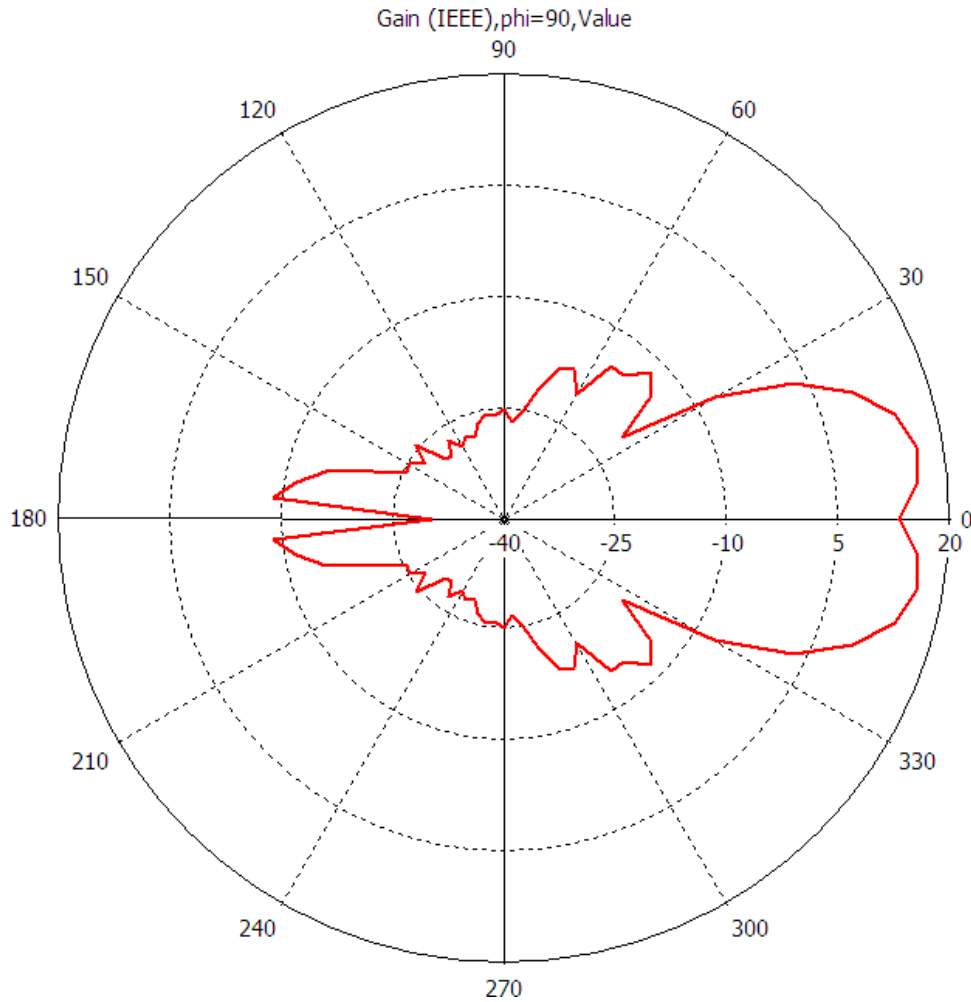


Figure 5.4: Antenna gain value at 6GHz in polar coordinates for first mode $\Phi = 90$

The antenna analysis was conducted to find out its main characteristics like the gain, directivity and reflection coefficient at different frequencies for different modes excited at the input side of the antenna feed.

A slight flare angle of 30 degree was provided at the output port of horn antennas, in order to smoothly match the impedance of the antenna with free space impedance for electromagnetic wave launching in free space. The aperture diameter was 412mm at the output side whereas the input side of the horn is matched with the waveguide of 580mm

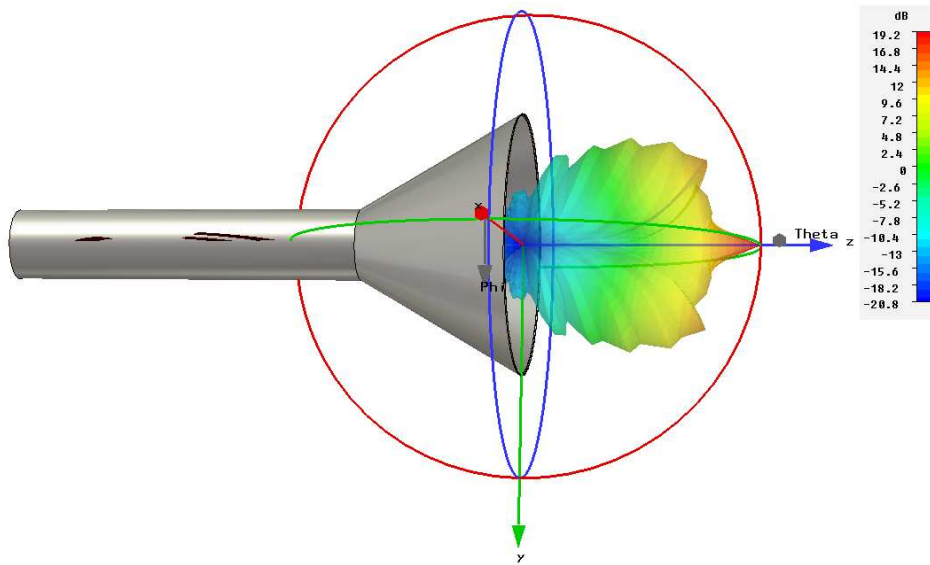


Figure 5.5: Far field radiation pattern at 6GHz for second mode

length and 112mm of inner diameter. The length of the horn antenna is 260mm. The antenna is made of stainless steel and can be evacuated for vacuum. The output end of antenna is having a stainless steel flange of 450mm diameter and 10mm thickness. This end of the antenna is closed with an acrylic disk of 25mm thickness with the diameter of 450mm.

The excitation, used in the modelling, given at the waveguide input port is shown in figure 5.1 and solution is obtained for the first six modes (Table 5.1) supported by the circular waveguide of horn antenna input side. The antenna gain, the reflection

Table 5.1: First six modes used for computation

Mode No	Mode Name	cutoff frequency (GHz)	Impedance(Ω)	$\beta(1/m)$
1	TE_{11}	1.56799	384.182	164.415
2	TM_{01}	3.26408	343.946	153.077
3	TE_{21}	3.57293	421.057	150.016
4	TM_{11}	4.2556	319.006	141.977
5	TE_{01}	4.53423	457.269	138.136
6	TM_{21}	5.42582	276.841	123.211

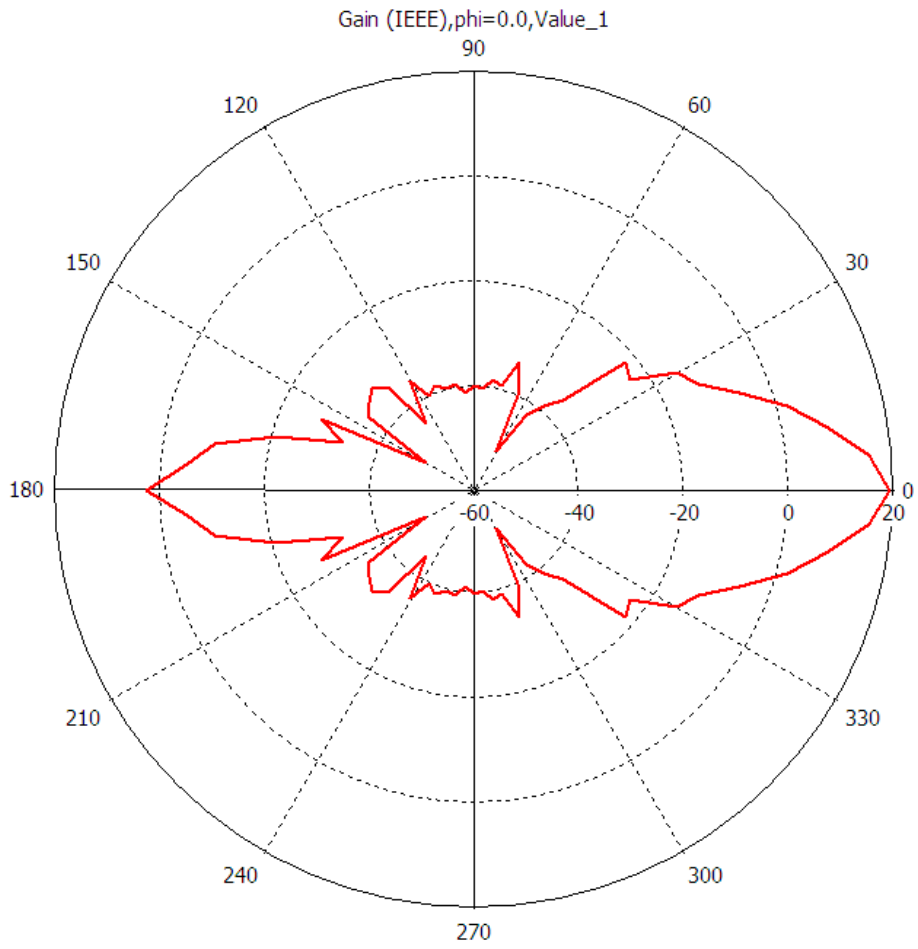


Figure 5.6: Antenna gain value at 6GHz in polar coordinates for second mode $\Phi = 0$

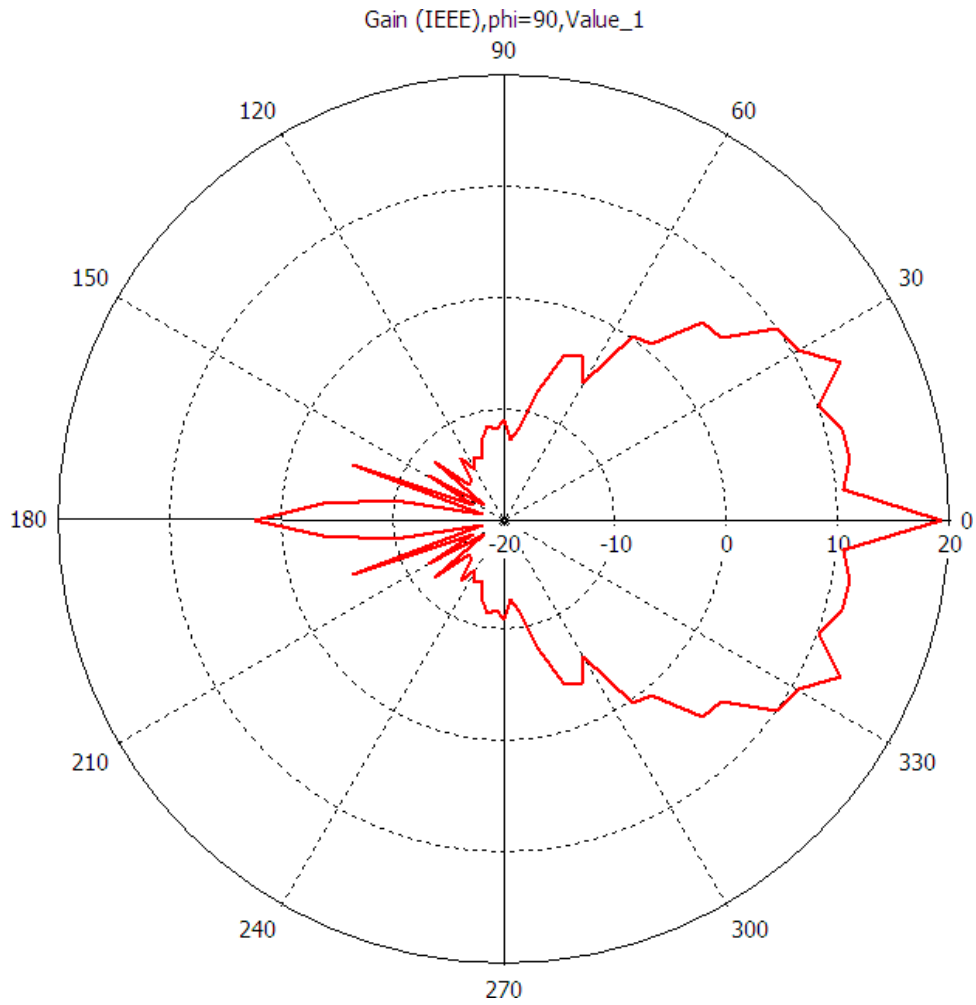


Figure 5.7: Antenna gain value at 6GHz in polar coordinates for second mode $\Phi = 90$

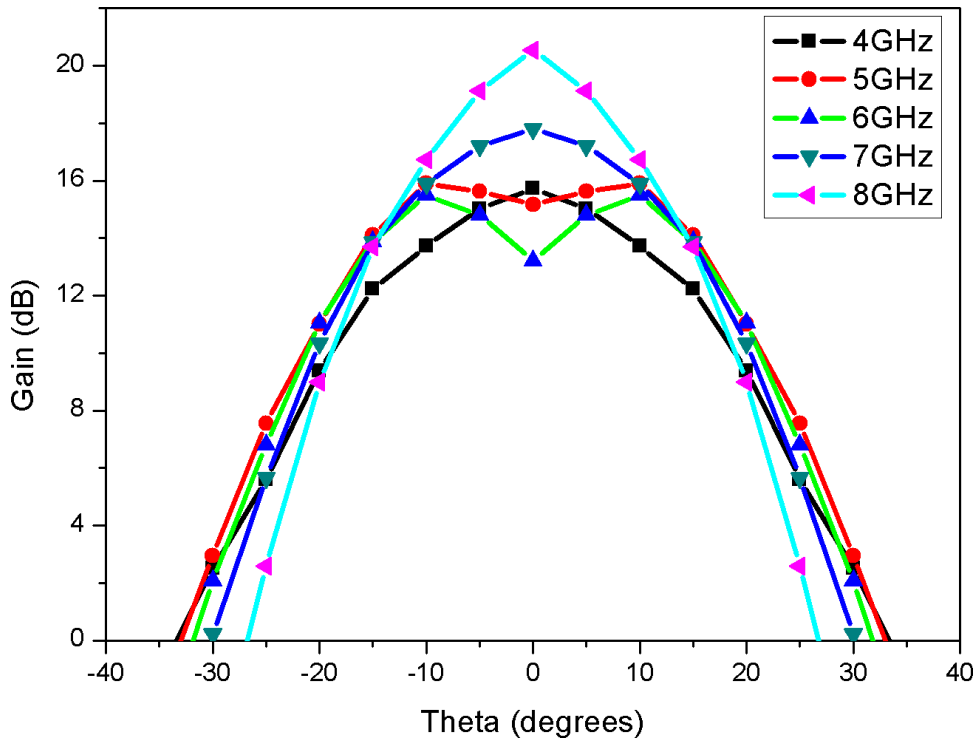


Figure 5.8: Antenna gain versus theta at $\Phi = 0$ for first mode at different frequencies

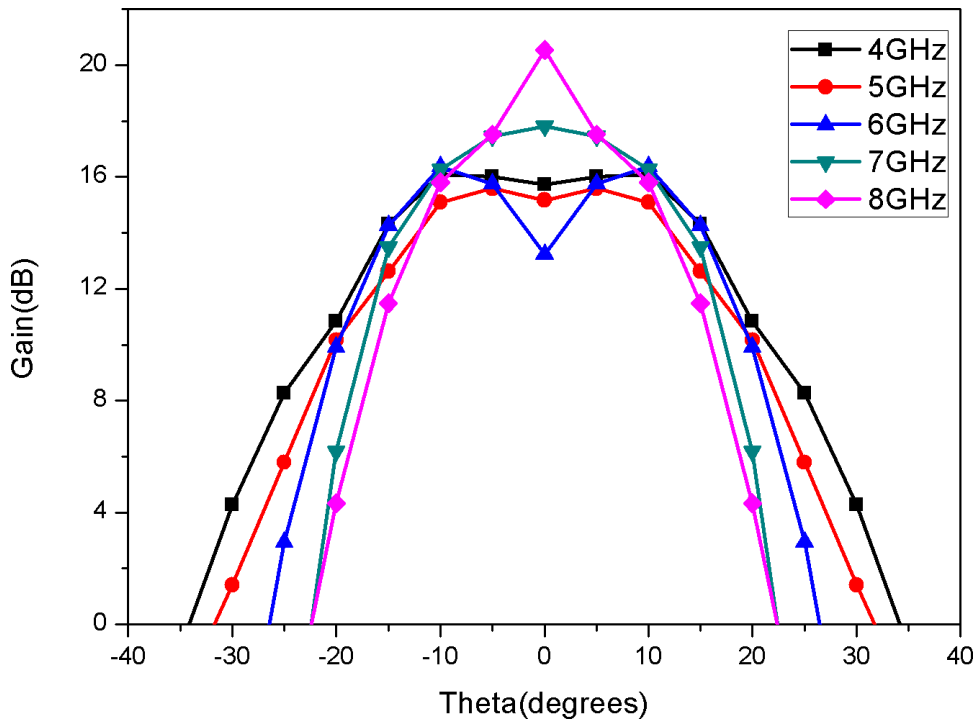


Figure 5.9: Antenna gain versus theta at $\Phi = 90$ for first mode at different frequencies

coefficient i.e. S11 parameter and VSWR is computed with the help of CST studio suite software [98] and the 3D radiation pattern for 6GHz frequency are shown in figure 5.2. Figure 5.3 and figure 5.4 show the gain values computed with the help of the results of figure 5.2 for $\Phi = 0, 90$ respectively for various Θ values in a polar plot.

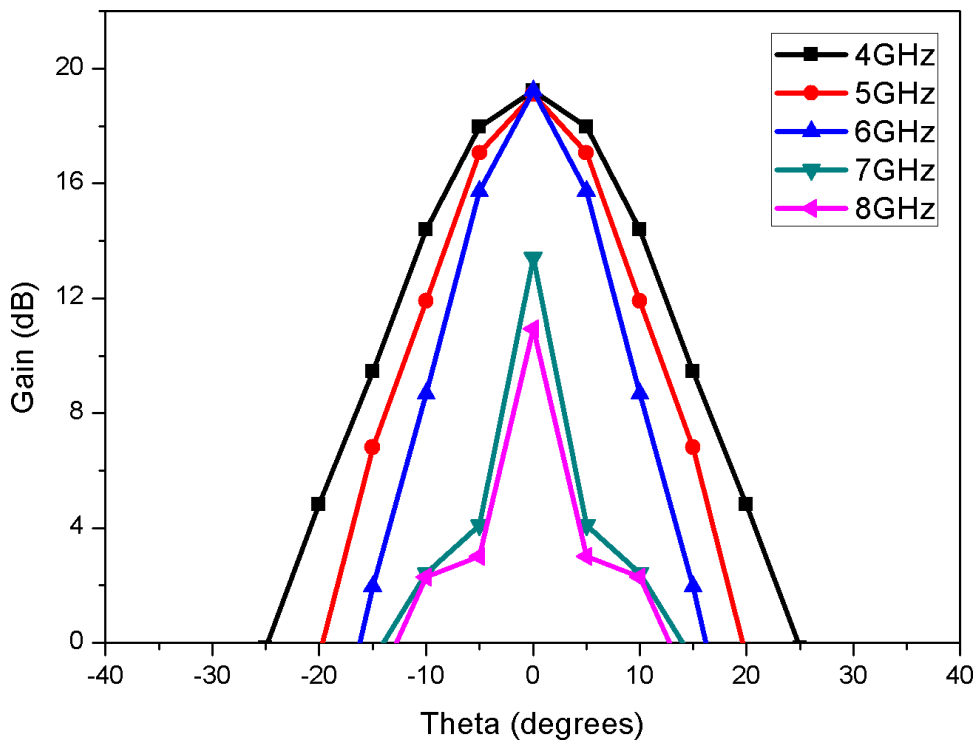


Figure 5.10: Antenna gain versus theta at $\Phi = 0$ for second mode at different frequencies

As far as the far field radiation pattern for the second mode is concerned it is shown in figure 5.5 and the results are plotted on polar curve in figure 5.6 and figure 5.7. In order to see the frequency dependency of the antenna gain pattern, the results were produced for different frequencies and the results are plotted in the figures 5.8 with 5.9, 5.10 with 5.11 and 5.12 with 5.13. An antenna gain of 17.7dB (directivity) is being shown by the computational results at 7GHz for the first or dominant mode at the axis of it. 3dB down beam width is nearly 30 degree for the conditions i.e. for the lowest order mode at 7GHz of computational frequency for $\Phi = 0$ whereas the beam width for

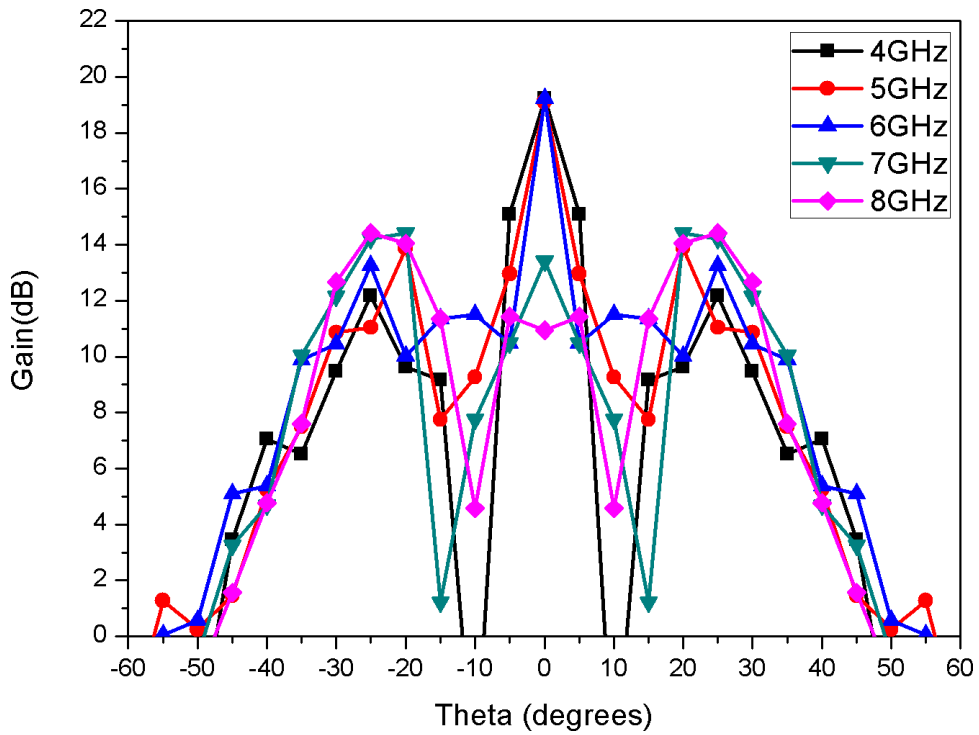


Figure 5.11: Antenna gain versus theta at $\Phi = 90$ for second mode at different frequencies

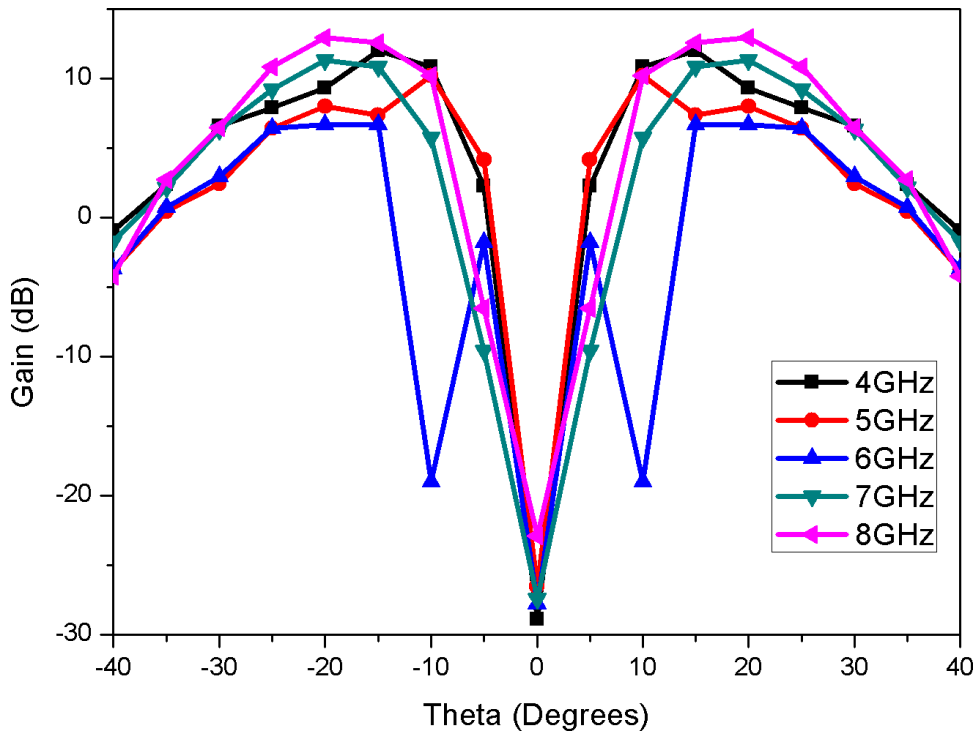


Figure 5.12: Antenna gain versus theta at $\Phi = 0$ for third mode at different frequencies

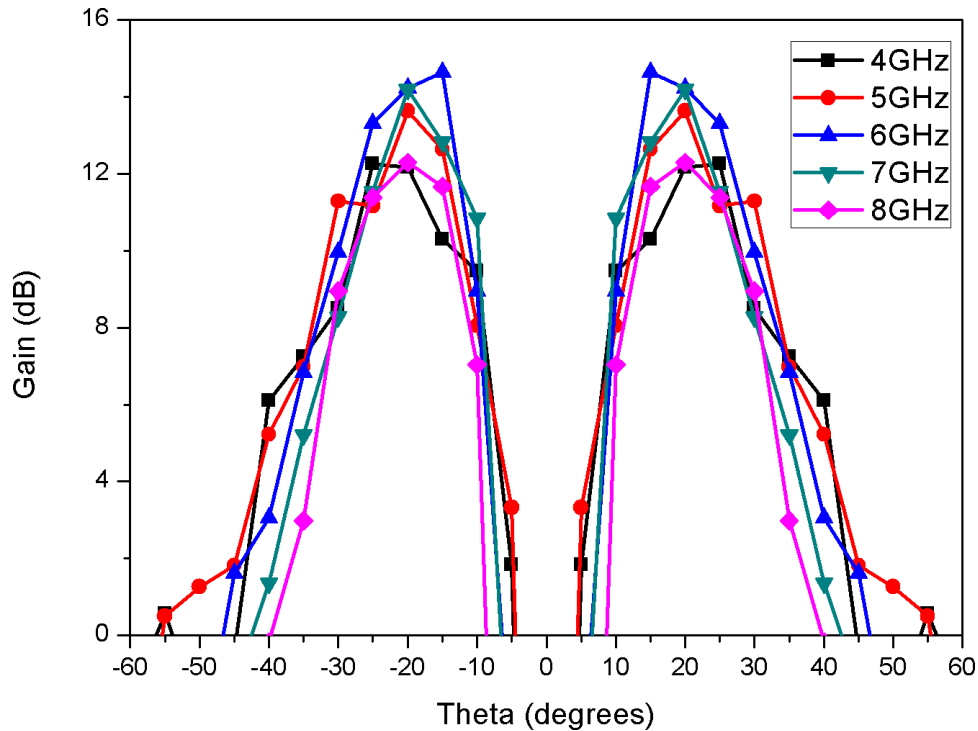


Figure 5.13: Antenna gain versus theta at $\Phi = 90$ for third mode at different frequencies

$\Phi = 90$ is also nearly 30 degree. The reflection coefficient denoted by S11 parameter is also shown for the reference in figures 5.14 and 5.15 as a function of the frequency for all the six fundamental modes without considering the cross coupling between two different modes. Finally in the figure 5.16, the VSWR for the horn antenna is presented which tells that the value is below 1.2 for various modes, excepting some low-frequency higher order modes, at different frequencies which is quite good for an antenna design for such purposes. One important thing coming out from this study that the designed antenna has nearly 16dB gain at a large aperture of 412mm diameter with beam width of 30 degrees. The large aperture will assist the handling of larger power expected from the vircator without causing the breakdown at output window of the antenna. All the radiation patterns are visualised and computed in 3-dimension and hence put a simple picture for further understanding of a rather complex problem of antenna. The solution is found in time domain so the frequency sweeping is rather easy and fast for different

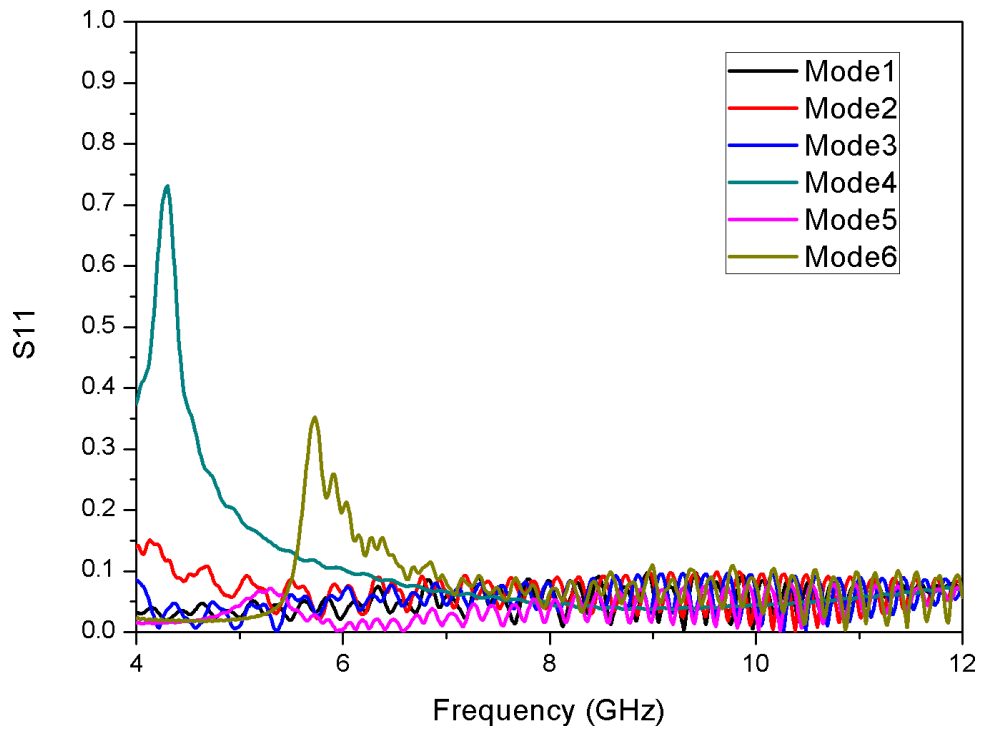
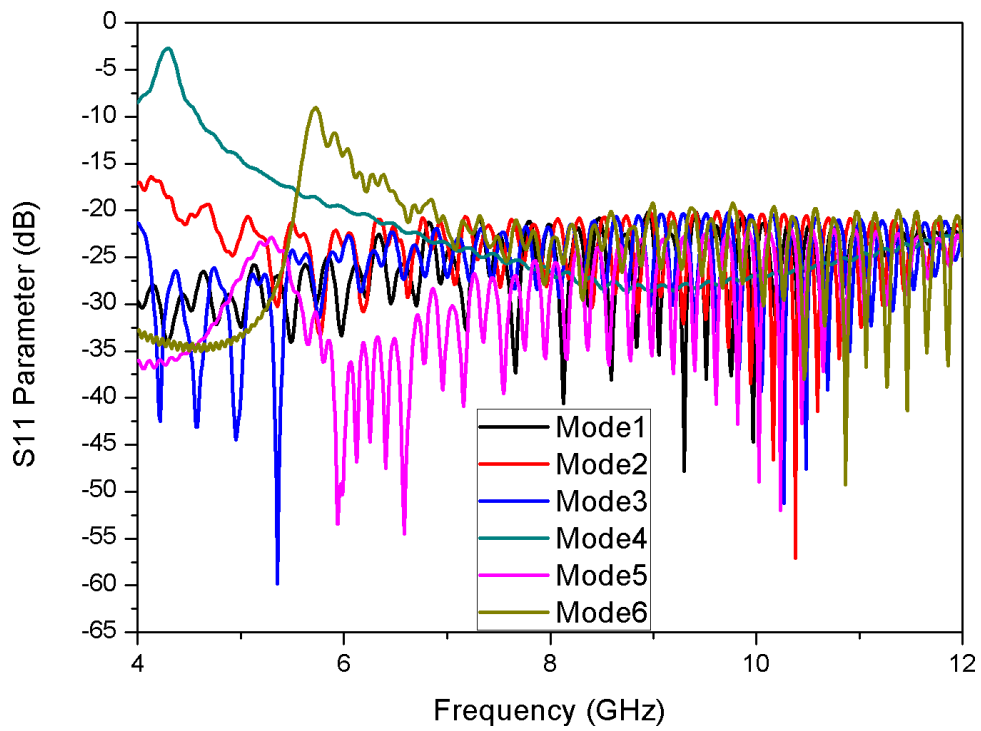


Figure 5.14: antenna reflection coefficient at different frequencies for different modes

Figure 5.15: S_{11} parameter on dB scale at different frequencies for different modes

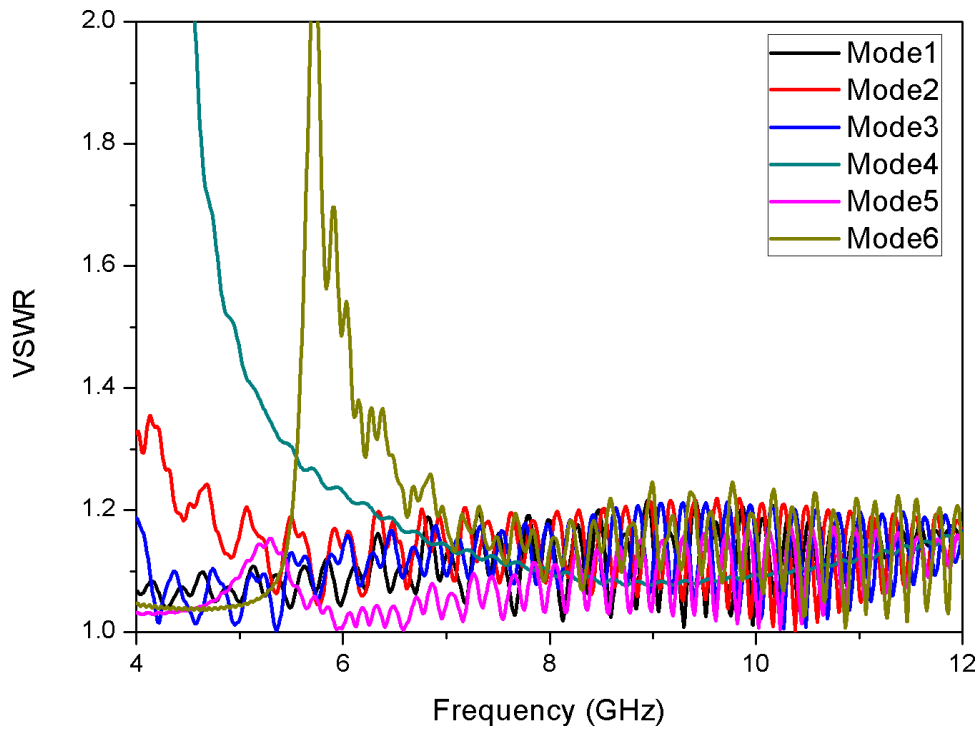


Figure 5.16: VSWR of the horn antenna for different modes

frequencies of computation. The reflectivity and the VSWR of the designed antenna are also quite low within the permissible limits of the normal antenna design for broadband microwave emission.

5.3 Conclusion

In this chapter the detailed analysis of the antenna used for the experiments mentioned in the third section of the chapter 6 has been done. It is seen from the dimensions of the waveguide of the experimental setup that the structure is overmoded for the frequencies being radiated from the system and hence six modes have been studied for the antenna. Maximum field intensity at the axis of the radiator also indicates that radiation is not purely the dominant mode. This detailed analysis is also helpful in determination of the peak powers being radiated from the radiator based on the gain calculations of the

radiating antenna at different frequencies and different modes based on the field measurements done at different locations away from the radiator.

6

VIRCATOR RESULTS

Axial virtual cathode oscillators are the devices which are recently being studied by various groups-worldwide [99, 100] as a source of high power microwave radiations operating with relatively much ease as compared with other conventional and well established high-power-microwave generating devices. This device requires quite a huge amount of electrical powers, in the form of power of generated electron beam inside it, which is converted to microwave power in the geometry of vircator.

The principle of operation of vircator is as given under. A high voltage source is con-

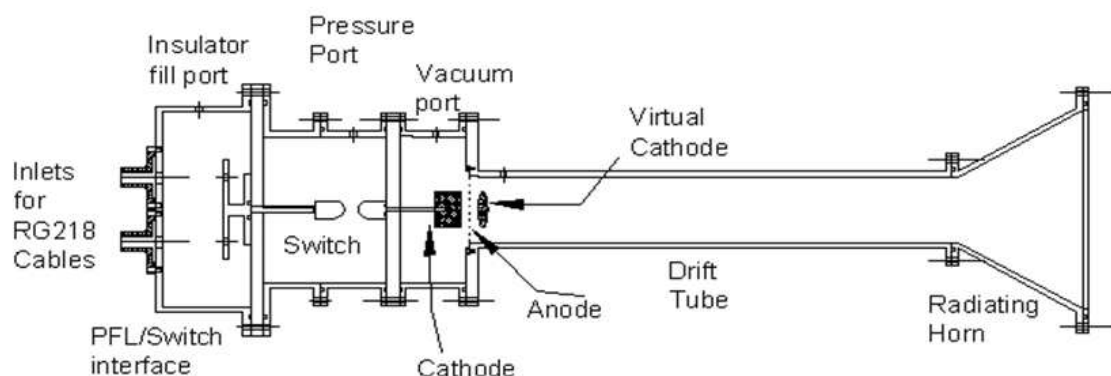


Figure 6.1: Schematic of Vircator Chamber assembly with cable based PFL

nected with the Electron beam diode which is part of vircator geometry inherently. In the case of axial vircator, which is in fact the case of present study, the electron beam diode is formed of cylindrical cathode and mesh/thin foil anode. The high power Electron beams are emitted from the surface of cathode mainly by two emission mechanisms viz. Field Emission and Explosive Electron Emission depending upon the material and surface properties of the cathode.

Once high power electron beam is generated it is accelerated towards anode by the same



Figure 6.2: Vircator Assembly

electric field which is responsible for its generation. As the electrons of the emitted beam reach the anode, some of them pass through anode depending upon the transparency for the anode. These passed electrons are forced to propagate inside a drift tube of vircator which interacts electromagnetically with the beam passing through it. The space charge effects causes the bending of cylindrical beam towards axis of drift tube and this results

in the formation of electron cloud of certain charge density inside the drift tube. This charge cloud is formed only when the electron beam current is higher than space charge limiting current of this drift tube. This charge cloud is also called virtual cathode. After formation of virtual cathode some part of the successive electrons emitted from cathode are reflected back by the virtual cathode. Because of this they get trapped between cathode and virtual cathode and keep on oscillating in the space between cathode and virtual cathode till they are lost either by diffusion or by hitting the foil/mesh. These oscillating electrons radiate the radiations depending upon their oscillating frequency which again depends upon the A-K gap and electron velocity considerably.

Other than the radiations caused by oscillating electrons between cathode and virtual

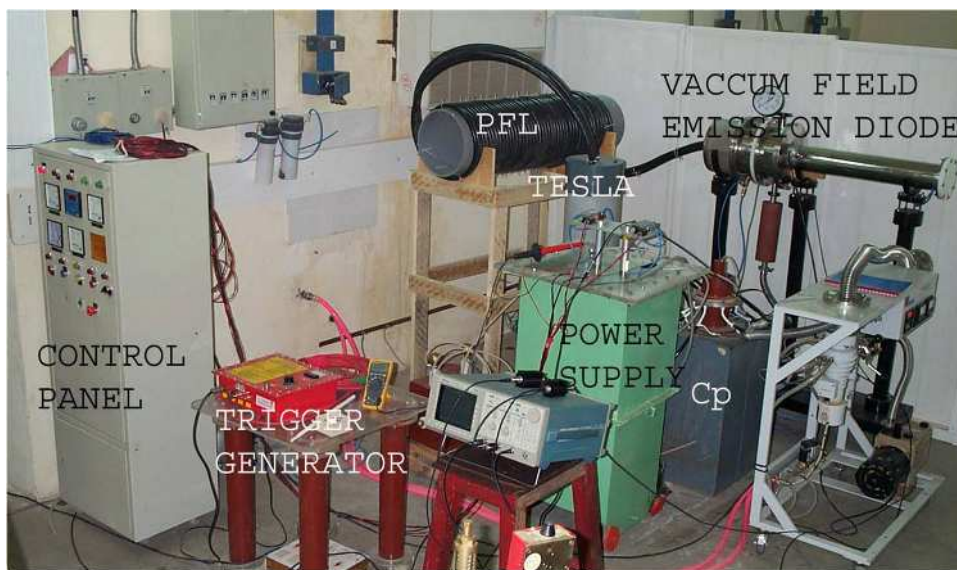


Figure 6.3: Pulsed power system and vacuum field emission diode

cathode, there is another mechanism which contributes to the total microwave radiations from the virtual cathode oscillator. The virtual cathode which is an electron cloud also keeps on oscillating in space and in time. The oscillation of the virtual cathode oscillator in space and time also causes the emission of electromagnetic radiation to take place. The frequency of the radiation from virtual cathode oscillations is dependent on

the electron plasma frequency of the charge cloud. Moreover there is always a loss of the electrons from the virtual cathode and electron beam in the form of drift and diffusion loss of electrons. This loss of electrons from the virtual cathode is compensated by the incoming electron beam which is emitted from the cathode. There is formation of plasma on the cathode surface and also on the anode surface caused by the impact of energetic electrons of the beam on it. This plasma also expands in all free directions and occupies the space in between the region of anode cathode. Once the plasma is filled in this region the electric field between anode cathode gap regions diminishes to a value where no further field emission of electrons takes place. The event is called diode closure. This requirement makes the pulse compression and pulse shaping necessary before applying it to the vircator.

6.1 Vircator Experiments:Set1



Figure 6.4: Impression of electron beam on S.S. mesh

Figure 6.1 is the schematic drawing of the first vircator which was made in the laboratory. This schematic drawing represents how the coaxial cables were connected

with the vircator chamber to produce electron beam in the system. It has inlets for four RG218 cables in it. the central conductors of each cable was shorted to single point connected with one end of discharge spark gap. the braids were simply terminated with the housing of the vircator chamber which was made with stainless steel. The antenna was not physically connected in these experiments and is used to only indicate that it was aimed to be used since the beginning of the experiments. Figure 6.2 is a close view on the way the connections between each of four cables and vircator chamber has been made. In these experiments the vacuum inside the chamber is better than 2×10^{-4} torr. Figure 6.3 is a full view of the complete experimental setup. The diameter of the drift tube of the vircator is 140mm. The cathode for these experiments, as is described earlier, is made of graphite which is stuck to the Aluminium by the silver epoxy which acts as conducting bonding agent between the two. The anode is made of anode mesh which has an optical transparency of 75%. These experiments gave a nice insight about the

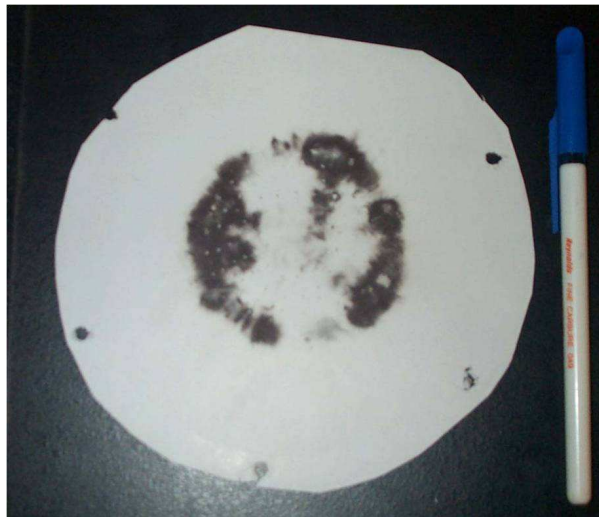


Figure 6.5: Impression of electron beam on thermal paper

system operation conditions and subsequent results and hence are of significance.

This set of experiments were started with 8mm of anode cathode spacings and no microwave was observed under these conditions. It was also quite interesting to note



Figure 6.6: Exposed dental X-ray film (exposure in five shots)

in these initial experiments, that the radiated X-rays measured from the electron beam system was 5mR when was integrated for four shots at 8mm anode cathode gap. At 8 mm anode cathode gap it was observed that the electron beam is annular in shape as is shown by figure 6.4. In the thermal paper recording of the beam caused burn on it, as is shown in figure 6.5 it is also evident that the beam is not perfectly uniform in the shape. Even though the x-rays were being produced the microwaves were nearly below the detectable limit of the diagnostics which comprised of the rectangular narrow band horn antennae having a limited bandwidth as is supported by the WR430 horn antenna. A dental X-ray film was exposed under this condition of experiments which was kept at the output side of the drift tube. A washer of S.S. was kept in the path of Xrays reaching the dental X-ray film. The image of the washer is being shown in figure 6.6. The motivation for conducting these experiments is to generate the electron beam and to find impressions of its presence. The results of this experiment were quite interesting. Continuing with the same experimental setup the A-K gap was further reduced to 5mm in this experiment so that a lesser impedance is offered by the diode expecting more current and formation of virtual cathode. At the 75% optical transparent SS mesh anode, microwave radiation is recorded by the microwave detector diode (envelop detection as is shown by figure 6.7) and also by a high frequency oscilloscope connected with a

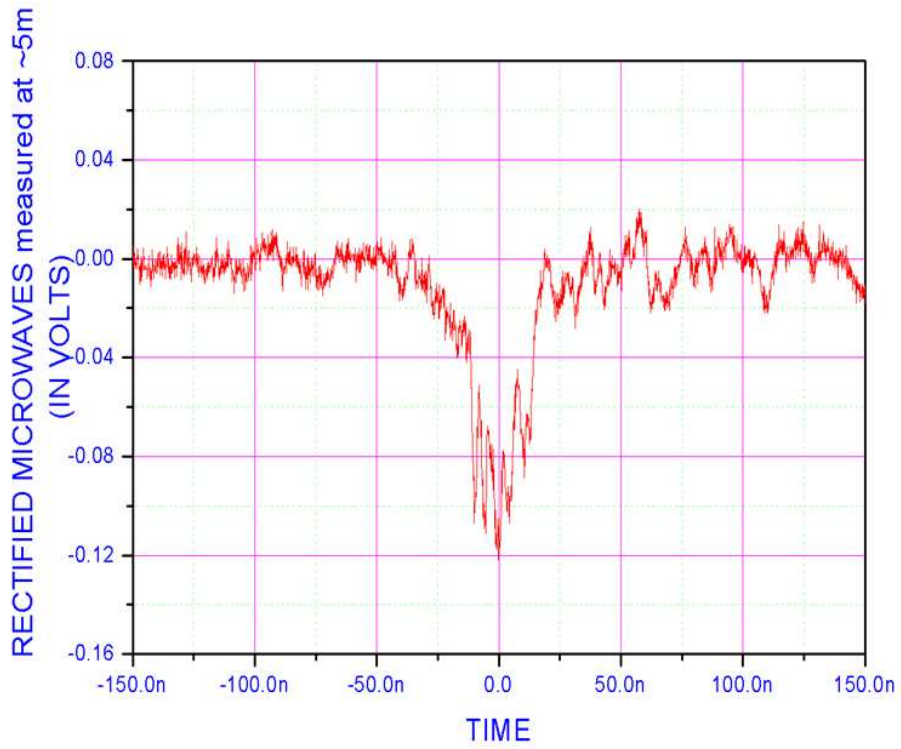


Figure 6.7: Microwave envelop as shown by detector diode

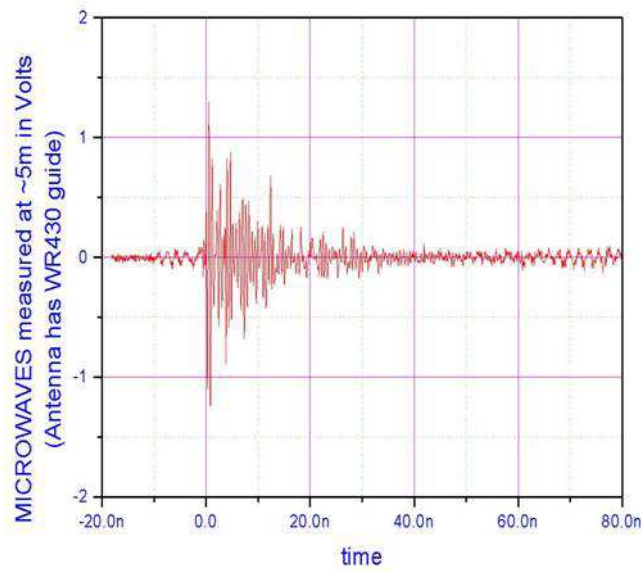


Figure 6.8: Received microwave signal

receiving antenna as is shown in figure 6.8. Dominating frequency of the received signal from the receiving antenna came out to be 2.5GHz (FFT of the oscilloscope record) and its duration is 25ns and is shown in figure 6.9. The interesting part is that even though the applied pulse for the vircator is of 88ns duration, the radiated pulse is shorter than the applied pulse. The charging voltage for the pulse forming line is 120kV only in these experiments. Since the maximum sampling rate of the oscilloscope used in these set

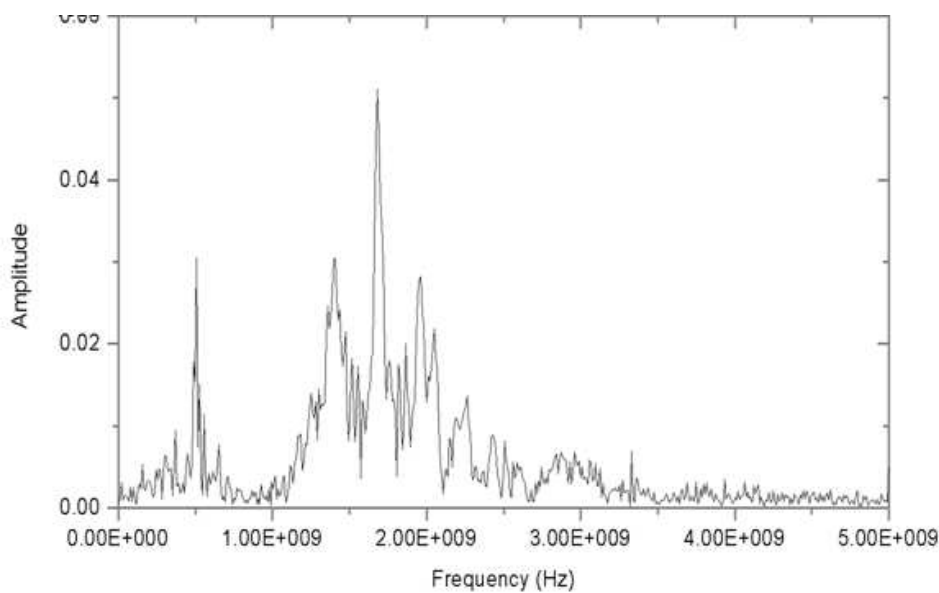


Figure 6.9: FFT of received microwaves

of experiments is limited to the 20Gsa/Second the limited bandwidth of the oscilloscope is 5GHz in the single shot. That is why the x-axis of the frequency curve is limited to 5GHz only in the figure 6.9. In order to be even more confirmed about the fields being radiated, an array of the neon lamps and gas filled fluorescent tubes were kept in front of the vircator. the glow of the neon lamps is shown in figure 6.10 and the glowing fluorescent tube is shown in figure 6.11. The glow in both of them at the time of exposure of vircator during operation also indicates about the fields being radiated from the system. After including the calibration factor of the designed high voltage probe(X40k) in the measured voltage between the anode and cathode of the vircator it

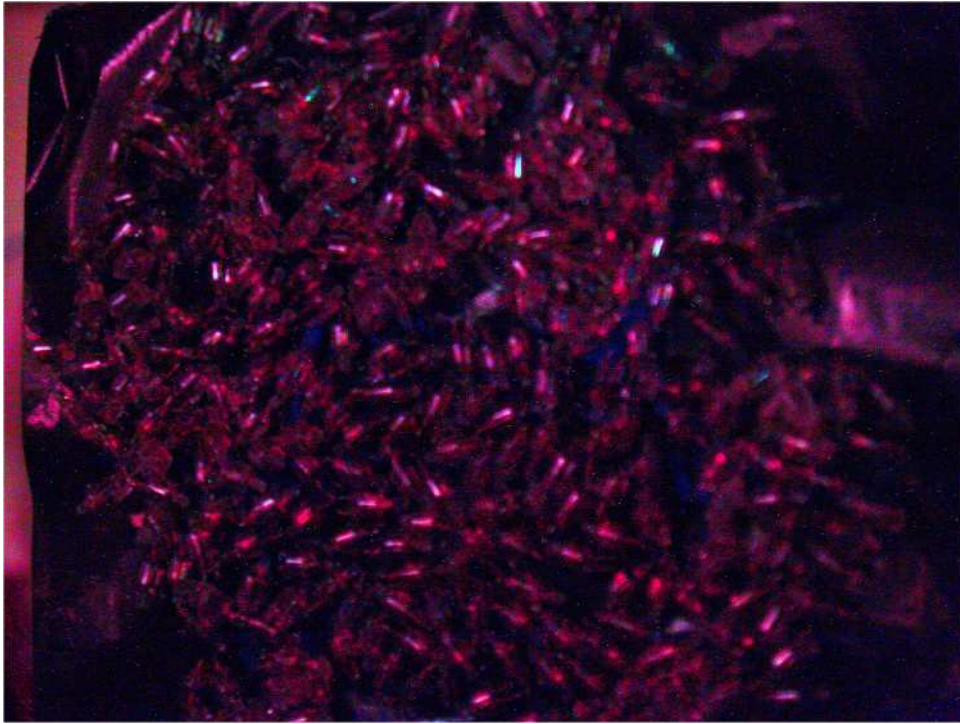


Figure 6.10: Glowing of neon lamps (red)

is seen that nearly 40kV of the voltage is being applied at the diode in this geometry and a record of it is shown in figure 6.12.

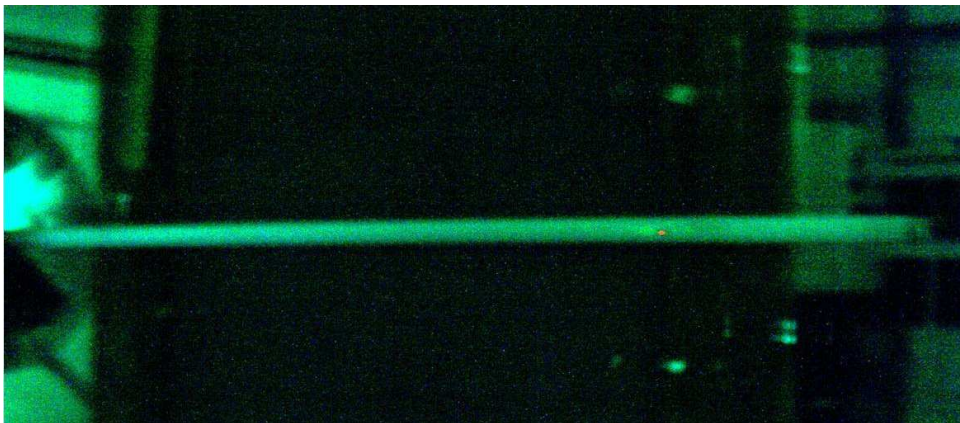


Figure 6.11: Glowing fluorescent tube in front of microwave radiations

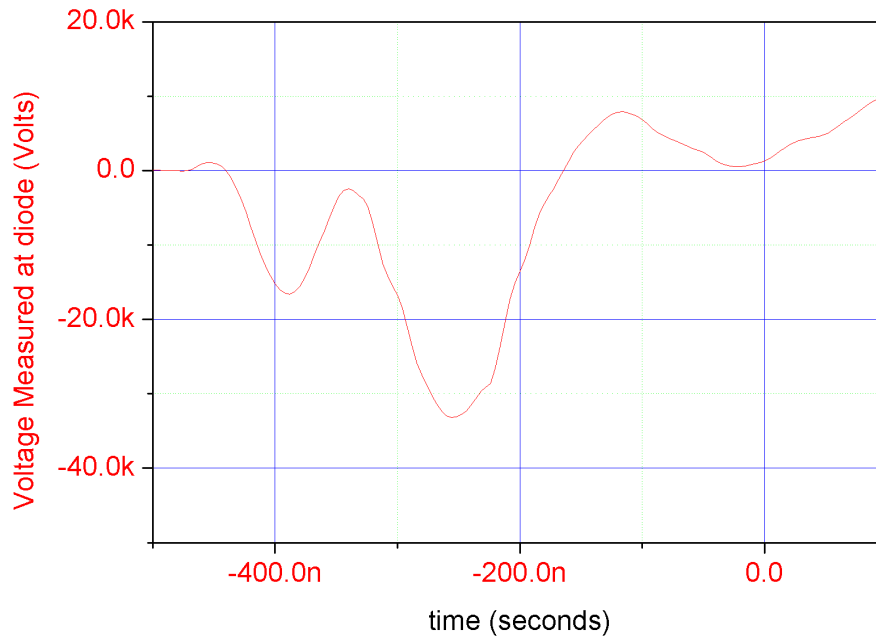


Figure 6.12: Voltage applied across the anode cathode gap

6.2 Vircator Experiments:Set2

To the best knowledge of the authors it is first system of its kind using coaxial cable based system driven by the compact pulsed power source to drive the complete assembly. Because of its compact nature, the system has potential of operating at repetitive mode also. The results of a bulkier pulsed power system driving a solid dielectric PFL and vircator connected to it have been mentioned in the previous section and some of them were published previously [101]. After producing the microwaves from the first set of experiments further efforts were made to enhance the radiation considerably by increasing the driving potential for the vircator and at the same time also to compactize the complete pulsed power assembly. As discussed above the vircator requires high electrical powers for its operation and only for very short durations. This is done by pulse-compression and pulse-shaping. An attempt has been made to do the pulse-compression

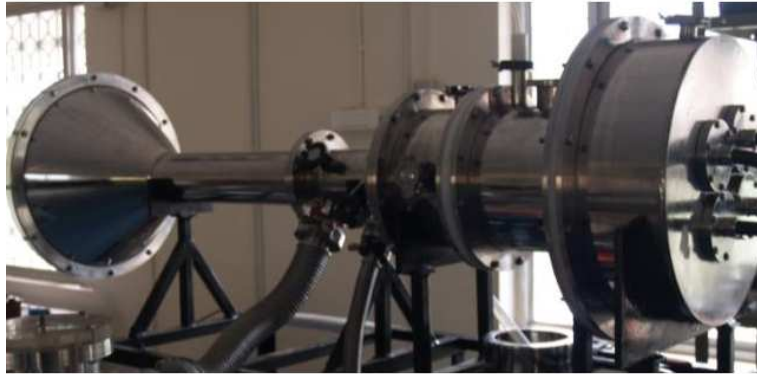


Figure 6.13: Axial virtual cathode oscillator System



Figure 6.14: Stainless Steel Cathode

and pulse-shaping by compact pulse compression system mentioned in the details given under. The experimental results are also presented after the system details.

6.2.1 Experimental Setup

The Virtual cathode oscillator in the present case has a measured vacuum of 2×10^{-4} mbar inside the chamber. The vacuum is created with the help of a diffusion pump of 500l/s pumping speed which is backed by a rotary pump. The vircator chamber is shown in figure 6.13 and is made of stainless steel. The cathode in the present experiments is made of S.S. electrode of 60mm diameter and is shown in figure 6.14. The anode is made of S.S. mesh of 80% optical transparency. In the present study at different PFL voltages, the anode cathode spacing is fixed at 4mm which is lesser than the previous case. The drift tube diameter is 140mm and estimated space charge limited current in this geometry is less than 1kA. A conical horn antenna is also designed for the system with input waveguide matching with the dimensions of drift tube. A conical horn antenna is also designed for the system with input waveguide matching with the dimensions of the drift tube. The vircator is operated using a solid dielectric pulsed forming line (PFL) made of four pieces of 50Ω , RG218 coaxial cables connected in parallel to make a net estimated impedance of 12.5Ω . The length of each cable is 12 meters and hence the estimated pulsed-width which is twice of its transit-time, is expected to be nearly 140ns which is longer than that of the previous case. The pulsed forming line is being charged by the compact pulsed transformer [122] which has its primary capacitor bank made in the shape of its primary. The capacitors used in the bank have shown very high power delivery driving a plasma focus device [102]. The connections between pulse transformer and pulse forming line is done using specialized connectors at the ground part in order to reduce the electric field strength generated between ends of sharp braid wires and inner conductor of the cable to such levels where the breakdown at feed point (as is shown

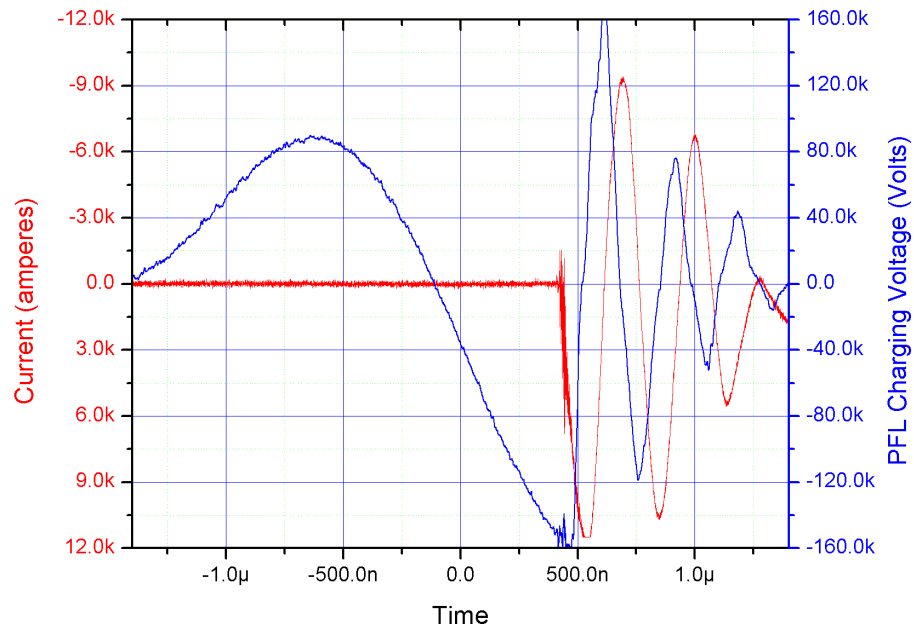


Figure 6.15: PFL Charging Voltage and PFL Discharge Current

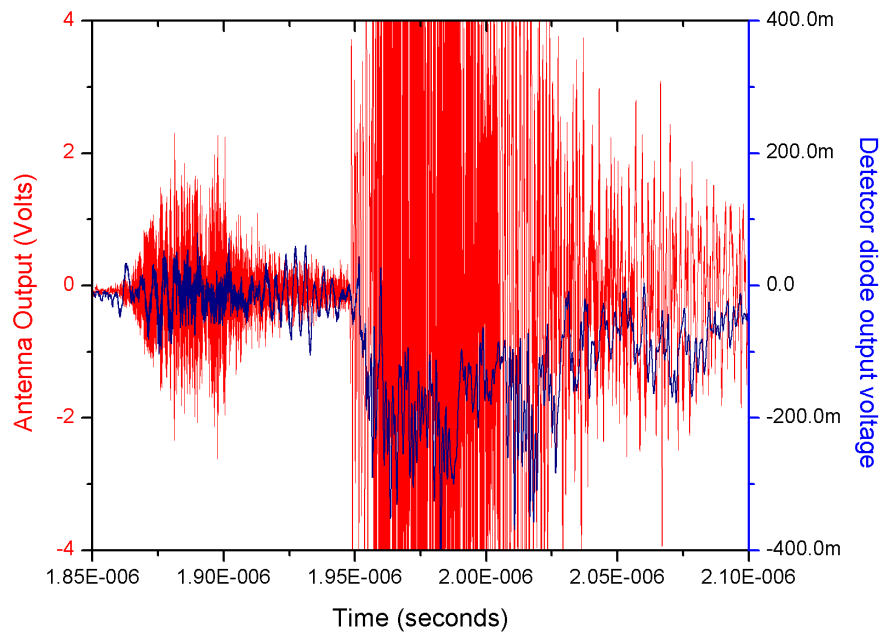


Figure 6.16: Receiving Antenna (kept at 1.2Meters from cathode) signal and envelop seen by the microwave detector diode (vircator operating with PFL at 160kV)

in figure 3.2) does not take place which, otherwise, happens only at 20kV only. The improved connections between the transformer and pulse forming line result in charging of PFL to still higher voltages reaching a maximum of 200kV. The compact transformer with the combination of Pulsed forming line is having 1:20 voltage gain when compared with primary charging voltage and PFL peak voltage reached at its second peak. The capacitor bank-*cum*-transformer, when first charged to 10kV and then discharged, delivers 200kV peak voltage in the second peak in $2.0\mu\text{s}$ at the Pulsed forming line which is connected to the Virtual cathode oscillator system using a self-triggered spark gap switch. As far as diagnostics are concerned, the standard diagnostics are used for the measurement of the PFL discharge current, PFL charging voltage, and microwave signal (both power envelop and frequency). For the measurement of pulsed forming line charging voltage we have used 10000X resistive voltage divider. For the measurement of currents we have used a 17ns rise time current transformer with standard sensitivity of 50V/kA. The current transformer output is connected to the oscilloscope using standard 20dB attenuator in order to reduce the voltage to the oscilloscope input requirements for the given current pulse. The current transformer is placed inside the spark gap chamber. The microwave signal is recorded on a 10GHz, 40GSa/sec oscilloscope using a double-ridged horn antenna having bandwidth of 800MHz to 18GHz. The receiving antenna is kept at 1.2meters distance from cathode location facing the drift tube which has no radiating antenna in these set of experiments. The receiving antenna is connected to the oscilloscope using high bandwidth cable having a cut-off at 12GHz. This signal coming directly from the receiving antenna to the oscilloscope is analyzed for its FFT to give frequency spectrum of radiated microwave signal. To see the power envelop of radiated microwave, the output of antenna is bifurcated and passed through microwave detector diode Agilent-423B and its output is smoothened to average out the acquisitions over 1ns (40samples) comparable to the rise time of diode. the diagnostics are mentioned in

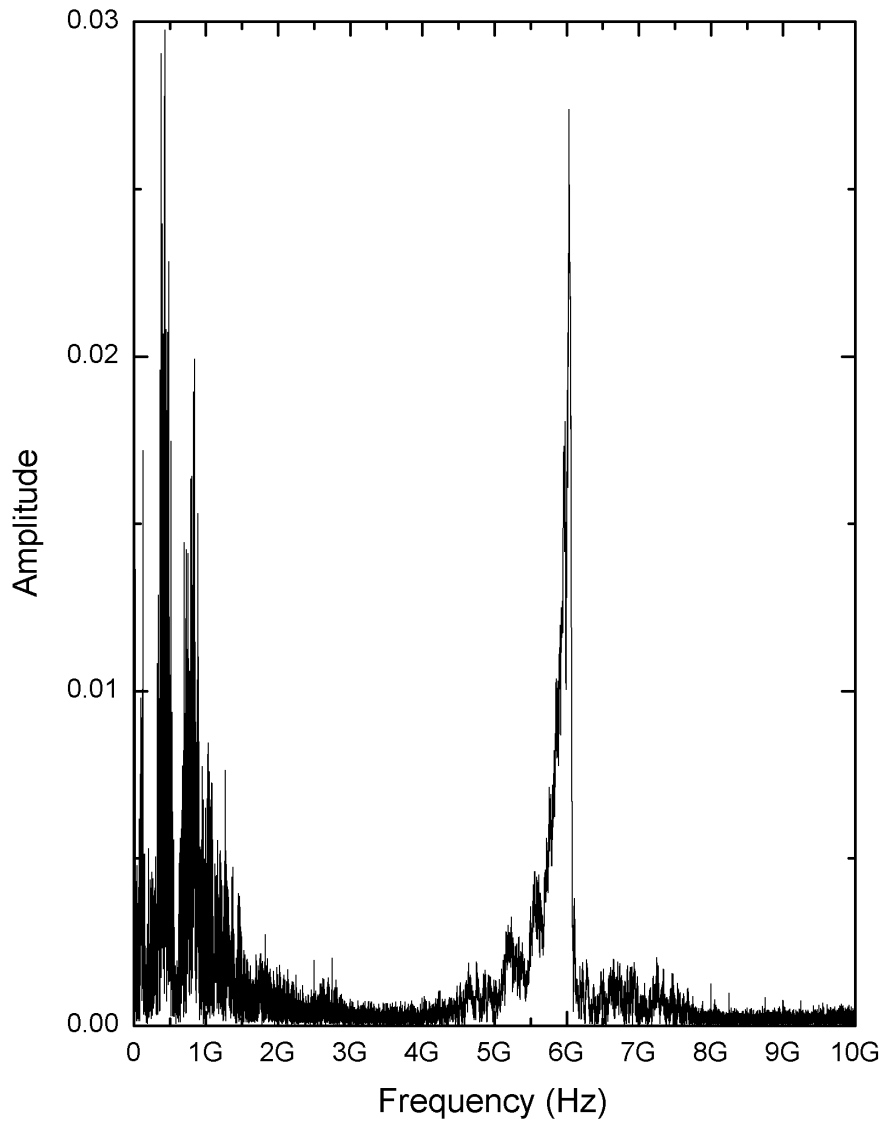


Figure 6.17: FFT of receiving antenna signal (vircator operating at 160kV PFL Voltage)

chapter 2.

6.2.2 Experimental Results

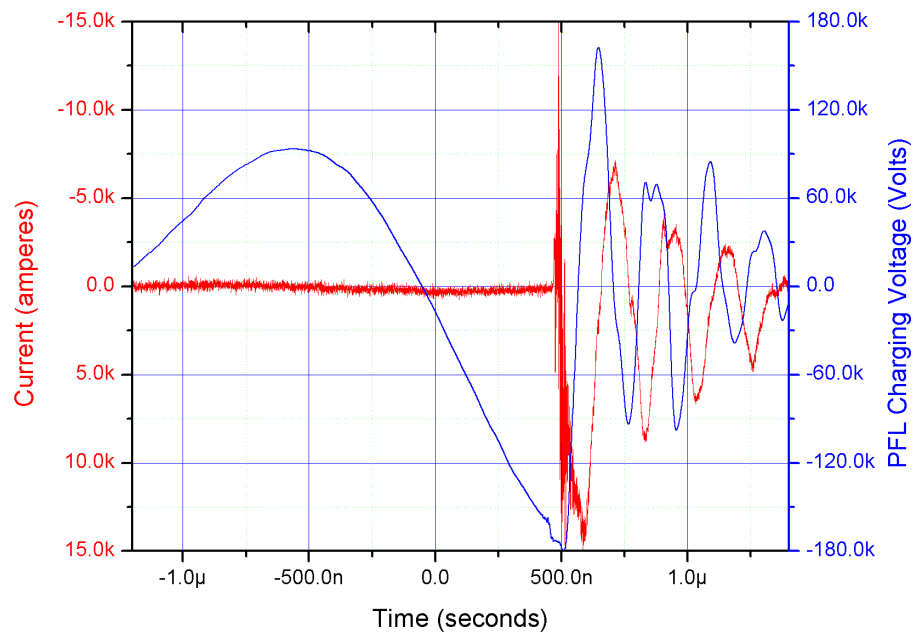


Figure 6.18: PFL Charging Voltage and PFL Discharge Current

Once a peak voltage of 200kV was achieved during the initial testing of the pulsed forming line the vircator which was connected to its output was operated in vacuum. It was noted that when the vacuum was not there inside the vircator, the high frequency components (of higher than 2.5GHz) in the FFT of antenna signal were not present. The microwave experiments with vircator were conducted at two different PFL-charging-voltages of 160kV and 180kV decided by the spark gap settings. Figure 6.15 shows the voltage measured at PFL charging end and discharge current of PFL measured using Current Transformer (CT). The peak discharge current reaching in the system is 12kA. The peak PFL charging voltage is 160kV and the small anode cathode gap leads to fast

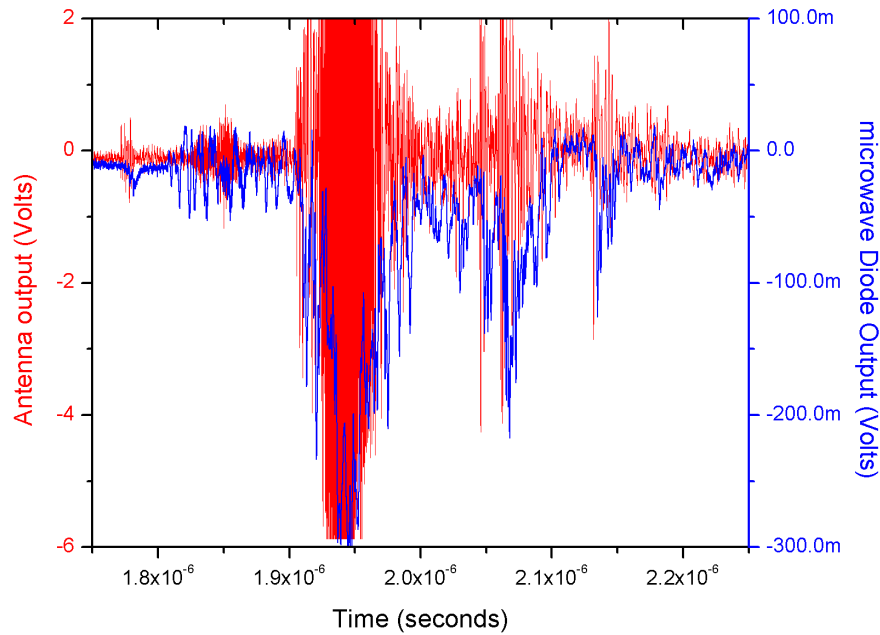


Figure 6.19: Receiving Antenna kept at 1.2Meters from Cathode signal and envelop seen by the microwave detector diode vircator operating at 180kV PFL Voltage

reduction of diode impedance. The net impedance of the complete discharge-circuit comes out to be nearly 13Ω . Figure 6.16 represents the microwave signals received from the antenna and fed to the oscilloscope at 50Ω input impedance. The microwave pulse record of not more than 50nanosecond duration also suggest that fast closure of diode is taking place because the applied high voltage pulse is nearly 140ns in duration. The reflections of voltage and current also suggest the same sequence of events to be happening in the vircator. Figure 6.17 is more informative in terms of the frequency content of radiated signal from the vircator. It is clearly visible from the spectrum that high frequency components of more than 5GHz are present in the signal. The vircator has successfully demonstrated the high frequency radiations from the compact pulsed power system. The other set of results achieved at 180kV of vircator operation are also very interesting and consistent. Figure 6.18 is the record of PFL charging voltage and

discharge current reaching 180kV and 14kA peak current again demonstrating the same 13Ω impedance of the discharge circuit. The respective microwave signal is shown in figure 6.19. The microwave envelop is of higher magnitude as compared with the signal

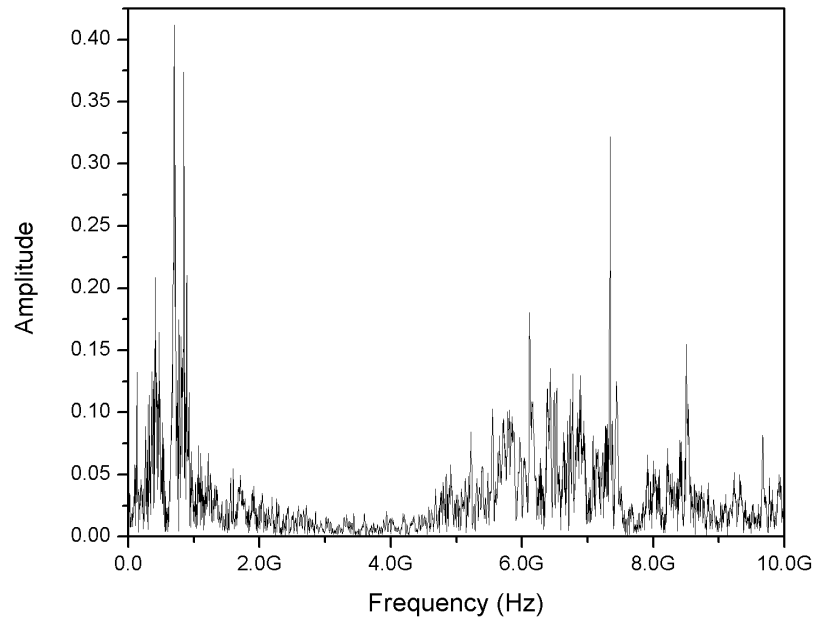


Figure 6.20: FFT of Receiving antenna signal vircator operating at 180kV PFL Voltage at 160kV indicating a higher emission of microwave at higher voltage. Figure 6.20 represents the FFT of radiated fields indicating that a frequency spectrum of greater than 5GHz is present as a result of vircator operation.

6.3 Vircator Experiments:Set3

6.3.1 Introduction

In this paper we are presenting the microwave emission results of a vircator which emits its radiation lying well-within the microwave range of electromagnetic spectrum viz

4-8GHz and the energy needed per shot is as low as 25joules only. In this reported experiment the pulse forming line is charged to a voltage of 160kV and the measured diode voltage is 50kV in the experiment. The primary energy is nearly 50joules only and hence the energy efficiency of the high voltage pulse transformer and pulse forming line combination for the given experiment is nearly 50%. The experiment is the first



Figure 6.21: Picture of virtual cathode oscillator assembly fitted with the cable based PFL

of its kind in establishing (experimentally) the low voltage operation of a conventional vircator, which has a planar cylindrical cathode and stainless steel mesh anode, for the microwave emission purpose. Moreover, because of the low voltage and low energy operation we could operate the whole system in repetitive mode and we could achieve as high as 4Hz operation with this device. Interestingly, the current density of the vel-

vet cathode used in the present experiment is nearly $300\text{A}/\text{cm}^2$ in the present reported set of experiments. One interesting observation emerging out from the present experiment is that in the low voltage operation of the vircator the beam acceleration potential is relatively low and hence the axial velocities of reflexing electrons (trapped between cathode and virtual cathode) is also limited and far less than $1.8 \times 10^8 \text{m/s}$ and hence with small anode cathode gaps like that of 3mm, which is the case of present experiments, it becomes feasible to achieve radiation frequency of 4-8GHz from the vircator. It has

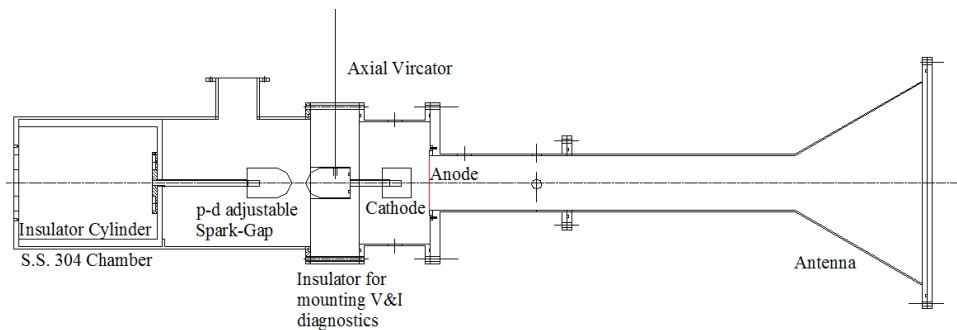


Figure 6.22: Geometrical drawing of the virtual cathode oscillator system

been shown in various studies which were conducted and reported so far in the context of axial Virtual Cathode Oscillator (VIRCATOR) that an axial Virtual Cathode Oscillator radiates in the microwave range of electromagnetic spectrum provided the voltage applied between anode and cathode is in the order of hundreds of kilovolts. Recently a detailed theoretical study [121] was presented for a proposed low-voltage conventional vircator which shows formation of secondary virtual cathode along with the existence of a primary virtual cathode. Moreover a theoretical estimation of as high as 7% efficiency is also reported in the same theoretical model. By using the word "conventional" the other mechanisms to assist the formation of virtual cathodes are excluded here for comparison viz. the application of external magnetic fields: [116], magnetron injection gun [115], shielding of the electron source from external magnetic field [117] and external

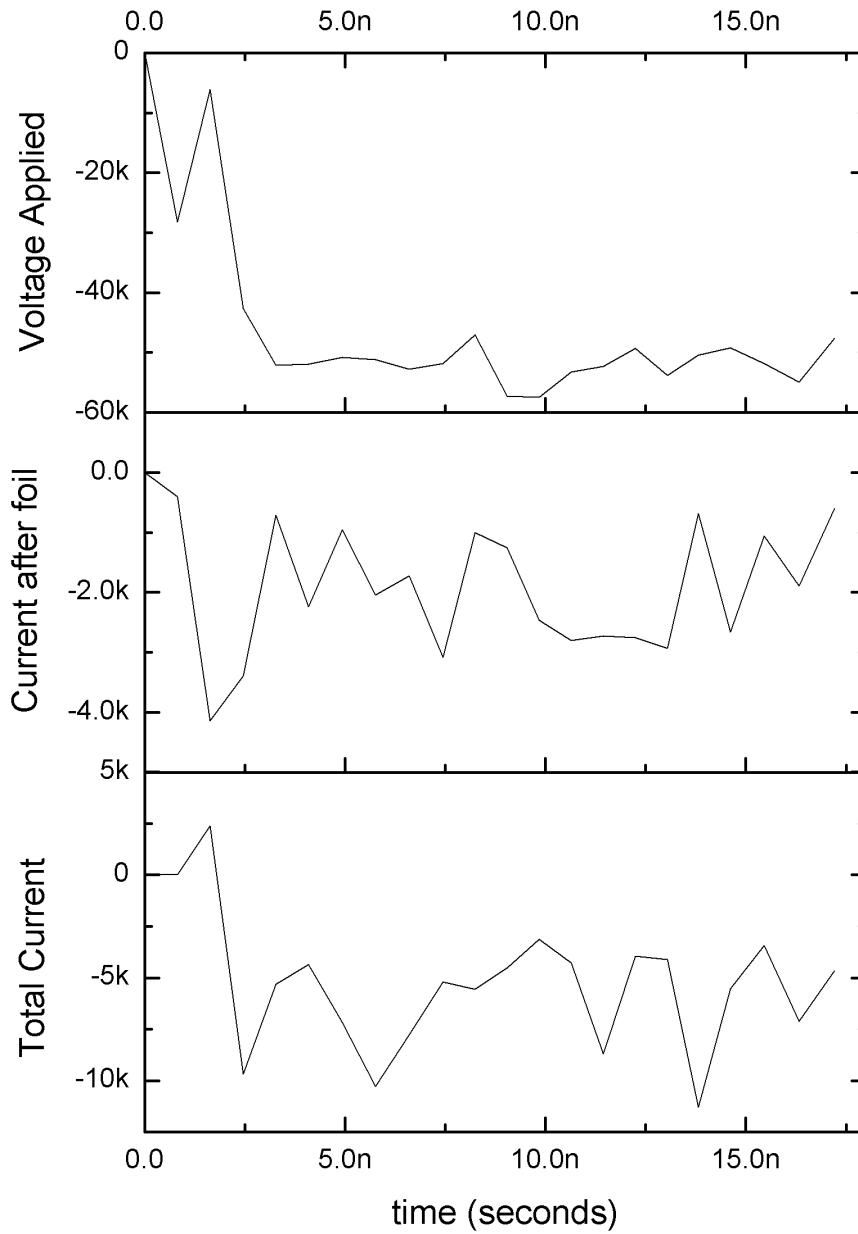


Figure 6.23: Simulation Voltage, total Current and the current after foil measured in the XOOPIC simulation

electric field: [110, 111]. A very interesting study regarding the effect of background gas and the ionization is also reported by [112–114] for low voltage vircator with decelerating electric field. Another low voltage vircator operation using pin type stainless steel cathode vircator by the application of 60kV accelerating voltage is also reported in the literature: [104]. Conventional axial-vircators are already well reported in the literature: [124], [105–107, 123]. As far as experimental point of view is concerned it

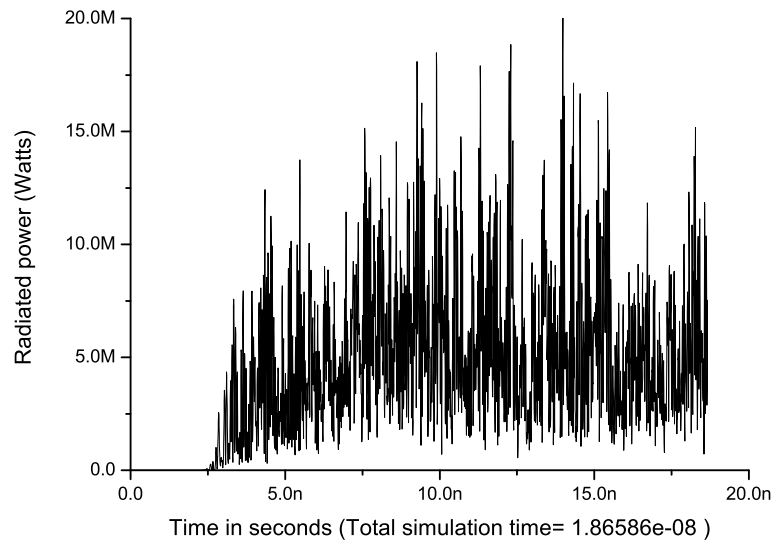


Figure 6.24: Power radiated in the simulation

becomes more and more tedious and complex task to make a pulsed power source which delivers higher electrical powers needed to drive the vircator at the hundreds of kilovolts of voltages. As the output voltage of the pulsed power source is increased, to meet the requirement of vircator, the associated system components become bulkier and bigger in size. This results from the requirement of breakdown strength of insulating materials used in the system design. It results in a quest to explore microwave emission characteristics of a vircator operating at the relatively lower voltages of operation which can be provided by a compact and easy-to-operate-with pulsed power source. Essentially

the problem gets bifurcated to two parts, one being engineering part to make a suitable compact and small pulsed power source and the other being to understand the physics of the axial virtual cathode oscillator when connected to such small and compact pulsed power source. A virtual cathode oscillator works when the current of a beam of charged

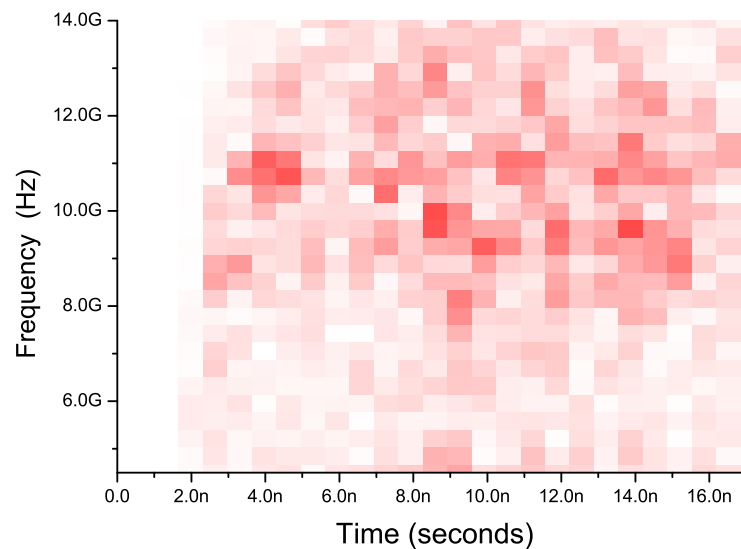


Figure 6.25: Instantaneous FFT of the radiated power and halved frequency to find the frequency spectrum of radiation in simulation.

particle moving inside a drift tube far exceeds the space charge limited current defined for that drift tube geometry. Under such circumstances the pinching inside the beam takes place and a virtual cathode is formed at the place where the density of charged particle is high and energy is in form of potential energy rather in form of kinetic energy. The region of these high density charge particles oscillates in space as well as in time leading to a radiation mostly defined by the density of the cloud of charge particles. Moreover the charges, which are still trying to replenish the beam current, get trapped between real and virtual cathode and also start radiating electromagnetic wave with a frequency depending upon reflection time for the charged particles between real and virtual cathodes.

6.3.2 Experimental Details

Viricator parameters In the present experiment we have used a viricator chamber made

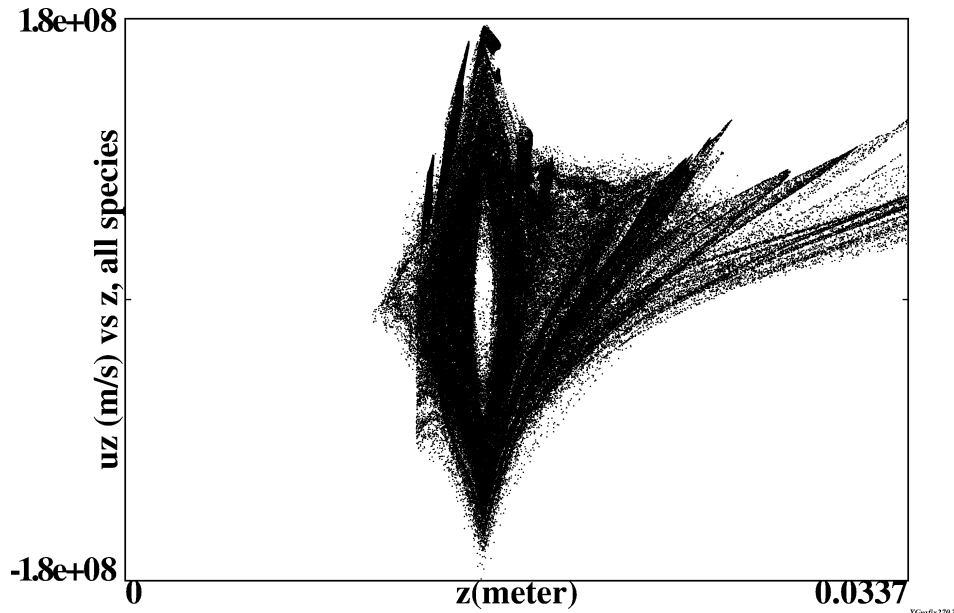


Figure 6.26: U_z versus z for the electrons trapped between cathode and virtual cathode at 18.66ns.

of stainless steel having a sheet thickness of 3mm. The cathode is made of aluminium which is covered with velvet on the electron emission surface using a silver epoxy based electrically conducting bonding agent. The diameter of the velvet area stuck on the aluminium is 50mm and the anode is made of stainless steel with an optical transparency of nearly 90%. In an interesting study done on carbon fibre cathodes [118,119] it has been shown that quite high ($280\text{-}440\text{A}/\text{cm}^2$) and almost uniform electron current densities are produced in carbon fibres. In a very recent published study by [120] the current densities in graphite s.s. nail cathode and carbon fibre cathodes at 200kV of applied voltage is also found to be similar. In the present set of experiments the gap between anode and cathode can be adjusted from 2mm to few centimetres. The electron-beam-diode zone of the viricator is evacuated to a measured 2×10^{-4} torr vacuum inside the viricator chamber. It is measured using the penning gauge connected with the vacuum chamber

directly. The vacuum measured at the mouth of the diffusion pump at the same time was still better than an order of magnitude. The vacuum inside the chamber is generated using a diffusion pump of 500litre/second pumping speed being backed by a rotary pump. The connection of the vacuum line between diffusion pump and the vircator is done using a 50mm diameter stainless steel bellow connected with a high voltage isolator of KF-50 port. The experiments were conducted with different anode cathode

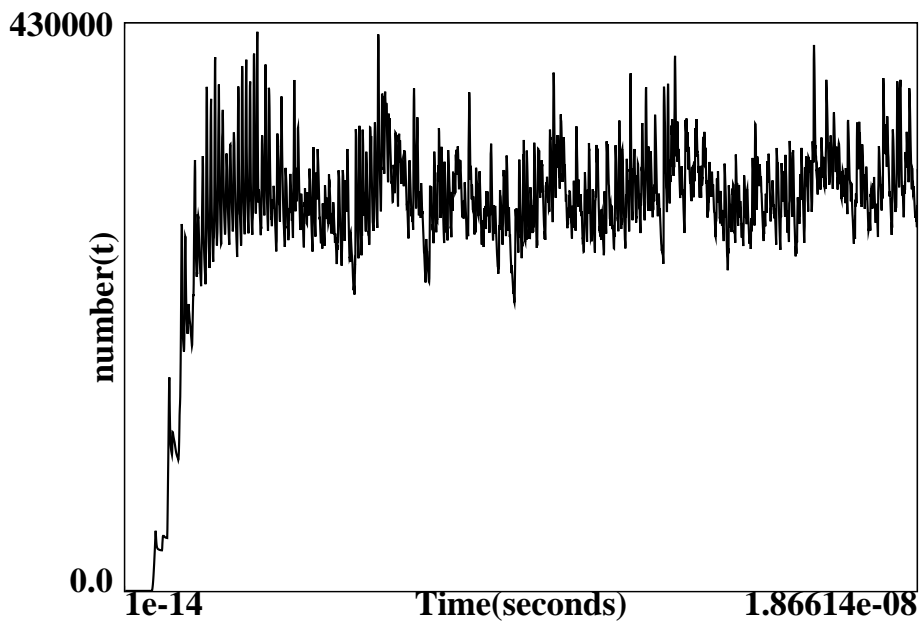


Figure 6.27: Number of simulation particles with time

XGrafix 2.70.2

gaps like 8mm, 7mm, 5mm and also at 3mm to enhance the microwave emission to a detectable/measurable value. It was observed during the series of such experiments that the anode-cathode gap of 3mm leads to maximum microwave radiation for fixed diameter of the cathode which is 50mm in all such cases of study. Consequently, we are presenting the results of 3mm anode-cathode spacing in this paper which has shown maximum microwave emission from the device. We also have connected a conical horn antenna to the vircator output window made of Nylon. The input of the conical horn antenna matches with the diameter of drift tube which is 112mm in dimension and out-

put side of the horn antenna is 412mm aperture diameter which is flared at an angle of 30° (cone half angle) from the antenna input end. The calculated gain of horn antenna is nearly 16dB at frequency of 6.0GHz. The length of the drift tube between antenna input port and anode is 1meter. The complete vircator system is made in such a way so that it can be fitted with the cable based pulse forming line (PFL) very easily The

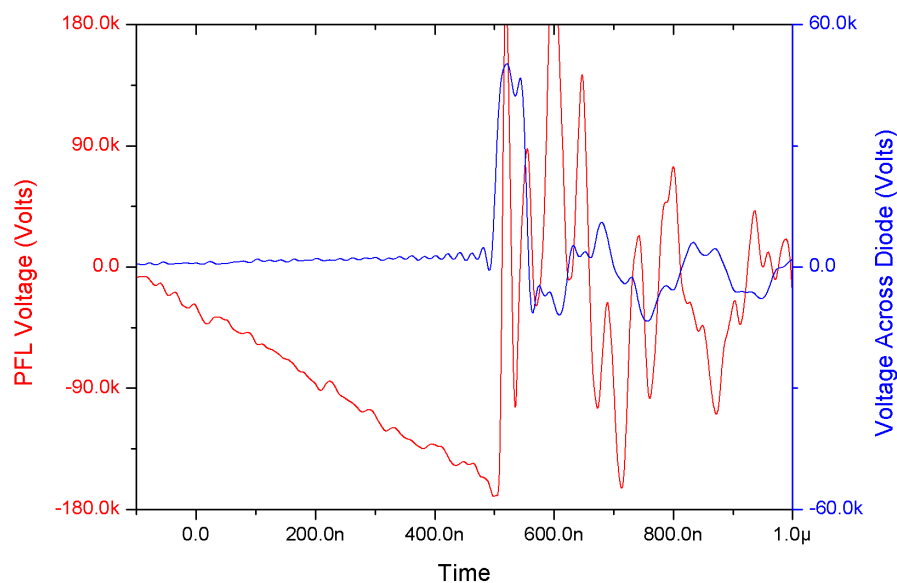


Figure 6.28: PFL charging Voltage and the diode voltage waveforms

central electrodes of all the four cables of PFL are press-fitted with a common point connected with one electrode of pressure-distance controlled spark gap which is connected between pulse forming line and the vircator and also controls the pulse forming line discharge into vircator. The braid part of the high voltage cables are connected to the S.S. chamber connected with the anode of the vircator using a flange based bolting method. Extra insulation inside the S.S. chamber between cable terminals is provided by using a properly shaped poly-propylene cylinder of 1.5inch thickness. The spark gap between the pulse forming line and vircator is filled with 2atm of absolute pressure of air. Figure 6.21 presents the physical picture of the virtual cathode oscillator used in

the experiment and figure 6.22 is geometrical drawing of the virtual cathode oscillator with input ports for 450kV, 60 Ω cables fitted with its standard connectors.

6.3.3 Energizing the vircator

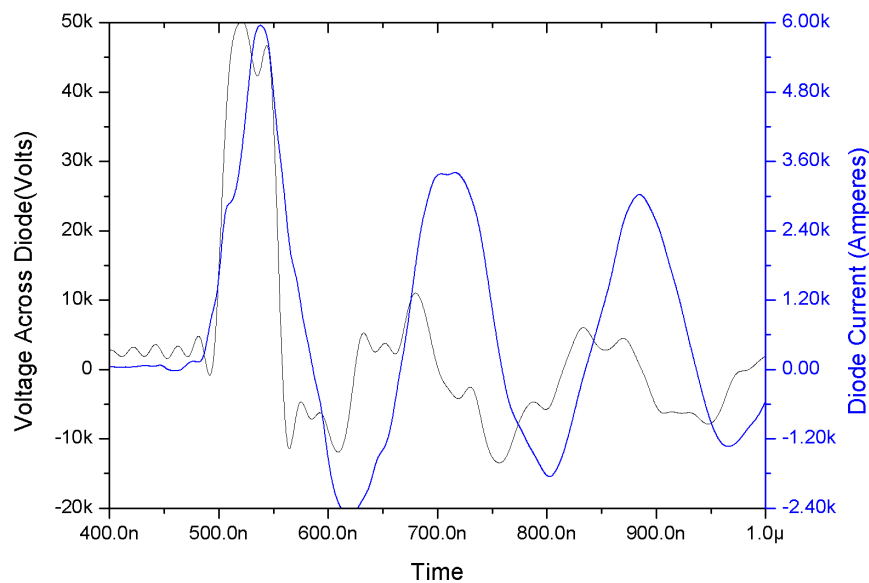


Figure 6.29: Diode voltage and diode current waveforms

The pulse forming line (PFL) is made using four equal lengths (5meters) of the high voltage (450kV) 60 Ω characteristic impedance cables connected in parallel to make a 450kV pulse forming line of 15 Ω characteristic impedance and nearly 50ns pulse-width. The capacitance of the pulse forming line is nearly 2nF. The pulse forming line is being charged using unipolar high voltage pulse in order to utilize the cable breakdown strength safely.

In order to characterize the vircator we have used the diagnostics (mentioned in detail in chapter 3) which are essentially electromagnetically coupled with the system and give their output as a time-dependent voltage pulse. To measure the diode current

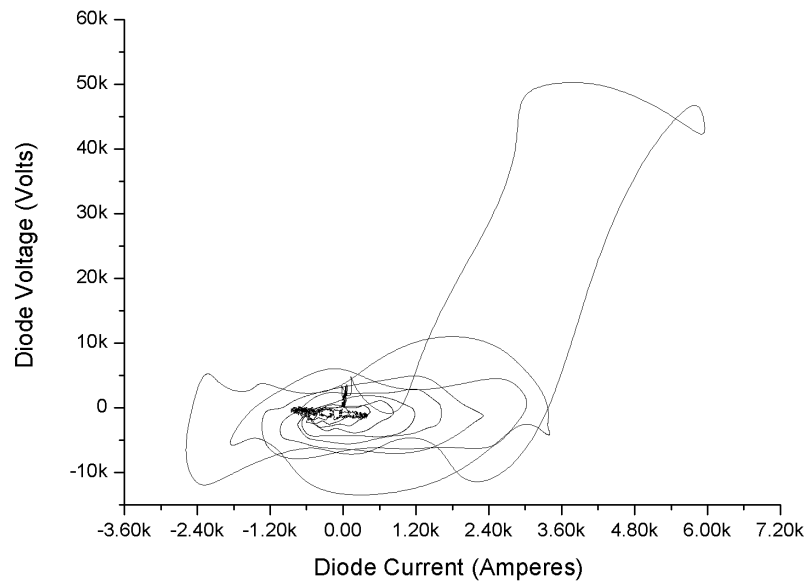


Figure 6.30: Diode voltage versus diode current showing single pulsed power dissipation

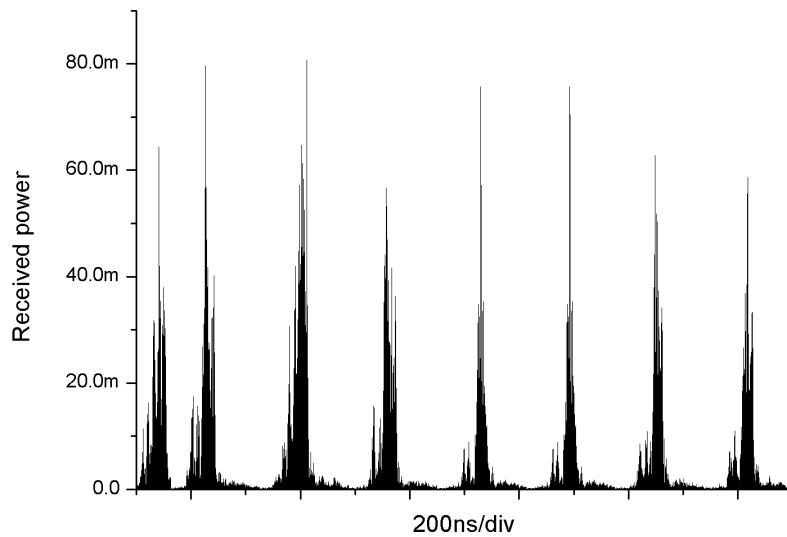


Figure 6.31: Microwave pulse with 40dB external attenuator measured at 2.5 meters from radiating antenna in 8 shots. (Power stability in different shots)

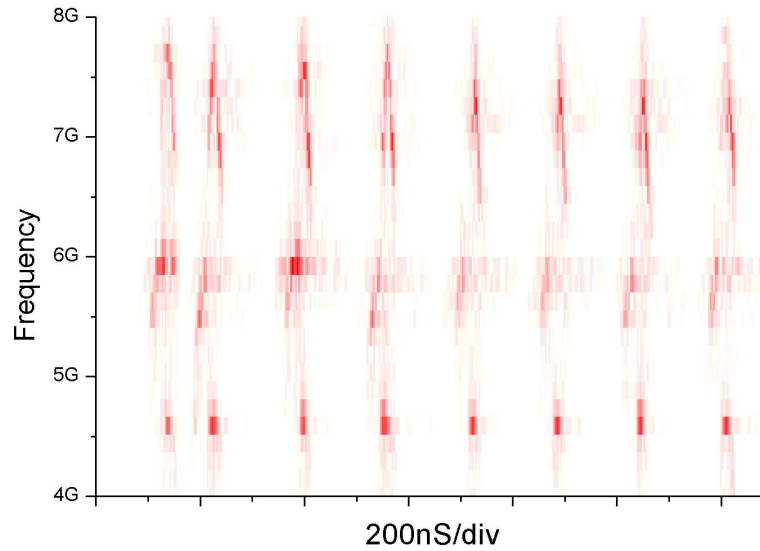


Figure 6.32: Instantaneous FFT of the acquisitions of previous electric field measurement. (Frequency stability in different shots)

and diode voltage we have used current transformer and voltage divider respectively. The voltage appearing at the diode is measured by a series cascading of two standard 100MHz bandwidth probes described in detail in chapter 2. The output waveform of the cascaded voltage divider is smoothed to 50MHz bandwidth by numerical techniques in order to incorporate the bandwidth loss of the cascaded probe resulted due to the series cascading and also due to additional connections used in the series cascading of the two similar probes as mentioned in chapter 2. The emitted microwaves are measured using wide-band double-ridged horn antenna with a gain of 12.5dB at nearly 6GHz with approximately flat frequency response from 4-8GHz connected to a high-bandwidth 50 Ω coaxial cable for final connection with the high bandwidth oscilloscope(10GHz, 40GSa/sec). To attenuate the received signal from the antenna, so that oscilloscope is not damaged by the input signal, we have used standard attenuators of broad DC-18GHz frequency range 40dB power attenuation depending upon the

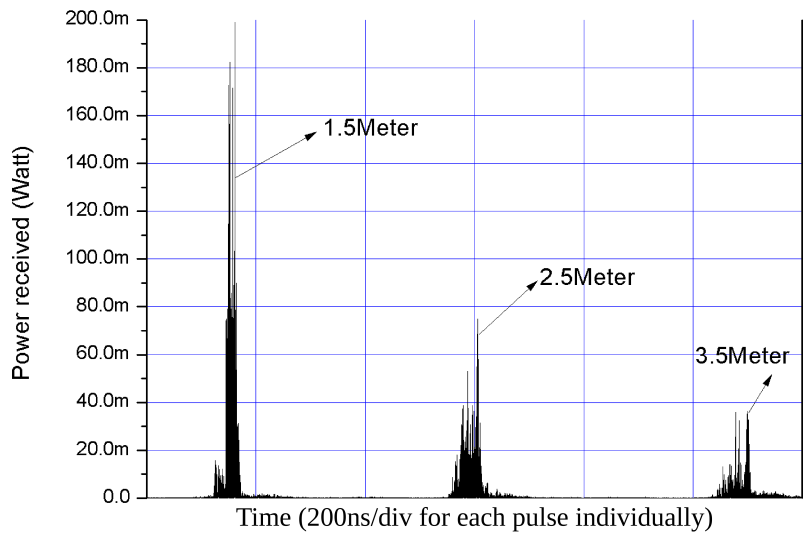


Figure 6.33: Microwave pulse with 40dB external attenuator measured at 1.5m, 2.5m and 3.5m from radiating antenna at the axis. (showing r^2 power attenuation) X-axis scale 200ns/div

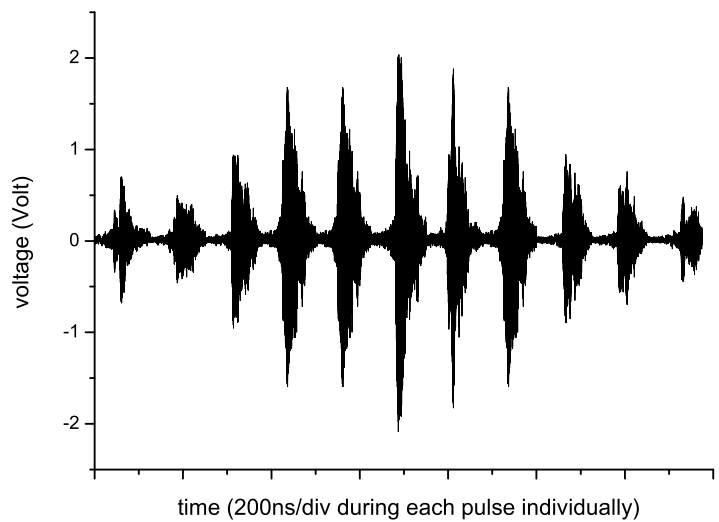


Figure 6.34: Electric field measured at 2.5meters from radiator when the receiving antenna is scanned from -45degree to 45degree on axis varying in angle of 7.5degree

measurement requirements. The attenuation imposed by the cables connecting the antenna with the oscilloscope is 3dB as is measured by the high frequency signal generator (operating in frequency range 4-10GHz) and the oscilloscope. The high bandwidth os-

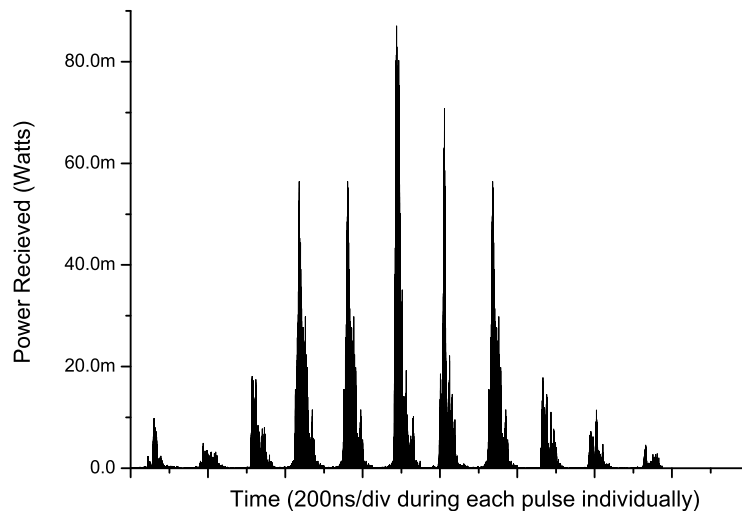


Figure 6.35: Power measured at 2.5meters from radiator when the receiving antenna is scanned from -45 degree to 45 degree on axis varying in angle of 7.5 degree

cilloscope with 10GHz bandwidth and 40GSa/s sampling rate was kept inside a 50dB shielded chamber with all its electrical power being provided by the uninterrupted power supply (UPS) kept inside the chamber. The diagnostic cable and power chord for UPS were provided inside the chamber using specialized input ports to maintain its shielding effectiveness for the frequencies of our concern.

Modelling Results (XOOPIC two and half dimensional particle-in-cell code) Extensive modelling for the results of low voltage vircator was done in a two and half dimensional computer code called XOOPIC (made available online by Plasma Theory Simulation Group, Electrical Computer Engineering Department, Michigan State University, and Nuclear engineering Department University of California, Berkeley) which uses particle in cell technique to solve the electromagnetic computational problem. The necessary

modifications in the available code were done in accordance with the scheme described by [121] et al and the results were obtained in the computation by using a time step of 0.01ps and a mesh size in axial direction is 0.25mm and in the radial direction is 0.5mm in the computational space. The applied voltage pulse total emitted current and current after the foil are collectively shown in the figure 6.23 The results are well depicting that the current emitted by the emitter is nearly 5-6kA which matches well with the obtained results for the same experimental setup as shown by the experimental results in the next section. The voltage pulse applied is having 1ns rise time and has been applied in radial direction through a gap which distributes the fields in the radial direction as per the radial location of respective mesh. Figure 6.24 shows the radiation pulse as measured at the output port as the integral of pointing flux at the output window. The graph shows that the emitted power is averaged at 5MW even though intermittent peaks of very short durations are seen for 15MW. The Fast Fourier Transform of the measured radiated power is shown in figure 6.25 and lies from 8GHz to 12GHz which is not very far away from our experimental findings reported in the next section. Figure 6.26 presents the u_z versus z graph of the charged particles trapped between the cathode and anode and is showing that the velocity is limited to $1.8 \times 10^8 m/s$ and hence the frequency of the radiation is not very high for very small gap spacings. Figure 6.27 presents the total number of simulation particles which is nearly 4.10^5 particles stabilized after 2nanoseconds from the beginning of the modelling. The number of simulation particles number of meshes and simulation time step decide the total time of computation or the problem space. For the computation of 18.66ns problem duration it is observed that computational run time is nearly 72hours on a 4GB RAM computer having 3GHz speed.

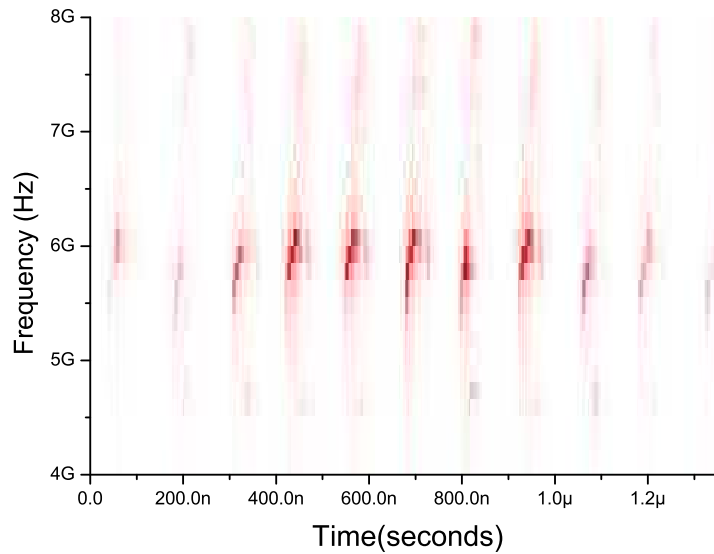


Figure 6.36: Instantaneous FFT of the signal of previous figure showing frequency stability between different shots. (Frequency(Hz) vs. Time(seconds))

6.3.4 Experimental Results

In figure 6.28 the pulse forming line charging voltage and the diode voltage is shown. It is shown that the charging of pulse forming line is done using monopolar pulse within $1\mu\text{S}$ from the beginning of the charging which is quite fast. The diode voltage is nearly 50kV peak which is very low for the conventional vircator operation as is mentioned in the literature to the best knowledge of the authors. In figure 6.29 the current and voltage inside the diode are simultaneously shown for showing a comparison and also to show that main power consumption is taking place in the first pulse only. Figure 6.30 shows single pulse dissipation in the vircator. It turns out that the diode current is 6kA leading to the diode impedance estimation of nearly 8ohms. As we know that the pulse forming line has a characteristic impedance of 15Ω and is charged to 160kV peak voltage hence a load impedance of 8Ω will have nearly 50kV voltage on it. It again shows that the voltage pulse appearing on the diode is well distributed as per the

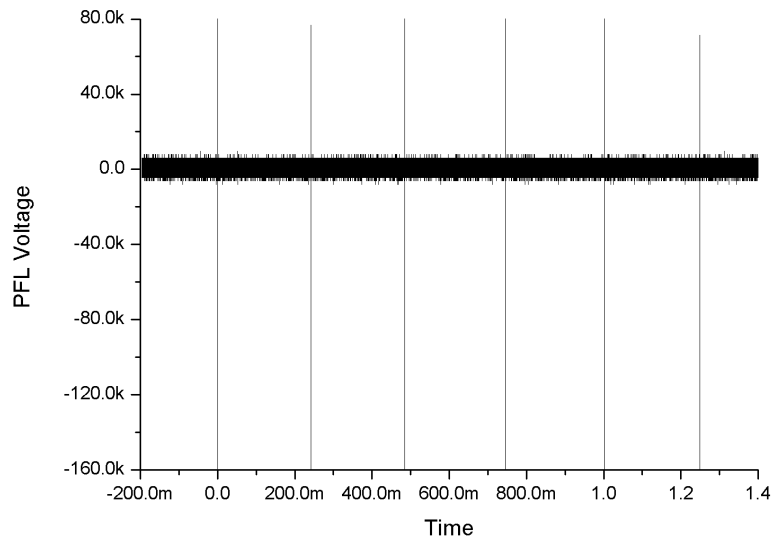


Figure 6.37: 4Hz discharge of the primary capacitor bank for the generation of the microwave in vircator; y-axis in volts

voltage division ratio with its source (PFL) impedance. The experiment was conducted to capture full amplitude by inserting a 40dB attenuator before the oscilloscope after the signal cable. The captured waveform is shown in figure 6.31 which is received by receiving antenna kept at 2.5meter away from radiating antenna. This figure contains the information about measured power in eight different shots showing that the power variation between different shots is insignificant. To show the frequency stability in the different shots the instantaneous FFT of the measured waveform of figure 6.31 is shown in figure 6.32. The frequency comes out to be ranging from 4.5GHz to 8GHz consistently in all the eight shots. To verify that the antenna measurements are done in the far field region we conducted the measurements at axis which are differing in the distance from the radiating antenna at three different points viz 1.5meters, 2.5meters and 3.5meters away from the radiating horn antenna. Three waveforms at each point were noted and plotted in form of figure 6.33 and it is evident from the figure that measurement at each point follows nearly r^2 dependency while going away from source

after 1.5meters away from radiating antenna hence the conducted measurement can be approximated with the far field measurement for the power estimation. Figure 6.34 and figure 6.35 show the measured electric field and measured power respectively when the receiving antenna was rotated with an angular displacement of 7.5degree from -45degree to +45degree in a radius of 2.5meters from the radiating antenna to capture the radiation pattern of vircator. A peak voltage of 85milliwatt at the central axis was measured with a cone half angle of 15 degree was observed by the noted radiation pattern and recorded. The peak radiated power after calibration factor put into the calculation comes out to be 0.85MW. The efficiency of the low voltage vircator reported in this paper is coming out to be nearly 0.3% if compared with the input power of the electron beam which is 50kV and 6kA. The spectral density as a function of time of the recorded waveform is shown in figure 6.36 which shows that the frequency content has chirping in every shot starting from 4GHz to 8GHz and the frequency content is not changing from shot to shot. The repetitive operation of the vircator is shown in figure 6.37 which shows the PFL voltage during this sequential shots at 4Hz. The respective radiation patterns of all sequential shots are shown in figure 6.38 with the time scale adjusted so that the we may easily compare the modulation and amplitude of each pulse to see the stability of radiation in different shots.

6.4 Conclusion

The results of the vircator driven by the different pulsed power sources are summarised in the table 6.1. It is quite evident at the end of this chapter that the systematic progress has been made starting from the first set of experiments conducted with a bulkier pulsed power generator to the third set of experiments which have been conducted using a compact pulsed power generator which is lighter in weight also.

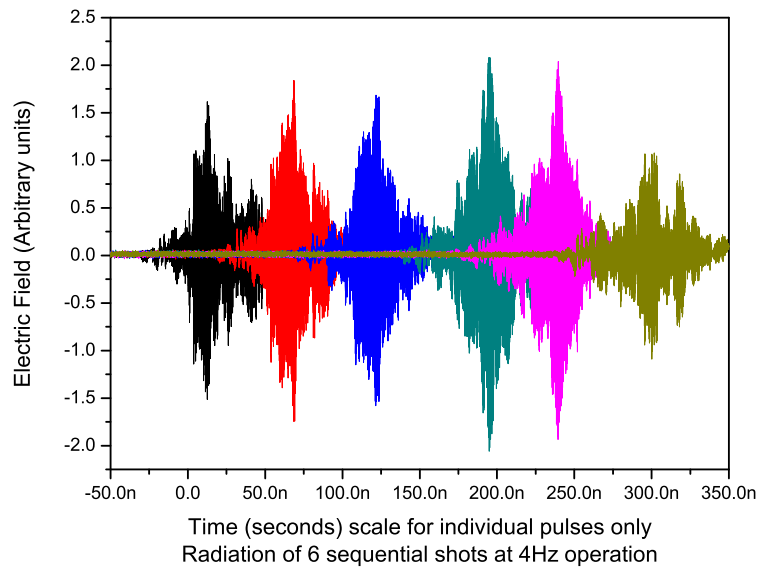


Figure 6.38: Radiation of vircator at 4Hz (6shots electric-field recorded) shifted in time scale to show the peaks and modulation

Table 6.1: Summary of vircator experiments

Sr. No	Description	First set	Second set	Third set
1	Diode voltage	7.1 μ F	2.46 μ F	3.5 μ F
2	PFL Voltage	120kV	160kV & 180kV	180kV
3	Anode Cathode Gap	5mm	4mm	3mm
4	Cathode Material	Graphite	S.S.	Red velvet
5	Cathode Diameter	60mm	60mm	50mm
6	Antenna	No	No	Yes
7	Results	2GHz Microwave for 20ns duration	6-7.5GHz for 50-60ns	Burst of 1MW at 4Hz repetition

A successful operation of vircator is demonstrated in the second set of experiments using a compact pulsed power source. The energy involved in each experiment was 125Joules making the system efficient in terms of power compression and shaping and also for a futuristic view of achieving repetitive operation.

In the third set of experiments, if we consider that the maximum area that can cause the formation of measured electron current is equal to the cathode area and the electron beam is nearly uniform, then interestingly the current densities achieved with velvet cathode are also nearly $300A/cm^2$. The simple method of capacitor bank charging topology makes it possible to operate the vircator at nearly 4Hz of repetition frequency which is shown in results of the discharge waveforms of the primary capacitor bank. The glow on neon lamps array and resetting of the computers kept in front of output window with assisted microwave coupling from the vircator are the qualitative inferences of electromagnetic emission from the vircator device whereas the Fast Fourier Transform of oscilloscope signal gives the frequency spectrum of radiated emission lying in the receiving range of the antenna. It comes out that the emission ranges in the range of 4-8GHz and frequency chirping during each shot is also well observed in the recorded radiation pulse of the virtual cathode oscillator. The shot to shot stability of power and frequency is also well demonstrated in the experiment. The experimental results are very much consistent with the extensive simulation/modelling results presented in this paper.

7

INDUCTIVE-STORAGE-CUM- OPENING-SWITCH DRIVEN VIRCATOR

In this chapter we are presenting the results of extensive study (experimental and theoretical) done on the exploding wire based opening switch *cum* inductive storage driver for driving a load of 10-20 Ω so that a driver may be made for delivering high electrical power for driving a vircator (virtual cathode oscillator) which has already been shown to be operating from 50kV voltage onwards leading to measurable experimental effects caused by emitted microwaves and is presented in chapter 6. The experiment reported in this chapter was conducted in two steps to deliver finally 1.5GW electrical power on 10 Ω load in very compact configuration and by using single optimized bare copper wire.

COMPONENTS OF EXPERIMENTAL SETUP

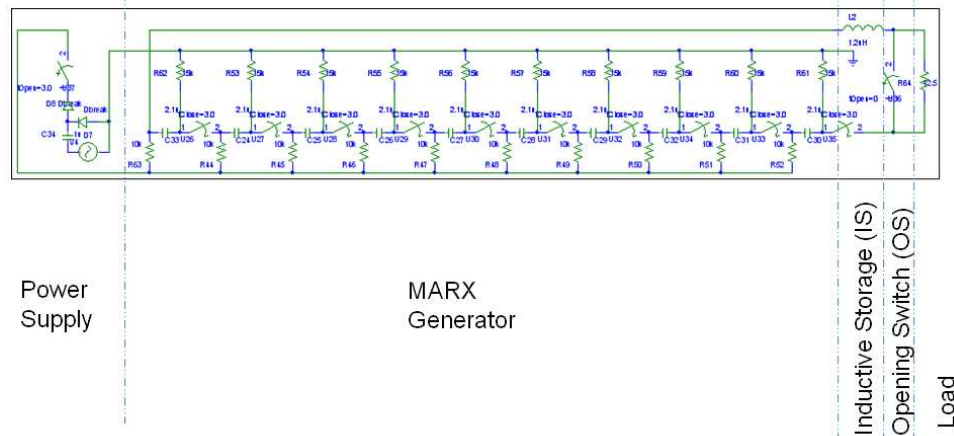


Figure 7.1: Schematic of inductive storage type pulsed power supply

7.1 500MW SYSTEM AND ITS MODELLING WITH THE VIRCATOR

Electrical energy storage methods are major design components for high-power-pulsed electrical delivery systems as they are part of essential involved mechanism of storing energy in long span of time and then delivering this energy in a desired load in very small time duration making the amount of peak power delivery in the order of Megawatts or Gigawatts. The loads requiring such high power delivery are mainly pulsed accelerators for electron and/or ion beams. This high electrical power is used for generation of pulsed high power electron beams, which, after its interaction with its neighbourhood, in turn generates high power microwaves (HPM) suitable for various applications. Moreover, antenna or Ultra Wide Band (UWB) systems also make use of such high electrical powers (of course after pulse conditioning) for direct generation of High Power Radio Frequency radiations. Broadly these energy storage methods can be divided in two parts one being capacitive energy storage and other being inductive energy storage. The energy density in inductive storage techniques can be order of magnitudes higher than that

of capacitive storage energy density. This advantage of high energy density of inductive storage method (i.e. realization of a compact pulsed power source) as compared to capacitive energy storage system) comes with added difficulty in the operation or optimization of the system.



Figure 7.2: Experimental Setup with Marx generator

The inductive storage driver works on following principle. When a current flowing through a circuit, which has inductor as a circuit component, is interrupted by use of an opening switch that changes its resistance very fast, the inductor tries to maintain the flow of currents through itself. If opening switch has another parallel circuit of high impedance load then this forced current will flow through that parallel load and a high voltage pulse (also of high power) will flow through the load.

7.1.1 Experimental arrangement

Inductive storage can be primed by a Marx Generator [135]. A compact Marx bank of 10 stages energizes the inductive storage driver. Each stage of the Marx bank consists of a capacitor of 2.1microfarad, which is charged to 4.5kV in parallel with other stages and

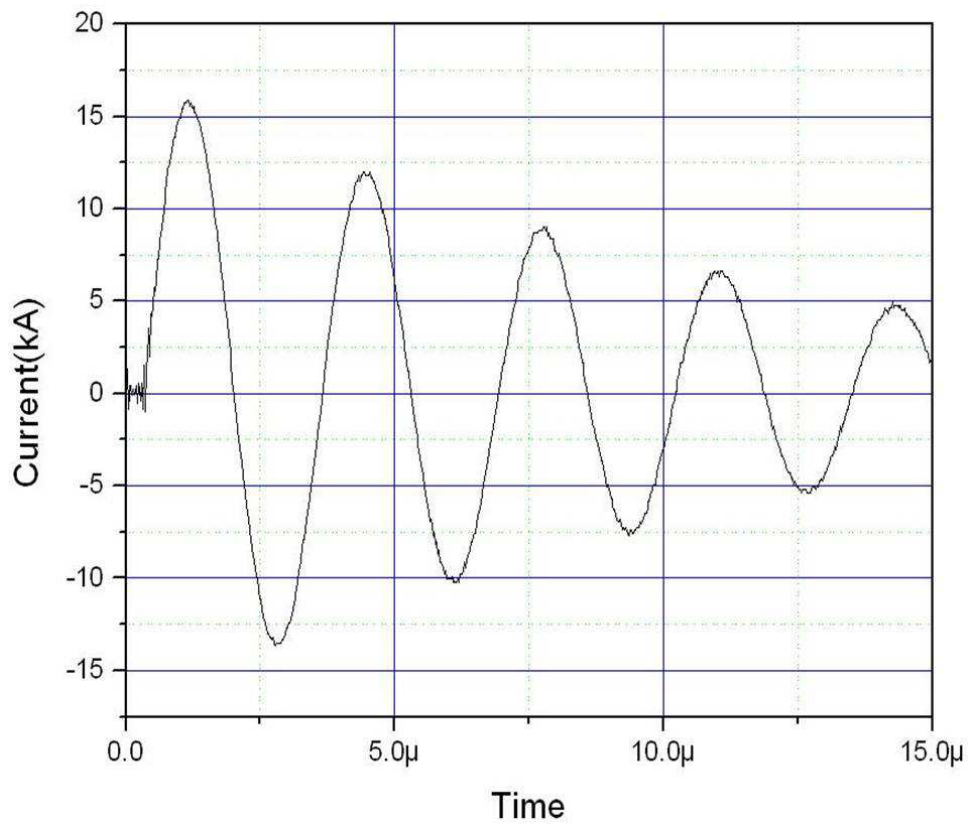


Figure 7.3: Short Circuit current of driver

is finally discharged in series to give open circuit voltage slightly less than the product of the charging voltage and number of stages. The trigger for the Marx generator is given by manual operating switch at the centre of 10 stages. The schematic of Marx generator and load assembly is presented in figure 7.1. The noteworthy point here when comparing with reference [135] is that the inductance driving opening-switch is not externally put into the circuit. It is the self-inductance of the geometry of the Marx bank plus the load inductance. This makes the generator compact. The weight of inductive storage driver is less than 10kgs. The charging system is also made portable as the

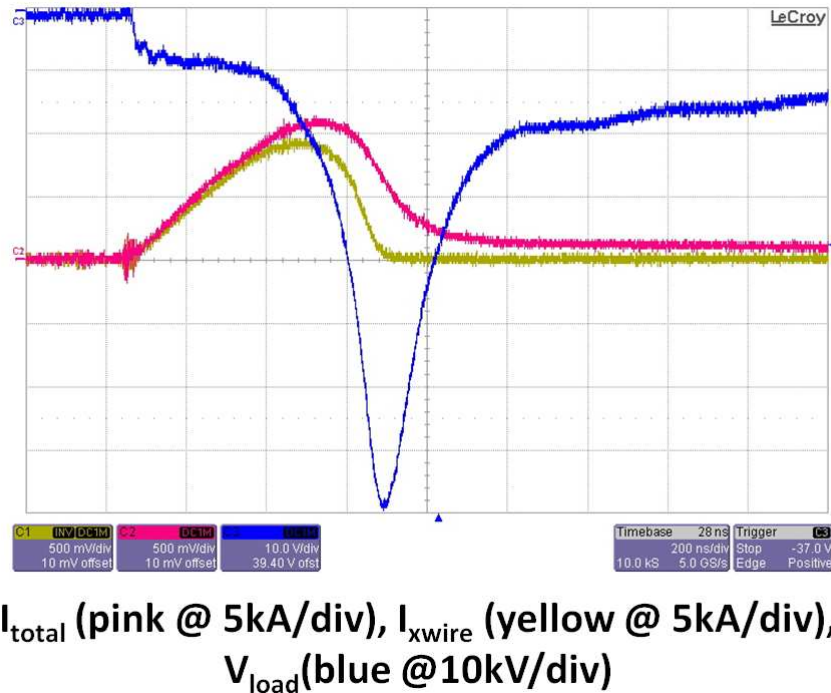
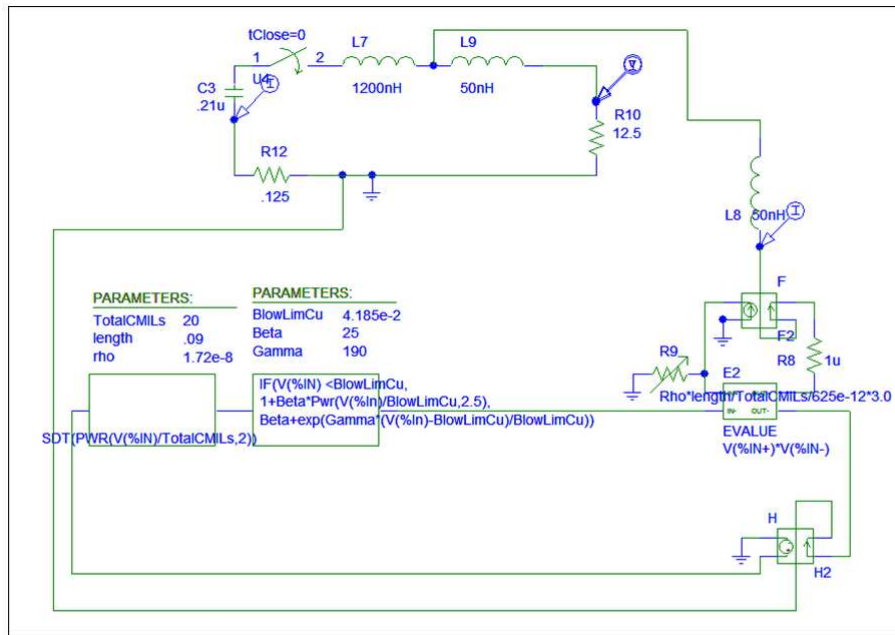


Figure 7.4: Total current (pink) 5kA/div, Exploding wire Current (yellow) 5kA/div, Load Voltage (blue) 10kV/div: Horizontal Scale 200ns/div

battery is used to initiate the inductive storage driver. It could have been made possible, as the energy/charge requirement for the operation of the system is not very high. The 12-volt DC is first converted to the 12Volt alternating pulses using astable-multivibrator of nearly 1A current ratings. The output of this astable-multivibrator is fed to the 9-0-

9 Volt to 1.6kV rms high voltage transformer. A voltage doubler circuit doubles the output of this transformer and then by passing it through a high voltage diode it is used for the charging of capacitor of Marx generator. The experimental setup is shown in figure 7.2. The air is used as the quenching media for the opening switch. The



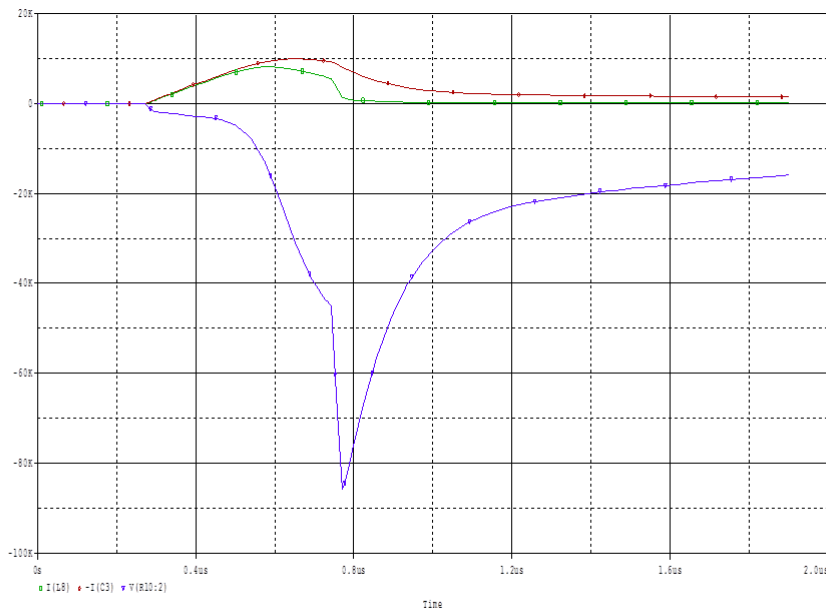
Equivalent Circuit of IS for fixed load viz 12.5 ohm

Figure 7.5: PSPICE model of inductive storage system

opening switch is exploding copper wire of optimized dimensions. The opening of exploding wire switch is optimized such that its explosion occurs at the peak of current flow through the inductive storage driver. The optimum length and optimum diameter of the opening switch in present system is experimentally found to be 9cms and 122 μ m respectively. The load used in the experiment is made from copper sulphate resistor. After early testing of generator, the ceramic disk resistors of high-energy ratings are used for the experiments.

For the measurement of the parameters of the inductive storage driver various current and voltage diagnostics have been used. Voltage measurement at the load is done using

a 75MHz 100kV voltage probe having 1000:1 attenuation ratio. Current measurement for total current and fuse current is done by high bandwidth current transformers with a sensitivity of 100V/A and 100X attenuator before the oscilloscope.



I_{total} (red) 10kA/div, I_{X_WIRE} (Green) 10kA/div, V_{Load} (blue) 10kV/div: Horizontal Scale Time @ 100ns/div

Figure 7.6: Total current (red) 10kA/div, Exploding wire current (Green) 10kA/div, Load Voltage (blue) 10kV/div: Horizontal Scale 100ns/div

7.1.2 Experimental Results

A peak discharge current of 16kA is observed during short circuit erection of Marx generator. The peak current is observed at 800ns delay from the beginning of discharge. The short circuit signal was recorded without using the opening switch i.e. by putting thick wire instead of thin exploding wire. The waveform is shown in Figure 7.3. Computationally it corresponds to the $1.2\mu\text{H}$ total circuit inductance of the driver. The erected capacitance of Marx generator is taken to be $0.21\mu\text{F}$. A circuit resistor of 0.125Ω is seen to be appearing in Marx bank discharge circuit considering 40kV erection voltage

which is nearly 90% of full erection voltage i.e. 45kV. The complete compact energy

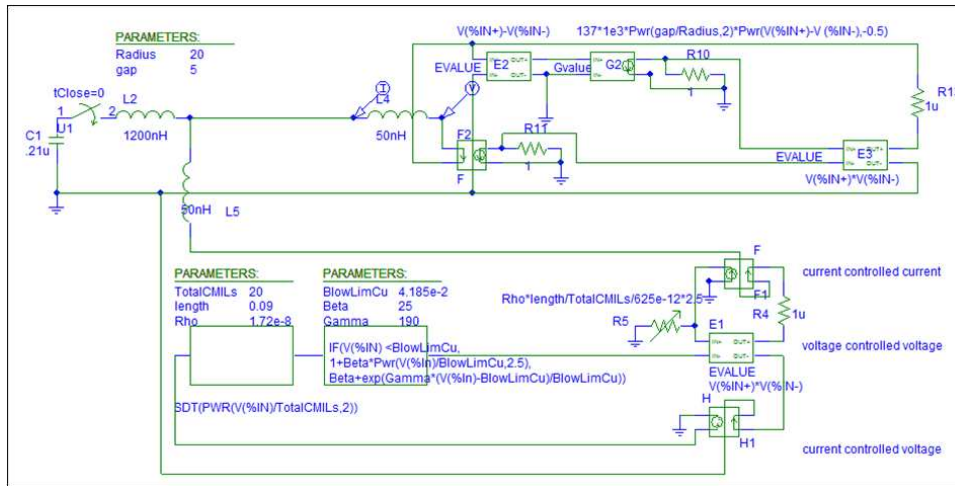


Figure 7.7: PSPICE model of inductive storage system with vacuum diode

storage device has shown its capability of delivering a peak of 80kV with 200ns FWHM (full width at half maximum) in a 12.5Ω load. The corresponding powers delivered to the load are 500MW. The corresponding waveform is shown in figure 7.4. The longer rise-time of the waveform is because of the reason of continuous flow of current in load right from the beginning of discharge. In order to sharpen the pulse a closing switch is also required and it will help in reducing the rise time of the load voltage pulse. This closing switch before the load connects the load by self-breakdown mechanism which disconnects the load during initial stages of opening switch action thereby clipping the initial slow rising part of voltage pulse. Nearly 50ns rise-time is expected in such cases. In order to simulate the whole experimental activity reported so far and to propose the interfacing of such system with different loads of interest we have taken the modelling mentioned in reference [48]. The spice [74] circuit solver is used to model and solve the circuit equations related to the physical phenomenon of heating of wire and then burst occurring at the end of event. The pspice equivalent schematic of our experimental arrangement is presented in figure 7.5. The complete Marx circuit is converged to its lumped parameters for the sake of simplicity in calculations. As the frequency is low the

lumped model is capable of simulating the desired currents to match the experimental values in short circuited system. The modelling results are presented in figure 7.6 with

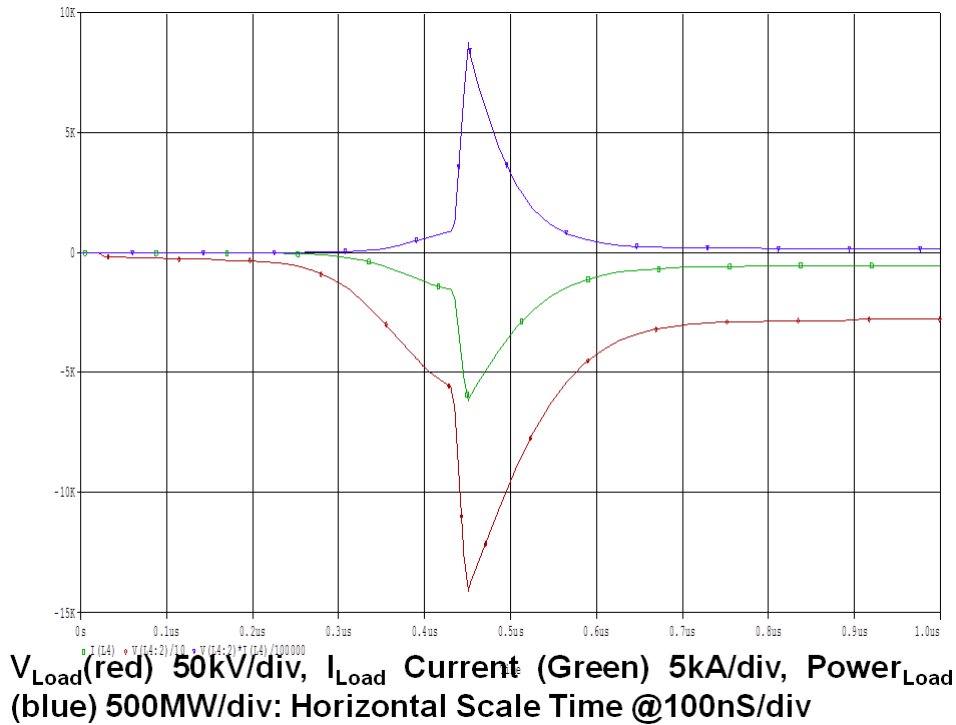


Figure 7.8: Load Voltage (red) 50kV/div, Load Current (Green) 5kA/div, Load Power (blue) 500MW/div: Horizontal Scale 100ns/div

dotted line style of waveform presentation. Respective scales are written using small divisions. Please note that in order to match experimentally achieved peak voltages, its pulse width, other current value parameters, it has been found that value of initial resistance should be kept nearly 2.5times higher than DC resistance. To some extent it seems reasonable also because skin effects are expected to dominate at higher frequencies leading to higher initial resistance values. The inductance of exploding wire and load are taken to be 50nH which is again on realistic assumptions. A slight mismatch of 80ns in the timings of the occurring peak voltage at load is seen in the simulation results. For higher impedance loads like antenna (50Ω, 75Ω etc) the expected theoretical (simple one without considering quenching of wire) power delivery is even higher because in-

ductive storage driver acts as a current source and the voltage appearing at the load is the product of the voltage at the load and current passing through the load. The only constraint in achieving such enormously high power delivery with inductive storage drivers is the voltage breakdown inside the exploding wire. Using suitable quenching media can increase the voltage breakdown limit of exploding wire. Once we have modelled

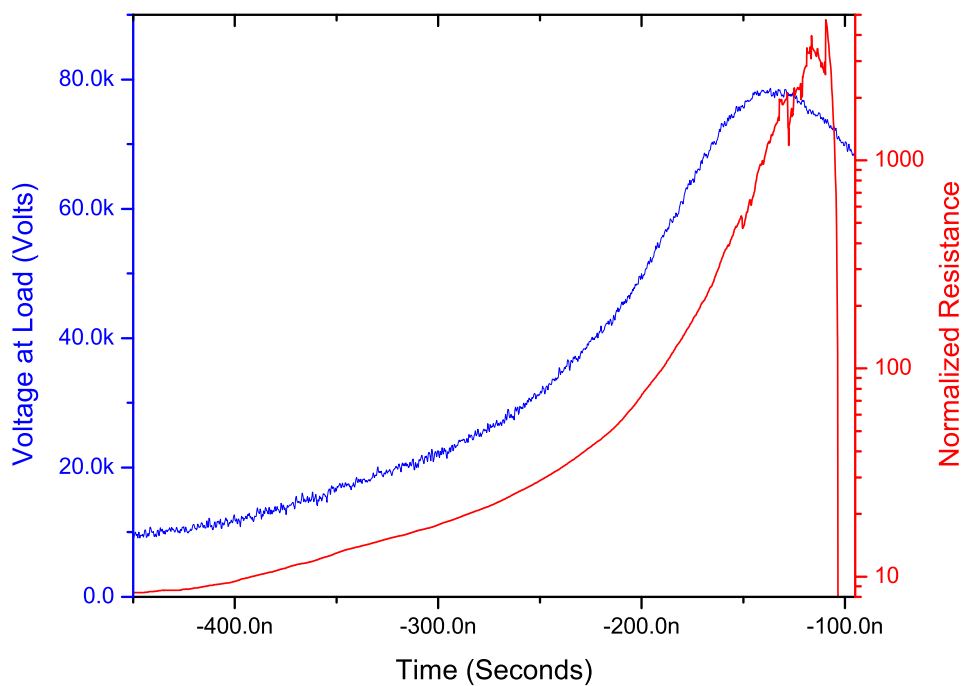


Figure 7.9: Normalized resistance of exploding copper wire

the inductive storage systems, we computed the amplitude and shape of the voltage and current and hence power pulse applied to a Vacuum field-emission-diode having a radius of 20mm and anode cathode gap of 5mm. For modelling the Vacuum field emission diode we have used the formula of impedance of planar electron beam diode which is in fact dependent on the voltage applied to it. This means one need to model a voltage controlled resistor following a relationship as that of field emission diode in planar ge-

ometry. The relationship of impedance (Z) of a diode in planar geometry is given by equation 1.2. The model of such assembly is shown in figure 7.7. The results of such modelling are shown in figure 7.8 with dotted line style of waveform presentation. The results predict the electrical behaviour of the system. A peak power of 0.9GW and a peak voltage of 140kV (100ns FWHM) is expected to be delivered by the pulsed power system in the electron beam load. Needless to say that rise times will be improved by putting a closing switch before the load. The normalized resistance of the exploding wire is shown in figure 7.9. Here the measured value of DC resistance (140m Ω) is used for normalization of the dynamic value of the resistance. The action on wire and the energy dissipated in the wire is shown in figure 7.10.

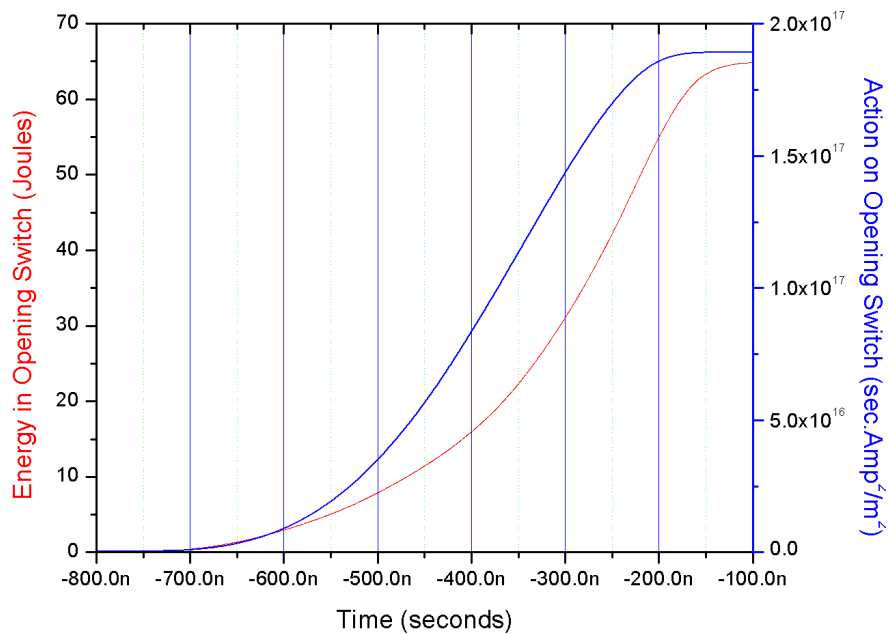


Figure 7.10: Action on wire and energy dissipated in wire

7.2 1.5GW Compact Generator

The results of a very-compact (confined into 0.20m cylindrical diameter and 0.75meter length) and light-weight (<15kg) pulsed-power generator, for driving HPM devices like vircator with load impedance of tens of ohms, are being presented in the paper. The load voltage at 10.5Ω is measured 125kV (150ns FWHM) with 1.5GW peak-power. The use of single-optimized-exploding-copper-wire along with the use of air for all the switches of the generator (closing switches of Marx generator and opening switch of exploding wire) make device very-attractive.

7.2.1 Introduction

The pulsed power generators for HPM load driving application become bulkier and heavier not only because of primary energy storage requirement, in many case explosives are used for electrical energy amplification for miniaturization, but also from the high voltage insulation requirement at different stages of power compression. If the environment is pressurized or in vacuum then the housing to create such environments make system bulkier and bigger. The aim of this work is to make a pulsed power generator which works in open air and is very easy to work with without compromising in the driving capability for a HPM load or similar load impedances. To have laboratory based setups it is not always possible to use explosive based electrical energy amplifiers and this constraint applies to this work as well and hence for the performance evaluation of the generator reported in this letter the devices which use the explosive means may be kept away from the consideration as they are not reusable. Moreover, it is also noteworthy here that idea of implementing more than single wire for optimized performance of inductive storage device itself is quite demanding in terms of preparing an optimized exploding wire assembly. Hence it was restricted not to use more than one single wire.

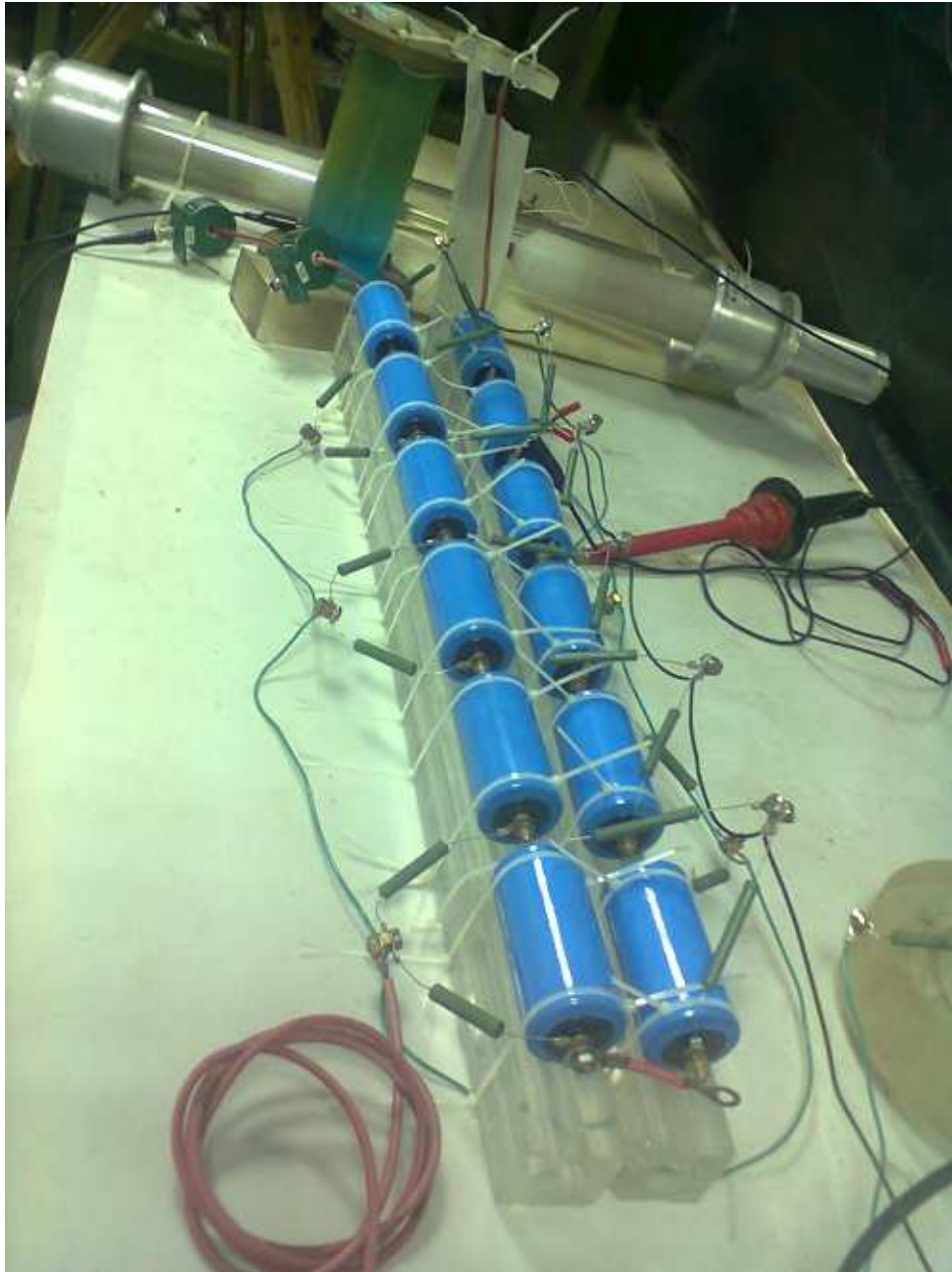


Figure 7.11: Experimental setup for the pulsed power source

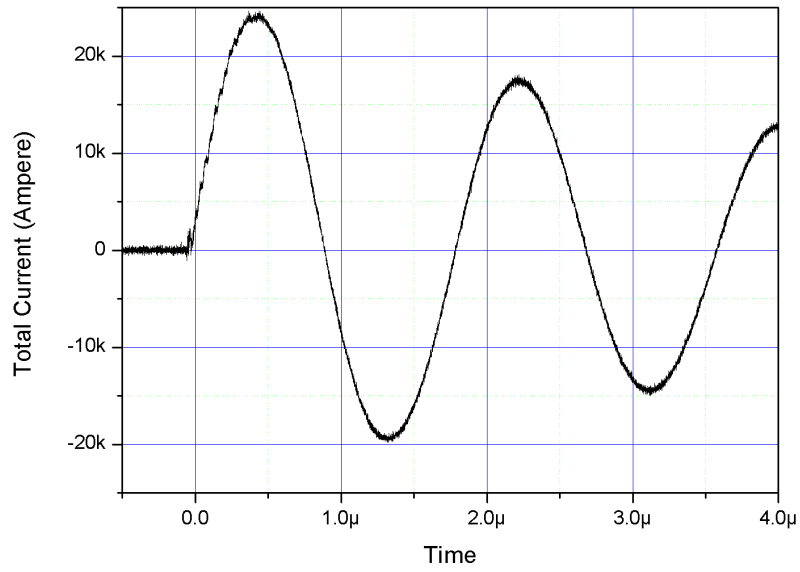


Figure 7.12: Short circuit current of the circuit

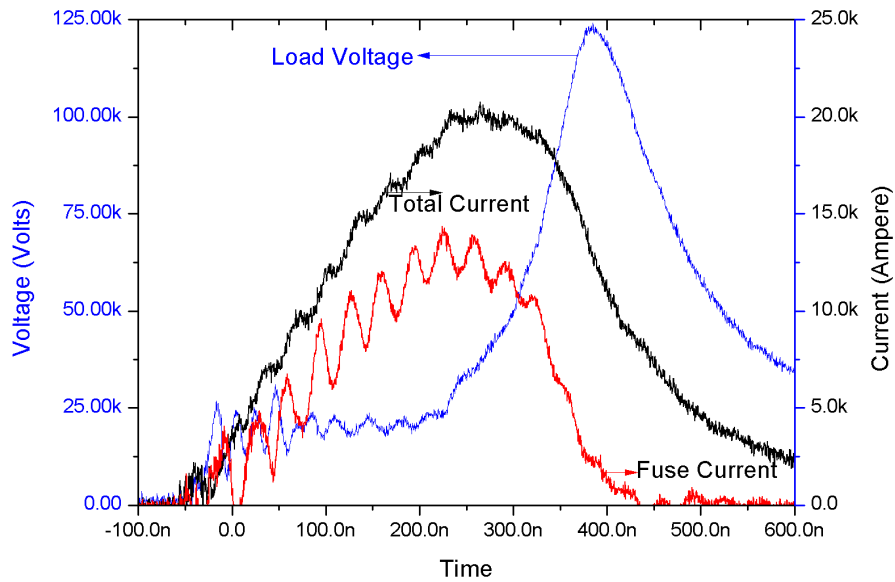


Figure 7.13: Load voltage and total current as well as fuse current of the circuit

Now as another requirement from the breakdown point of view, the length of wire should be sufficient to withstand the generated voltages in the air. Hence a longer wire of nearly 15cm is chosen to be used for the experiment. In another way, approximate length of 15cm of the exploding wire was the aim of designing the pulsed power source. Earlier in a different system we have worked with a length of 9cm and could reach a peak voltage of 80kV only in nearly 13Ω diode [142]. Once approximately length is decided, based on the previous experience and approximate estimation, it is found that 122micron diameter copper wire should suffice for such currents which are 25kA and reaching in nearly 500ns to their peak values. In order to generate such currents inside an inductive storage device, a Marx generator scheme was implemented using 12stages each of $0.68\mu\text{F}$ and a peak charging voltage of 10kV with peak energy of 39joules. This leads to the erected capacitance of 55nF and erected voltage of 120kV. Interestingly the Marx generator was made in such a way that it has two straight lines each having six stages and separated with increasing distance from trigger side (opposite to the load side) to the load side. The trigger for Marx generator discharge is provided with manual switch in between two halves of the Marx assembly. The separation between two straight lines of Marx generator also provides the inductance to the circuit which acts as inductive storage element in the circuit (see figure 7.11). It is quite interesting to note that because of the full access on every component of experimental setup, it takes only less than two minutes to change the exploding fuse wire and prepare the setup for next shot, which is not possible in the cases of pressurization of source or in the cases of explosive pulse amplifiers which can't be reused because of their very devastating nature. Table 7.1 represents the previous noted experiments where the Marx generator was used to energize the inductive storage device and then the opening switch (electro-exploding wire based) conditions the power going into the load. Reference [125] is very bulky as it requires huge energy to drive the wire for lightning application and reference [131]

is made using single spark gap and is also quite heavy using many wires in pressurized gas. Reference [132, 135] have too low current to drive the vircator as the total current output is limited to a few kAs which is just equal to even charge limited current of vircator, needed to be exceeded for virtual cathode formation. Reference [136] has driven the vircator to 20GW and 60GW in a big generator.

7.2.2 Experimental Results

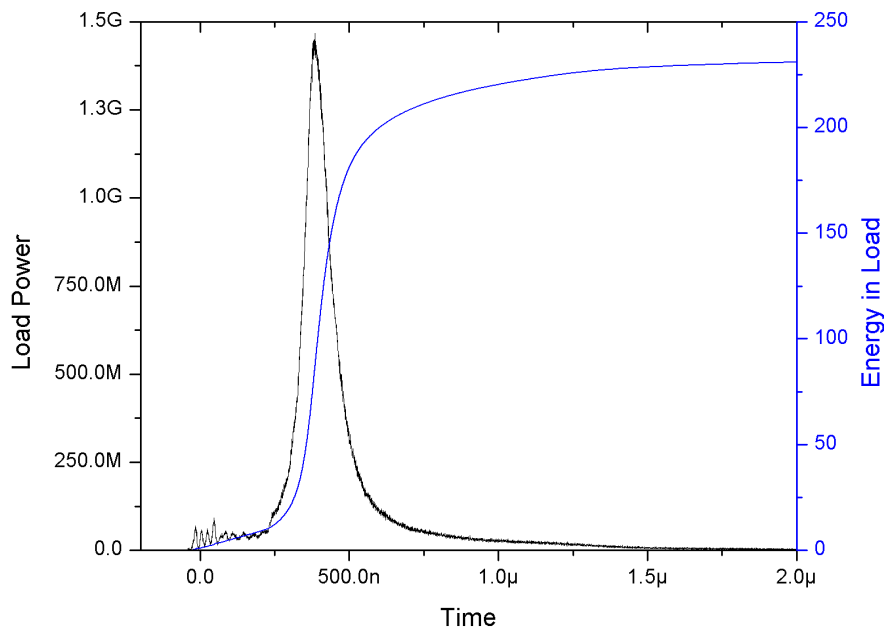


Figure 7.14: The power and energy dissipated in the 10.5Ω load

Figure 7.12 shows the short circuit current of the Marx generator based inductive storage device reported in this letter. In this acquisition the exploding wire was replaced with thick copper wire so that no change in circuit resistance takes place during current discharge and it is seen that the peak current in the discharge is 25kA when the Marx is discharged at 9kV charging of each stage. The time period and the peak amplitude

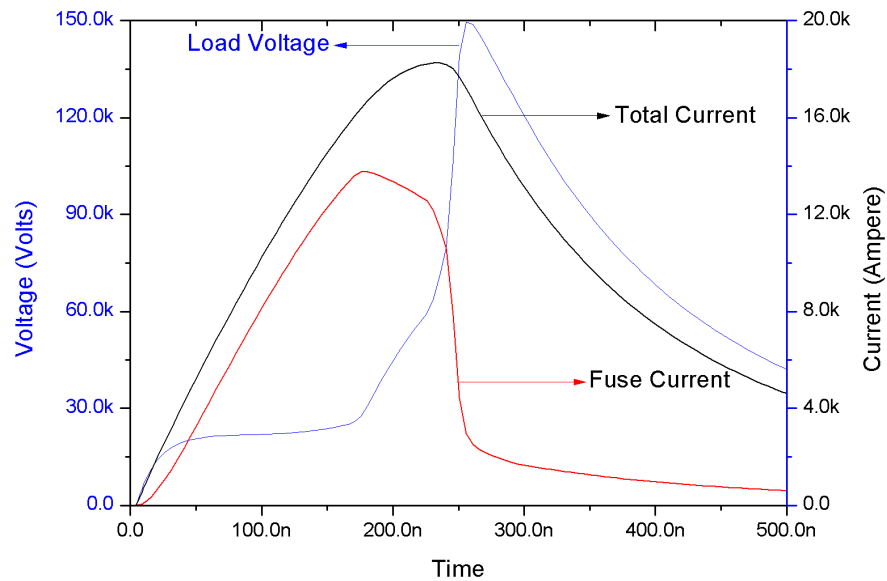


Figure 7.15: Modelling results of the pulsed power generator with 10.5Ω load without including delayed burst

with the voltage reversal taken into the consideration, it is inferred that the inductance is $0.9\mu\text{H}$ and the series circuit resistance is $400\text{m}\Omega$. The series inductance associated with the exploding wire is 200nH as is shown by the voltage pulse. The slightly lesser value of the fuse current as compared with the total circuit current, suggests that the part of current flows through the load which is connected in parallel to the fuse location presently shorted with thick wire. In the figure 7.13 the voltage across the load of 10.5Ω made of copper sulphate solution is shown along with the current waveforms of total current and the fuse current. It is shown that a voltage of 123kV is seen across the load with FWHM of 150ns . Figure 7.14 shows the amount of energy dissipated in load and also the power reached into the load. The energy dissipated in the load is quite a good fraction of the total energy of the capacitor bank at the outset. The power dissipated in the load is nearly 1.5GW .

7.2.3 Discussion with Analysis of Results

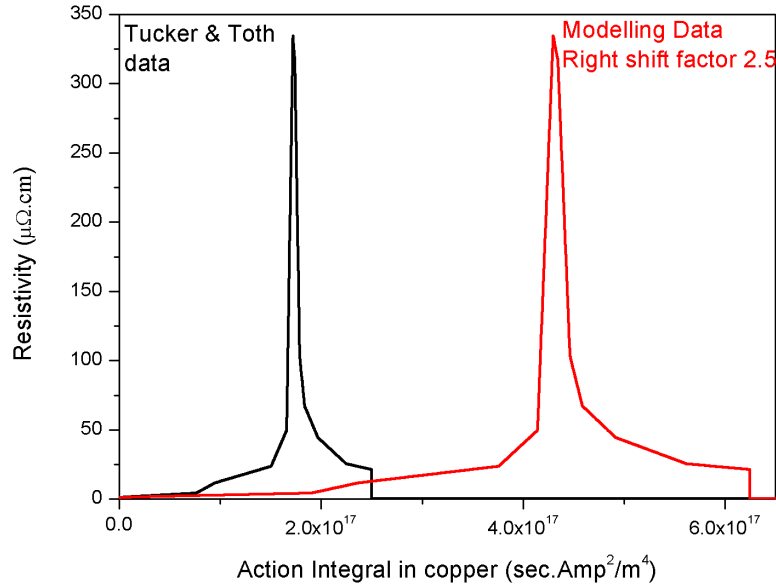


Figure 7.16: Original and modified resistivity of copper based on action integral

A modelling for the pulsed power generator along with the load is done. For action dependent resistivity value of the copper wire, the model proposed by Tucker and Toth [137] is used as basic guideline which is essentially limited to $10^{11} \text{ Amp}/\text{m}^2$ current densities and invites further studies for removal of this limitation. In order to simplify the computations using this model, equation based fitting has been successfully used in the past in which an event of burst (beginning of vaporization) is defined (action at burst is named action-to-burst and is noted to be $1.7 \times 10^{17} \text{ Amp}^2 \cdot \text{sec}/\text{m}^4$) below and above which the resistivity varies differently with the action [138]. In some other cases of modelling a third equation defining arcing is also considered [139] to achieve physical conditions in modelling. In later studied couple of references [132, 138] the action-to-burst is found to be $4.1 \times 10^{17} \text{ Amp}^2 \cdot \text{sec}/\text{m}^4$ and $4.7 \times 10^{17} \text{ Amp}^2 \cdot \text{sec}/\text{m}^4$ for current densities of $1 \times 10^{12} \text{ Amp}/\text{m}^2$ it was also proposed that to interpolate the action-to-burst between

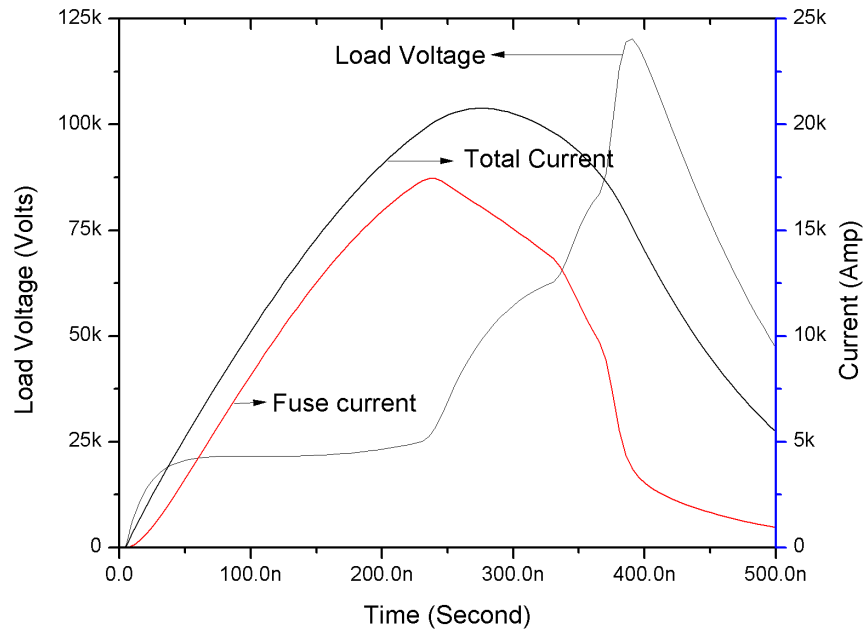


Figure 7.17: Modelling results of the pulsed power generator with 10.5Ω load including delayed burst

these values a linear fitting can be used [138] as the event of vaporization is delayed in higher current densities [132, 138]. Rather using equation based resistivity model which follows the trend of Tucker and Toth model for different phases, we have digitized the waveform of Tucker and Toth model and then we used this database for present modelling directly with linear interpolation between consecutive data points. The modelling results are shown in figure 7.15. The waveforms of the two cases are certainly having phase mismatch i.e. peaks are not occurring at same interval from the beginning of the discharge in modelling and experimental results. Moreover peak values of the voltage generated are differing by 20%. In order to remove this discrepancy, in a simplest approach, we tried different action dependent resistivity curves which were having same shape as that of Tucker and Toth model but were having scaled values of action integral (to include delayed burst by super heating) to solve the present experimental problem.

Figure 7.17 shows the results of the model which is scaled by a factor of 2.5 (as is shown in figure 7.16) on action axis of the Tucker and Toth model. An excellent match between experimental values and modelling results are obtained under this condition and if we back calculate the value of action-to-burst using this scaled model, it comes out to be $4.25 \times 10^{17} \text{ Amp}^4 \cdot \text{sec}/\text{m}^4$ which is nearly in same to so far reported values. The higher values of scaling factors applied for the resistivity model drastically reduce the computed load voltages and hence show that they can't be the solution of the present experimental case.

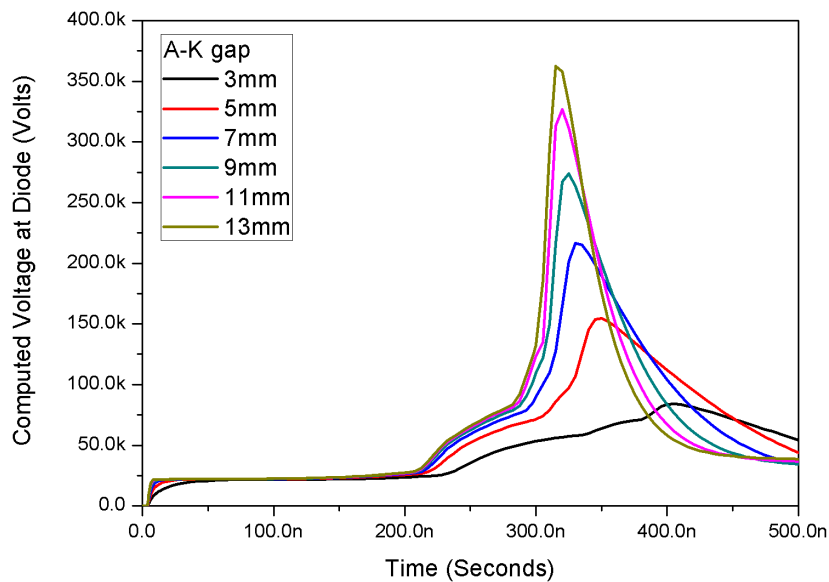


Figure 7.18: The computed diode voltage for different A-K gap

7.2.4 Summary

A reusable, ultra-compact and light-weight pulsed power generator is made using single optimized exploding wire in combination to the Marx bank driven inductive storage device. To reach similar or higher powers in loads, the demonstration of explosively

driven compact pulsed power sources is well reported but they can't be reused and require special environments which protects personnel from explosive hazards. Moreover the single capacitor bank driven systems are also very heavy and big and also involve very large amount of the initial energies. As the single capacitor banks are slow, they use multiple wires for the optimized current interruption which may not be very handy. Interestingly, this compact generator can also be used for the generation of high pressure, low density metal plasma as the current rise rate is 70Amp/ns and the current densities $1 \times 10^{12} \text{Amp/m}^2$ and 0.9GW peak power is dissipated into the wire which is in the same range as were previously utilized for experiments [140]. Even though the device is different, however, the present system is compared with the ultra compact Marx generator designed to directly drive reflex triode vircator at high repetition rates [141]. For 18.5Ω load impedance the present generator is modelled and found to deliver 200kV of load voltages which is 2GW load power and is same as that of the compact Marx generator reported previously. In other words if modelled for load of 10.5Ω the Marx generator delivers nearly same voltage and same powers as that is reported in the present experiment. Dimension wise the present system is comparable with the system reported previously however the weight of the present generator is quite low as compared with the weight of compact Marx based generator. Certainly the Marx based system (37kg weight reported for [141]) can be used in the repetitive mode but requires additional sub-systems to maintain high pressure SF_6 and air/nitrogen inside the Marx generator vessel. Additionally the cost of all the 12 capacitors used in the presently reported system is only 40USD and this feature is no less attractive when compared with the cost of 80 to 100 capacitors used in the compact Marx generator. The modelling results of this pulsed power system are presented in figures 7.17 7.18 and 7.19 for the diode impedances modelled on the basis of equation 1.2 without considering the gap closure event caused by expansion of plasma at the cathode and the anode. The results show the

voltage, current and power delivered at diodes for different anode cathode spacings and a fixed cathode diameter of 50mm.

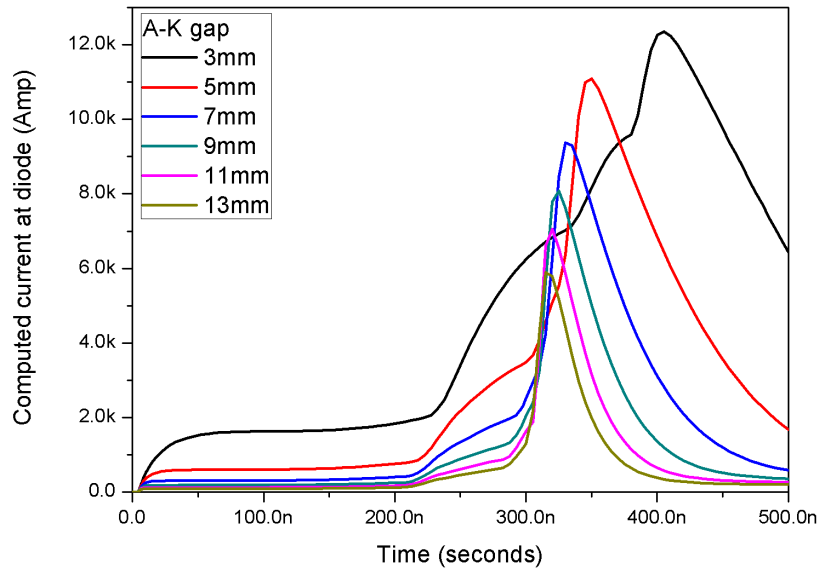


Figure 7.19: The computed diode current for different A-K gap

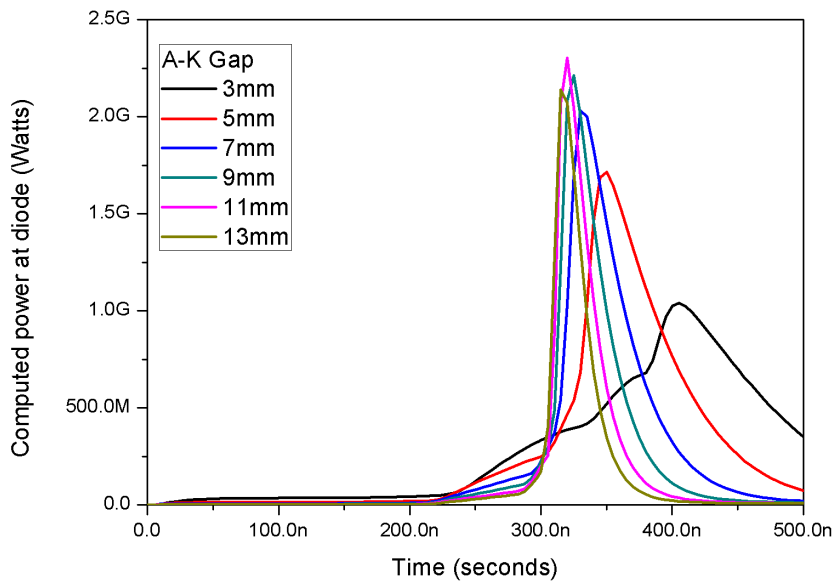


Figure 7.20: The computed diode power for different A-K gap

Table 7.1: Marx Generator driven Inductive Storage based pulsed power generator

S.No	Remarks	stages	$C_{marx}L_{marx}$	V_{marx}	I_{peak}	Wire	$Z_{load} V_{load}$	E_{marx}
1	Ref. [125] 6kV/m 720kg wt.	2 3	$2.85\mu\text{F}$ $1.9\mu\text{F}$	80kV 270kV	$I_{fuse} 10\text{kA}$	Enameled Cu 200 μm 36m	Xwire	46kJ 69kJ
2	Ref. [131]	2 stages bipolar 1 spark	$1\mu\text{F}$ $1.5\mu\text{H}$	180kV	150kA	56cm 0.35mmsq	10 Ω 500-600kV	16kJ
3	Ref. [132] 240mm dia 800mm len	16-18	580pF	250kV	0.1,1.0,2.0kA (estimated)	36,45,10 μm dia	overheating in fuse	18J
4	Ref. [135] size 60cm.120cm.150cm	5 stage	80nF $47.7\mu\text{H}$ $177\mu\text{H}$	100kV	$I_{fuse} 1.2\text{kA}$	35cm 40cm	20k Ω 600kV	400J
5	Present Thesis	12 stages	$.055\mu\text{F}$	120kV	25kA	122 μm 15cm	10.5 Ω 123kV	400J
6	Ref. [136] N_2 at 2atm Marina	6 stages	$0.53\mu\text{F}$ $10\mu\text{H}$	300kV	25kA	-	-	23kJ
7	Ref. [136] N_2 at 2atm 3 Marina in		$1.6\mu\text{F}$	360kV - -	100kA - -	-	-	104kJ

7.3 Conclusion

The inductive storage driver is very cheap and compact and is developed using indigenous components. The system is being enhanced for its power delivery capacity. One way to do this may be use of better quenching media and longer exploding wires which will certainly require higher amount of energies to start with. The work towards the interfacing of the driver with electron beam generator for pulse microwave generation is under consideration. For this purpose the present load (which are of fixed values like 12.5Ω of 500MW case and 10.5Ω for 1.5GW case) will be replaced by the vacuum field emission diode.

8

CONCLUSION & FUTURE WORKS

A compact pulse transformers are designed developed and tested to have desired coupling co-efficients between the primary and secondary depending upon the coaxial cable base PFL parameters for two sets of experiments. The transformers have been made with a very novel design technique in which the primary capacitor bank takes shape of primary turn of pulse transformer. The voltage gain value, between primary and secondary, as high as 1:20 has been achieved with such designed pulse transformer. The transformer is very compact and uses air as insulation to avoid the additional insulation weight up to 250kV of secondary voltages applied on PFL. The detailed modelling 3D of such pulse transformer supports the deign and results of the pulse transformer.

For the first time the PFL made of high voltage coaxial cables, available commercially, has been made to give low impedance pulsed power generator (four in parallel to four times enhance current delivery capability and reduce generator impedance to one fourth) for the generation of electron beams in vircator geometry. With the ever-increasing use and production and associated improvement in the insulation technology of modern XLPE cables for HV transmission networks the scope of making such generators is very promising in future. Such a generator has also been tested for microwave

radiation at 4Hz operation frequency of the generator in a burst mode. Two such generator with different cables have been made and were experimented successfully driving a vircator device. The peak electrical power delivery capability to matched loads of these generators is 650MW and 3.3GW respectively for 12.5Ω and 15Ω loads. For repetitive and compact driver for a vircator such generator may find its use as far as reliability of its operation and ease of handling is concerned for the expert operating hands.

The experimental demonstration for 4Hz repetitive operation of axial virtual cathode oscillator driven by a compact driver is done. The radiation frequency chirps between 4-8GHz. The measured microwave power is 1MW and peaks at the centre of radiation pattern. The beam width of radiation is approximately 30° where the power reduces by half of its peak power which is occurring at the centre of axis. The efficiency of the vircator is found to be 0.3% for input electrical power to radiated microwave peak power.

The vircator is conventional geometry has been operated at the lowest ever reported voltages of 50kV with considerable microwave power emission. The beam generation at such low voltages have been found to be nearly similar with that when a high voltage is applied on cathode. The field enhancement is done by reducing anode cathode gap to as low as 3mm for such low voltage operation and having a good amount of electron beam generation leading to virtual cathode formation. A current density as high as $300\text{A}/\text{cm}^2$ has been attained by the use of velvet cathode even at the application of 50kV voltage.

It is also found experimentally that while operating at low voltage the kinetic energy of electrons is limited to $1.5 \times 10^8 \text{m/s}$ and hence with smaller A-K gap distances the frequency of radiation can be kept below 10GHz. The particle in cell modelling of vircator supports our experimental results to a good extent. The modelling was done with the help of XOOPIC, two and half dimensional particle-in-cell code.

A broadband conical horn antenna in order to maximize the radiation in free space

and to maximize them on the axis of vircator was designed with the supported 3D computer modelling and was implemented after the vircator. The antenna is broadband as is shown by its VSWR curve. The radiation was found to be maximum at the axis of vircator after the antenna.

A very novel inductive storage technique based pulsed power generator has been made to drive a vircator of nearly similar impedances as are experimented with the capacitive storage based pulsed power generator. The inductive storage based generator can come within 20cm diameter and 75cm length and used a copper wire of 122 μ m diameter and 15cm length. It is fed by a 12stage Marx generator made of axial capacitors and all the switches (closing or opening) are in air. The generator has less than 15kg weight and has been tested to deliver 1.5GW electrical power to 10.5 Ω load at peak 125kV and 150ns FWHM. The peak power computed for the matching load impedance vircator with anode cathode gap of 13mm and 5cm cathode diameter is nearly 2GW and a peak voltage of 200kV. This ultra compact generator is useful for single shot application and also to those places where one can afford to take second shot in next couple of minutes by simply mounting new exploding copper wire.

In and extensive modelling of opening switch performance of exploding copper wire with simple and fast modelling technique it has been found that a current density of $1 \times 10^{12} \text{ amp}/\text{m}^2$ is what we have loaded the copper wire with. The action integral to burst for such super heating correspond to highest values only reported in couple of references of exploding wires and the value is $4.25 \times 10^{17} \text{ Amp}^2/\text{m}^4$.

Future Works

As far as future works in the context of the present works are concerned, the following is some of the advancements which may be taken up. The cable based pulsed forming line may be made for reduced impedance by increasing number of cables and a simplest and quite effective way would be to add the two more cables i.e. total of six number of

60Ω of cables effectively delivering 10Ω PFL impedance capable of delivering higher peak powers like 5GW in matched loads. The dimensions of the input coupler of PFL allows the fitting of these two cables easily at present.

The other technical change may be incorporated by the merging of six cables to make a PFL system by three lengths and charging the PFL at the spark gap end of the PFL. This leads to a completely closed and further compact assembly.

The vacuum pumping system may either be completely removed from the vircator i.e. after vacuum sealing of the vircator tube or also by pumping using ion pump which is backed by small diffusion pump or turbo molecular pump for long life of the desired vacuum inside the vircator.

Looking at the complexity of design and development involved in the compact pulsed power sources at the outset only vircator with simple geometry was considered to be used in integrated system. In future the other competitive devices radiating high power microwave radiation may be used in place of vircator of simple geometry with the same or similar pulse power generator.

In the 4Hz operation it is seen that upto six pulses the microwave emission is almost consistent whereas after six pulses the microwave emission is reducing at the current levels studied so far. The next burst of the shots also was quite consistent in the beginning but a systematic study is to be done to conclude further. Single shot operation shot to shot effects may be further studied for determining an estimate of the life of velvet cathode dependent on the current densities attained in the system.

In the case of compact inductive storage based pulse power generator, further work may be done to make the system self supportive so that it may be used directly with the loads. This can be done by making the spark gaps of the marks which are embedded at the end of the capacitors. The data of explosion of conductors achieved with the generator may further help for optimization based on the best choice of the material for exploding wire.

- [1] Markus Zahn, Yoshimichi Ohki, David B. Fenneman, Ronald J. Gripshover, Victor H Gehman Jr *Proceedings of the IEEE* Volume 74 pp 1182-1221 (1986)
- [2] S.J. Sackett *Presentation of Sixth Symposium on Engineering Problems of Fusion Research* (1975)
- [3] M Kammon, M.J. Tsuk and J K White *IEEE transactions on Microwave Theory and Techniques* Vol 42 NO 9 (1994)
- [4] J Benford J A Swegle Edl Schamiloglu **High Power Microwaves** Taylor and Francis (2006)
- [5] M Leijon, M Dahlgren, L Walfridsson, L. Ming, A. Jaksts *IEEE Electrical Insulation Magazine* (2001)
- [6] Y. Murata, S. Katakai and M. Kanaoka *IEEE transactions on Dielectrics and electrical insulation* Vol 3 No 3 (1996)
- [7] J.P. Steiner F.D. Martzloff *IEEE international symposium on electrical insulation* Toronto Canada (1990)
- [8] T. Tanaka T. Itaya, S Katakai, Y Murata, K Takahashi *Proceedings of International symposium on electrical insulating materials in conjunction with Asian international conference on dielectrics and electrical insulation and the 30th symposium on electrical insulating materials* Toyohashi Japan (1998)
- [9] A Lindblom, P Appelgren, A Larrsson S E Nyholm, J Isberg, H Bernhoff *IEEE transactions on plasma science* Vol 31 No 6 (2003)
- [10] C Mayoux *IEEE transactions on dielectrics and electrical insulation* Vol 7 No5 (2000)

- [11] N Shimizu C Laurent *IEEE Transactions on Dielectrics and Electrical Insulation* Vol 5 No 5 (1998)
- [12] U Riechert M Eberhardt, J Kindersberger, J Speck *IEEE International Conference on conduction and breakdown in Solid Dielectrics* Vasteras Sweden (1998)
- [13] U Reichert J Kindersberger J Speck *High Voltage Engineering Symposium* (1999)
- [14] U Riechert R Vogelsang J Kindersberger *12th International Symposium on High Voltage Engineering ISH* Bangalore India (2001)
- [15] Y Zang J Lewinder C Alquie *IEEE Transactions on Dielectrics and Electrical Insulation* Vol 3 No 6 (1996)
- [16] W. G. Chase and H. K. Moore, **Exploding Wires** Plenum Press, Inc., New York, (1959), Vol. 1, pp. 7-16.
- [17] W. G. Chase and M. A. Levine, *Journal of Applied Physics*, vol. 31, no. 7, p. 1298, Jul. (1960)
- [18] C. Cho, Young-Wook Choi, W. Jiang *Journal of the Korean Physical Society* Vol. 47, No. 6, (2005) pp. 987 990
- [19] Z.Mao, X.Zou, X. Wang, X. Liu, and W.Jiang, *Laser and Particle Beams* (2009) pp 1-7
- [20] Antonios E. Vlastós *Journal Applied Physics* 38, 4993 (1967)
- [21] Antonios E. Vlastós *Journal Applied Physics* 39, 3081 (1968)
- [22] A. E. Vlastos, *Journal Applied Physics* 40, 4752 (1969).
- [23] A. E. Vlastós, *Journal Applied Physics* vol. 44, no. 5, pp. 2193-2196, (1973)

- [24] I.M. Vitkovitsky V.E.Scherrer *Journal of Applied Physics* 52(4) April (1981) pp3012 3015
- [25] B.M. Novac, M.Magureanu and I.R. Smith *Journal of Physics D Applied Physics* 31 (1998) pp L57 58
- [26] M. J. Taylor, *Journal of Physics D* 35, 700 (2002).
- [27] R. Baksht, Y.Yankelevich, I. Ziv, A. Pokryvailo, *Proc. of 14th Int. Pulsed Power Conference* 748-751, (2003)
- [28] V.N. Korobenko and A.D. Rakhel *Physical Review B* 75 064208 (2007) pp 064208-1 to 8
- [29] A.D. Rakhel, G.S. Sarkisov *15th Symposium on thermo physical properties* June 22-27, (2003)
- [30] R.E. Reinovsky, J.H. Goforth, I.R. Lindemuth and H. Oona *International workshop on high power opening switches* Novosibirsk (1989)
- [31] R.E.Reinovsky, D.L. Smith, W.L. Baker, J.H.Degnan, R.P. Henderson R.J. Kohn, D.A.Kloc, N.F. Roderick *IEEE transaction on plasma science* PS-10 No2 June (1982)
- [32] M.A.Elsayed, A.A. Neuber, J.C. Dickens, J.W. Walter, M.Kristiansen L.L.Altgibers *Review of Scientific Instruments* 83 024705 (2012)
- [33] V.A. Demidev, A.S. Boriskin, N.V. Stephenov, I.V.Konovalov, S.A.Kazakov, K.V.Shibalko, Yu.V.Vlasov, V.A.Yanenko, I.V. Rozhnov, S.N. Golosov, E.V. Shapovalov, A.S. Shuvalov *Instruments and Experimental Techniques*, 48 no5 (2005) pp 630-635

- [34] J. Stephens, A. Neuber, and M. Kristiansen, *Physics of Plasmas*, vol. 19, no. 3, pp. 032702-1-032702-8, (2012)
- [35] J. Stephens, W. Mischke, and A. A. Neuber, *IEEE Transactions on Plasma Science*, Vol. 40, No. 10, (2012)
- [36] D. B. Sinars, T. A. Shelkovenko, S. A. Pikuz, M. Hu, V. M. Romanova, K. M. Chandler, J. B. Greenly, D. A. Hammer, and B. R. Kusse *Physics of Plasmas*, vol. 5, no. 2, (2000).
- [37] D. Veksler, A. Sayapin, S.Efimov, Ya.E. Krasik *IEEE transaction on plasma science* Vol 37 No 1 (2009) pp 88-98
- [38] Ya. Krasik, S.Efimov, A.Fedotov, D. Sheftman,A.Sayapin, V. Tz.Gurovich, A. Grinenko *29th ICPIG* (2009) Mexico
- [39] A. Grinenko, S. Efimov, A. Fedotov, Ya. E. Krasik, and I. Schnitzer *Physics of Plasmas* 13, 052703 (2006)
- [40] L.Gilburd, S Efimov, A Fedotov Gefen, V. TZ. Gurovich, G. Bazalitski, O Antonov, YA.E. Krasik *Laser and particle Beams* (2012)
- [41] Toru Sasaki, Yuuri Yano, Mitsuo Nakajima, Tohru Kawamura and Kazuhika Horioka *Laser and Particle Beams* Volume 24 Issue 03 (2006), pp 371-380
- [42] H Domingos, J Scaturro, L J Hays *IEEE transactions on components, hybrids and manufacturing technology* Vol CHMT-4 No 4 (1981)
- [43] S. I Shkuratov E.F Talantsev J. C. Dickens, M Kristiansen *IEEE Pulsed power Conference Proceedings* (2003)
- [44] R Shukla A Shyam *Review of Scientific Instruments* 85 Issue 3 (2014)

- [45] R B Miller *Intense Charged Particle Beams* Plenum New York (1982)
- [46] R Shukla, A Shyam, S Chaturvedi, R Kumar , P Sarkar, D Lathi, V. Chaudhary, R Verma, K. Debnath, J M Sonara B Adhikary, K Shah *Papers on technical meeting on Plasma Science and Technology, IEE Japan* (2004) pp 25-28
- [47] Buccur M. Novac, Marco Istenic, Jing Liu, Ivor R Smith, John Brown, Martin Hubbard, Patrick Appelgren, Mattias Elfsberg, Tomas Hurtig, Cecilia Moller, Anders Larsson, Sten E Nyholm *IEEE transaction on plasma Science* Vol. 34 No 5 (October 2006)
- [48] Andreas A. Neuber *Explosively driven pulsed power* Springer (2005)
- [49] Balanis *op.cit*
- [50] Pvt communication with Richard Adler from North Star USA
- [51] R J Adler **Pulsed Power Formulary** (2001)
- [52] R Shukla, A Shyam *Laser and Particle Beams* 31 Issue 04 pp 627-634 (2013)
- [53] Adam Lindblom Hans Bernhoff, Mattias Elfsberg, Tomas Hurtuig, Anders Larsson *IEEE transaction on plasma science* 37 No 1 (January 2009) p 236-242
- [54] I C Somerville S J MacGregor O Farish *Measurement Science and Technology* 1 pp 865-868(1990)
- [55] V Nassisi *Review of Scientific Instruments* 68 No 2 (1997)
- [56] V Nassisi F Felloni D Doria A Lorusso *Review of scientific Instruments* 74 No 12 (2003)
- [57] V Nassisi F Felloni D Doria A Lorusso *Measurement Science and Technology* 15 pp 244-247 (2004)

- [58] A Schuette, H Rodrigo *Review of Scientific Instruments* 67 No. 10 (1996)
- [59] Z Zeng, L Ma *Review of Scientific Instruments* 72 No5 (2001)
- [60] SK Sharma, P Deb, R Shukla P Banerjee, T. Prabakaran, R Das, B Das, B Adhikary, A Shyam *Journal of Korean Physical Society* 59 3468 (2011)
- [61] Adam Lindblom, Hans Bernhoff, Jan Isberg, Mats Leijon *IEEE transactions on Plasma Science* 34, 5 (2006) pp 1838-1844
- [62] M Rivaletto, P Pignolet *European Physics Journal Applied Physics* 3 pp 159-167(1998)
- [63] Y Carmel, S Eylon, E Shohet *Journal of Physics E Scientific Instruments* 11 (1978)
- [64] F A Tuema, S J MacGregor, R A Fouracre *Measurement Science and Technology* 9 pp1989-1993 (1998)
- [65] S M Turnbull, S J MacGregor J A Harrower *Measurement Science and Technology* 11 (2000)
- [66] S J MacGregor, S M Turnbull, F A Tuema *Measurement Science and Technology* 5 (1994)
- [67] J O Rossi, M Ueda , J J Borroso *IEEE transactions on Plasma Science* Vol 30 No 5 pp 1622-1626 (2002)
- [68] J O Rossi, J J Borroso , M Ueda *IEEE transactions on Plasma Science* Vol 34 No 5 pp 1846-1852 (2006)
- [69] D K Gupta, P I John *Sadhana* Vol 26 Part 5 (2001)

- [70] R Verma, A Shyam, S. Chaturvedi, R Kumar, D Lathi, P Sarkar, V Chaudhary, R Shukla, K Debnath, S Sharma, J Sonara, K Shah B Adhikary T jigna, J Piyush *Proceedings on IEEE conference on Power Modulators* (2004)
- [71] R Verma, A Shyam, K Shah *Sadhana* Volume 31 Part 5 (2006)
- [72] R Shukla, A Shyam, Pulsed power group *Proceedings of First Euro Asean Pulsed Power conference* Chengdu China (2006)
- [73] R Shukla, S K Sharma, P Banerjee, R Das, T Prabakaran, P Deb, B. K. Das, B Adhikary, R Verma, A Shyam *Journal of Physics : Conference Series* (2012)
- [74] *Pspice* www.orcad.com
- [75] D.Finkelstein, P. Goldberg, J. Shuchatowitz *Review of Scientific Instruments* Vol 37 No 2 pp 159 (1966)
- [76] E.A. Abramyan *Internal Report Institute of Nuclear Physics Novosibirsk* (1970)
- [77] E.A. Abramyan *IEEE Transactions on Nuclear Society* NS-18,3,447-455 (1971).
- [78] C.R.J. Hoffman, *Review Scientific Instruments* 46, 1-4 (1975)
- [79] I. Boscolo, G. Brautti, R. Coisson, M. Leo, and A. Luches *Rev. Sci. Instrum.* 46, 11 (1975)
- [80] I. Boscolo, G. Brautti, M. Leo, A. Luches, M.R. Perrone *Journal of Vacuum Science Technology* Vol 12, No 6 , pp 1194-1196 (1975)
- [81] I. Boscolo, M. Leo, A. Luches, L. Provenzano *Review of Scientific Instruments* Vol 48 No 7 (1977)
- [82] A.Luches A. Perrone *Review of Scientific Instruments* Vol 49 No 12 pp 1629-1630(1978)

- [83] E.G. Cook L.L. Raginato *IEEE transactions on Electronic Devices* Vol Ed-26 No.10 (1979)
- [84] Matsuzawa and S. Suganomata, *Review of Scientific Instruments* 53, 694-696 (1982).
- [85] K.K. Jain, D.Chennareddy, P.I.John, Y.C. Saxena, *Sadhana* 9,1 (1986)
- [86] Di Nicolai, *Review of Scientific Instruments*, 73, 3332 (2002)
- [87] J. L. Reed, *Review of Scientific Instruments*, 59, 10 (1988)
- [88] J. R. Reed, *Review of Scientific Instruments*, 76, 104702 (2005)
- [89] J. R. Reed, *Review of Scientific Instruments*, 77, 033301 (2006)
- [90] P. Sarkar, S.W. Braidwood, I.R. Smith, B.M. Novac, R.A. Miller, R.M. Craven, *IEEE Trans. on Plasma Science* 34,5 (2006)
- [91] M Isteni , B M Novac , J Luo , R Kumar and I R Smith *J. Phys. D: Appl. Phys.*39, 21(2006)
- [92] C. A. Balanis **Antenna theory : Analysis and Design** 3rd edition Wiley- Interscience (2005)
- [93] C. A. Balanis E. Holtzman **Circular waveguides Encyclopedia of RF and Microwave Engineering** (2005)
- [94] C S Lee S W Lee S L Chuang *IEEE transactions on microwave theory and techniques* MTT-33 No 3 (1985)
- [95] Eric C Becker **M S Thesis University of Missouri Columbia** (2011)
- [96] M G Schorr, F J Beck *Journal of applied physics* Vol 21 No8 (1950)

- [97] A. King *Proceedings of the IRE* Vol 38 No 3 (1950)
- [98] *Computer Simulation Technology AG* www.cst.com
- [99] A Roy, S K Singh, R Menon, D Senthil Kumar, S Khandekar, V B Somu, S Chottray, P C Saroj, K V Nagesh, K C Mittal D P Chakravarty (2010) *IEEE Trans. Plasma Sci.* 7 (38) p 1538-1545
- [100] T Queller, A Shlapakovski, Ya E Krasik (2010) *J.Appl.Phys.* 10 103302
- [101] R Shukla, S K Sharma, A Shyam April 2010 *J. of Nepal Phys. Soc.* 26, No. 1, p 29-34
- [102] R Shukla, S K Sharma, P Banerjee, R Das, P Deb, T Prabahar, B K Das, B Adhikary, A shyam (2010) *Rev. Sci. Instruments* 81 83501
- [103] R Shukla, A Shyam, S Chaturvedi, R Kumar, D K Lathi. V. Chaudhary, R Verma, K Debnath, S Sharma J Sonara, K Shah, B Adhikary *IEEE International Pulsed power Conference 2005* Montenary USA
- [104] Betzios P. V., Uzunoglu N. K. (December 2009) *Microwave Review or Mikrota-lasnarevija* 15(2), 24-28,
- [105] Chen Y., Mankowski J., Walter J., Kristiansen M., Gale R., (2007) *IEEE Transactions on Dielectrics and Electrical Insulation* Vol. 14, pp. 1037-1044,
- [106] Choi E. H., Choi M. C., Choi S. H., Song K. B., Jung Y., Seo Y. H., Shin H. M., Uhm H. S., Lim D. W., Kim C. H., Lee J. M., and Ahn J. W., (2002) *IEEE Transactions on Plasma Science* Vol. 30, pp. 1728-1732,
- [107] Choi E.-H., Choi M.C., Jung Y., Chong M.W., Ko J.J., Seo Y., Cho G., Uhm H. S., and Suk H., (2000) *IEEE Transactions on Plasma Science* Vol. 28, pp. 2128-2134,

- [108] J A Nation *Particle Accelerators* 10 (1979)
- [109] K V Nagesh *Proceedings on Technology of electrical insulation and high voltage pulse techniques*(1982)
- [110] Egorov E. N., Kalinin Yu. A., Koronovskii A.A., Hramov A.E., Morozov M.V. (2006) *Technical Physics Letters*, 32(5), 402-405
- [111] Egorov E. N., Kalinin Yu. A., Koronovskii A.A., Hramov A.E., (2007) *Technical Physics*, 52(10), 1387-1390
- [112] Filatov R.A., Hramov A.E., Bliokh Y.P., Koronovskii A.A., Felsteiner J. (2009) *Phys. Plasma* 16 033106 doi:10.1063/1.3080200
- [113] Filatov R.A., Kalinin Yu.A., Khramov A.E., Trubetskov D.I. (2006) *Radiophysics and Quantum Electronics* 49(10) 769
- [114] Filatov R.A., Koronovskii A.A., Kurkin S. A., Hramov A.E. (2012) *Physics Bulletin of the Russian Academy of Sciences* 76(12) 1336-1338
- [115] Kalinin Yu. A., Starodubov A. V. (December 2011) *Technical Physics Letters* 37 (12) 1104-1105
- [116] Kurkin S. A., Koronovskii A. A. and Hramov A. E (2011) *Technical Physics Letters* 37(4) 356-359
- [117] Kurkin S. A., Hramov A. E., Koronovskii A. A., (2011) *Technical Physics Letters*, Volume 37, Issue 2, pp.144-147
- [118] Li, LM; Liu, L ; Xu, QF; Chen, GX; Chang, L ; Wan, H ; Wen, JC (2009) *Laser and Particle Beams* Volume: 27 Issue: 2 Pages: 335-344

- [119] Li, LM ; Chang, L ; Zhang, L ; Liu, J ; Chen, G ; Wen, J (2012) n *Laser and Particle Beams* Volume: 30 Issue: 4 Pages: 541-551
- [120] Roy A ; Menon R; Sharma V; Patel A; Sharma A; Chakravarthy D. P. (2013) *Laser and Particle Beams* Volume 31 pages: 45-54
- [121] Singh G., Chaturvedi S., (June 2008) *IEEE Transaction on Plasma Science* 36(3) 694-700
- [122] Shukla R., Banerjee P., Sharma S.K., Das R., Deb P., Prabakaran T., Das B., Adhikary B., Verma R., and Shyam A., *Review of Scientific Instruments* (2011); 82, 106103
- [123] Turchi P. J., and Peterkin R. E., (1998) *IEEE Transactions on Plasma Science* 26, pp. 1485-1491,
- [124] Yatsuzuka M., Nakayama M., Tanigawa M., Nobuhara S., Young D., and Ishihara O., (1998). *IEEE Transactions on Plasma Science* 26 , pp.1314-1321,
- [125] R. Sinton, R. van Herel, W. Enright, P. Bodger *J. Appl. Phys.* 110, 093303 (2011)
- [126] R. Sinton, C. Hammond, W. Enright, and P. Bodger, *Techcon Asia Pacific* Sydney, Australia, (2009), pp. 211-219.
- [127] R. Sinton, R. van Herel, W. Enright, and P. Bodger, *IEEE Trans. Plasma Sci.* 38, 1015 (2010)
- [128] R. Sinton, R. van Herel, W. Enright, and P. Bodger, *Journal Applied Physics* 108, 053304 (2010).
- [129] R. Sinton, R. van Herel, W. Enright, and P. Bodger, *Australasian Universities Power Engineering Conference* Christchurch, New Zealand, (2010)

- [130] R. Sinton, R. van Herel, W. Enright, and P. Bodger, *Asia-Pacific Power and Energy Engineering Conference* Wuhan, China, (2011)
- [131] Hao Shi Rong, Xie Wei Ping, Ding Bonan Wang Minhua, Yang Yu, Wu You Cheng, Dai Ying min, Zhang Nan Chuan, Han Wen Hui *High Voltage Engineering* Vol. 35 no 3 (2009) (In Chinese)
- [132] L.I Chemezova, G. A. Mesyats, V. S. Sedoi, B. N. Semin, V. V. Valevich *IEEE 18th international symposium on discharges and electrical insulation in vacuum* Eindhoven (1998)
- [133] N. Shimomura, M. Nagata, H. Akiyama, *11th IEEE International Pulsed Power Conference* (1997)
- [134] N. Shimomura, M. Nagata and H. Akiyama *IEEE International Conference on Plasma Science conference records abstracts* (1999)
- [135] Shimomura N. Nagata M., Akiyama H. *Japanese Journal of Applied Physics* Vol 40 (2001) part 1 no 6A
- [136] A.V. Kharlov, B.M. Kovalchuk, S.V. Loginov, G.V. Smorudov, A. M. volkov, A.A.Zherlitsin *14th international symposium on high current electronics* Tomsk (2006)
- [137] T.J. Tucker and R.P.Toth **SAND75-0041** (1975)
- [138] T.Heeren, **PhD Dissertation**, Electrical Engineering, Texas Tech University Lubbock TX (2003)
- [139] K.A.O'Connor, R.D. Curry *IEEE transactions on plasma science* Vol 38 No 10 (2010)

- [140] G.S. Sarkisov, S.E. Rosenthal, K. Cochrane, K.W. Struve, C. Deeney, D.H. McDaniel, *Physical Review E* (71) 046404 (2005)
- [141] Neuber, A.A. Y.J., Dickens, J.C., Kristiansen, M. *IEEE Pulsed Power Conference 2005* (2005) doi: 10.1109/PPC.2005.300570
- [142] R. Shukla, P. Banerjee, S. K. Sharma, R. Das, P. Deb, T. Prabakar, B. K. Das, B. Adhikary, A. Shyam *International Symposium on Microwaves* (2010) Bangalore India